STRUCTURAL BASIS FOR PUTRESCINE ACTIVATION, SUBSTRATE SPECIFICITY AND INHIBITOR DESIGN OF HUMAN *S*-ADENOSYLMETHIONINE DECARBOXYLASE

A Dissertation

Presented to the Faculty of the Graduate School

of Cornell University

In Partial Fulfillment of the Requirements for the Degree of

Doctor of Philosophy

by

Shridhar Bale

May 2009

STRUCTURAL BASIS FOR PUTRESCINE ACTIVATION, SUBSTRATE SPECIFICITY AND INHIBITOR DESIGN OF HUMAN *S*-ADENOSYLMETHIONINE DECARBOXYLASE

Shridhar Bale, Ph. D.

Cornell University 2009

Structure Based Drug Design is an emerging tool employed in industry as well as academia in the design and discovery of therapeutically relevant molecules. The enzyme *S*-Adenosylmethionine decarboxylase (AdoMetDC) is a critical enzyme in the polyamine biosynthetic pathway and an attractive target for design of anti-cancer and anti-proliferative compounds. The polyamines putrescine, spermidine and sperimine are ubiquitous aliphatic cations essential for cell growth, differentiation, and proliferation. The crystal structure of human, potato and bacterial AdoMetDC have been determined previously. The crystal structure of human AdoMetDC with *S*-adenosylmethionine methyl ester (MeAdoMet) and putrescine bound provided insights into the interactions of the substrate and putrescine with the enzyme. It is well known that putrescine activates the autoprocessing and decarboxylation of human AdoMetDC. To understand the structural basis of the activation, crystal structures of the wild type enzyme and the D174N, E178Q, and E256Q mutants were obtained in the putrescine free form. Putrescine was added to the E178Q and E256Q mutants and the crystal structures obtained. The crystal structures of the putrescine free mutants with MeAdoMet bound were also obtained. A comparison of the crystal structures reveals the details of putrescine activation of Human AdoMetDC. Based on the structural information of the active site and MeAdoMet binding interactions, a series of compounds were synthesized. The crystal structure of human AdoMetDC with a

member of each of the series was obtained. The structures coupled to biochemical results and quantum chemical calculations revealed details about the substrate specificity of AdoMetDC. The ligands were bound to AdoMetDC with the adenine base in the higher energy *syn* conformation. A series of compounds with substitutions at the C^8 position of the adenine base were obtained. These compounds turned out to be more potent inhibitors than the unsubstituted parent compounds. The crystal structure of processed form of AdoMetDC from *Thermotoga maritima* and complexed to MeAdoMet and 5'-Deoxy-5'-dimethyl thioadenosine (MMTA) were also obtained. The conservation of the binding mode of ligands in prokaryotes suggests the extension of inhibitors of human AdoMetDC to other therapeutically relevant species.

BIOGRAPHICAL SKETCH

Shridhar Bale is the second son of Mr. Bale Rajanna and Mrs. Bale Lakshmi. He was born in Raikal, Andhra Pradesh, India. He received his primary education at Oxford Grammar School, Hyderabad where he spent most of his childhood. He attended college at Tetrahedron Junior College, Hyderabad. His interest in mathematics and science prompted him to write the Joint Entrance Examination for admission into the prestigious Indian Institutes of Technology. After completing his college education in 1998, he secured admission into IIT Mumbai for the 5 year Integrated Masters of Science program in Chemistry.

At IIT Mumbai - he was interested in learning more about Chemistry. The course curriculum at IIT, which is designed to have a conceptual knowledge of engineering as well as science, helped him broaden his perspective about basic sciences in general. Apart from gaining professional and scientific knowledge at IIT Mumbai, he was a constant participant in the inter hostel competitions and cultural programs. This helped him immensely in developing good team working and interpersonal skills.

During his 5 years at IIT Mumbai, Shridhar was involved in many research projects, which motivated him to pursue a career in research. He was selected for admission to the graduate school by the Department of Chemistry and Chemical Biology, Cornell University, Ithaca, NY, USA for the Fall of 2003. He was very excited to be a part of such a prestigious university and his stay at Cornell helped him to develop as a researcher. He was fascinated by the structure and function of enzymes and he joined the lab of Prof. Steve Ealick. During his stay at Cornell, Shridhar expanded his knowledge in the area of structural biology applied to drug design and enzyme function.

Apart from studying structural biology, Shridhar is also interested in cricket and has immense knowledge about the game and aspires to become a good critique of the game. He is also interested in movies, music and literature. After completing graduate studies at Cornell, Shridhar is headed to Dr. Erica Ollmann Saphire's group at The Scripps Research Institute as a postdoctoral associate. At Scripps, he would be pursuing research on structural biology applied to pathogenesis of HIV and Ebola viruses.

Dedicated to my parents, siblings and all the teachers who continue to show love, support and inspiration.

ACKNOWLEDGMENTS

I thank my advisor, Professor Steven E. Ealick, for his support, guidance and teaching me the principles of X-ray crystallography and allowing me to work on a drug design project. I am indebted to my advisor for helping me develop a critical viewpoint of my work, drawing just conclusions and the freedom given to me over the period of my graduate work. I thank Professors Anthony E. Pegg, Wayne C. Guida, John A. Secrist III, William Waud, and Diane E. McCloskey for being exemplary collaborators on the polyamine project. I thank Professor Tadhg Begley for being a collaborator on the thiamin biosynthesis project and also serving on my committee. I thank Professors Brian Crane and Hening Lin for serving on my committee and providing insights into my research work. I thank Ms. Leslie Kinsland for her assistance in numerous ways. I thank all the former and present Ealick lab members for their wonderful support and technical help. I thank the staff of NE-CAT and CHESS for their assistance with data collection. I thank Cynthia Kinsland and staff of the protein production facility for the clones and protein. I thank the Begley lab members for the collaboration, biochemical insights and fun moments. I thank my friends at Cornell and all around the world who made my days brighter and cheerful. Finally, I thank everybody who is directly and indirectly involved with my graduate work at Cornell University.

TABLE OF CONTENTS

LIST OF FIGURES

LIST OF TABLES

LIST OF ABBREVIATIONS

AdoMetDC, *S*-adenosylmethionine decarboxylase

MeAdoMet, *S*-adenosylmethionine methyl ester

Put, putrescine

AdoMet, *S*-adenosylmethionine

dcAdoMet, *S*-adenosyl-5′-(3-methylthiopropylamine)

ODC, ornithine decarboxylase

ITC, isothermal titration calorimetry

DTT, dithiothreitol

WT, wild type

TCEP, tris(2-carboxyethyl)phosphine

EDTA, ethylenediaminetetraacetic acid

DFMO, α-difluoromethylornithine

MGBG, methylglyoxal *bis*(guanylhydrazone)

MHZPA, 5′-deoxy-5′-[(3-hydrazinopropyl) methylamino]adenosine

MAOEA, 5′-[(2-aminooxyethyl)methylamino]-5′-deoxyadenosine

MHZEA, 5′-deoxy-5′-[(3-hydrazinoethyl)methylamino)adenosine

hAdoMetDC, human *S*-adenosylmethionine decarboxylase

DMF, dimethylformamide

Tris, tris(hydroxymethyl)aminomethane

PEG, poly(ethylene glycol)

CCD, charge-coupled device

HEPES, N-(2-hydroxyethyl)piperazine-N′-2-ethanesulfonic acid

DIEA, diisopropylethylamine

SAH, S-adenosyl homocysteine

MMTA, 5'-Deoxy-5'-dimethyl thioadenosine

MTA, 5'-Deoxy-5'-methyl thioadenosine

DMAMA, 5’-Deoxy-5’-(N-dimethyl)amino-8-methyl adenosine

CGP48664A, 4-amidinoindan-1-one-2'-amidinohydrazone

Brij-35, polyoxyethyleneglycol dodecyl ether

HF, Hartree-Fock

LMP2, Local Moller-Plesset second-order perturbation

SCRF, self consistent reaction field

TmAdoMetDC, *Thermotoga maritima* AdoMetDC

TbAdoMetDC, *Trypanosoma brucei* AdoMetDC

PLP, Pyridoxal-5´-phosphate

CHAPTER 1

STRUCTURAL BIOLOGY IN DRUG DESIGN

Section 1.1. Structural Biology

Structural biology studies biological processes from a structural view point. The structural details of the molecule of interest can be obtained by numerous methods such as X-ray crystallography, nuclear magnetic resonance spectroscopy (NMR), electron microscopy, laser spectroscopy, and circular dichrosim. X-ray crystallography is a powerful method used to obtain the atomic position of all atoms in the molecule of interest when arranged in the form of a crystal lattice. This method is routinely used to study the structure of molecules varying from small inorganic salts to large macromolecular assemblies comprising of proteins, nucleic acids etc. X-ray crystallography is currently the most accurate tool in determining the atomic coordinates of macromoleucles. The structural information of biologically relevant macromolecules aids in understanding phenomenon such as catalysis, binding, structure, signaling and transport.

Determination of structure by X-ray crystallography primarily involves the processes of (1) growing 3-D crystals of macromolecule of interest (2) shooting a focused beam of X-rays through the crystal and obtaining a diffraction pattern (3) obtaining the electron density of the macromolecule using various phasing techniques and (4) building the model of the macromolecule based on the electron density maps and refinement of the model. Crystals of macromolecules are usually obtained by incubating pure and homogenous macromolecule with suitable precipitating agents. The electron density of the macromolecule is a Fourier transform involving the intensity of spots on the diffraction pattern and the phase of each reflection. The phase value of the each reflection cannot be measured experimentally and hence has to be inferred indirectly. Many methods have been developed to solve the “phase

problem". Multiple isomorphous replacement (MIR) involves soaking of a heavy atom into the protein crystals. The change in scattering upon addition of heavy atom is analyzed for phase determination. The most powerful technique for solving the phase problem is multi-wavelength anomalous diffraction (MAD). The anomalous diffraction of atoms is wavelength dependant and is carefully measured by collecting data at two different wavelengths. Single-wavelength anomalous diffraction (SAD) phasing technique is routinely used to obtain the phase information. For this technique, the methionine residues in the protein are replaced with selenomethionine, which acts as a heavy atom. Molecular replacement is the widely used phasing method where the initial phases of the model are obtained from the structure of a homologous protein with sufficient sequence identity. Direct methods is a powerful phasing tool suitable for small molecule structures or with high resolution data. This method looks for statistical relationships between sets of structure factors and estimates the phase values for those reflections.

Section 1.2. Structure based drug design

The determination of 3-D structure of macromolecules of therapeutic interest has always been a major research for industry as well as academia. In most of the cases, the structure would reveal the ligand binding site, which could be used for rational design of molecules with better potency (*1, 2*). More recently, virtual screening programs perform screening of libraries of millions of compounds to the active site to obtain a lead compound for further development. The virtual screening process is an effective way to obtain novel lead compounds and reduce drug discovery costs. The lead compounds are tested using biochemical methods for potency and promising candidates are developed further. The development of HIV protease inhibitors Nelfinavir and Amprenavir and the influenza drug Relenza have been aided

by structural studies (*2*). The drugs Captopril, Dorzolamide, Zanamivir are a few examples that have been rationally developed from a structural viewpoint (*3, 4*).

Structure based drug design requires that targets have an experimentally determined crystal structure to high accuracy. However, there are a lot of targets that do not have an experimentally determined crystal structure. In those cases, homology modeling provides reasonably accurate structural information of macromolecules tough to crystallize (*5, 6*). In many cases, the structural information from homology modeling has been vital in making key changes to the targets for successful crystallization. As of now more than 40 drugs designed through structural means have entered clinical trials. As a result, the use of structure in drug discovery is gaining more importance in recent times.

Section 1.3. Polyamine biosynthesis and targets

The polyamines putrescine, spermidine and spermine are simple aliphatic cations implicated in cell growth and proliferation (*7, 8*). At physiological conditions, the polyamines are positively charged with the positive charges separated from each other by the aliphatic carbon chain. The polyamines are known to bind to the negative charged DNA, RNA and nucleic acids (*9*). They are also known to maintain chromatin conformation and regulate specific gene expression (*10-12*). In addition, polyamines are also implicated in ion-channel regulation, membrane stability and free radical scavenging (*13, 14*). Elevated levels of polyamines are found in rapidly proliferative cells, which make the polyamine biosynthetic pathway an attractive target for antiproliferative diseases and cancer chemotheraphy.

The polyamine levels in the cells are maintained by the regulation of the biosynthetic enzymes, catabolic enzymes and transport in/out of the cellular membrane. The polyamine biosynthetic pathway has two separate branches, the products of which are used in the production of all the polyamines (Figure 1.1). In the

first branch of the pathway, putrescine is produced by the decarboxylation of ornithine by ornithine decarboxylase (ODC). In plants, an alternate pathway also produces putrescine. The amino acid arginine is decarboxylated to agmatine by arginine decarboxylase. Agmatine is hydrolyzed to putrescine by agmatine ureohydrolase. In the second branch of the pathway, *S*-adenosylmethionine (AdoMet) is decarboxylated to decarboxylated *S*-adenosylmethionine (dcAdoMet) by *S*-adenosylmethionine decarboxylase (AdoMetDC). The aminopropyl group from dcAdoMet is transferred to putrescine to form spermidine and in the next step the aminopropyl group is transferred to spermidine to form spermine. These transfer reactions are catalyzed by spermidine synthase and spermine synthase respectively. In the catabolic pathway, the joint action of the enzymes spermidine/spermine N1-acetyltransferase and polyamine oxidase convert spermine to spermidine and spermidine to putrescine in each step respectively.

The inhibitors to the polyamine biosynthetic pathway and the activators of the catabolic pathway have shown promise as antiproliferative agents. The biggest success of the inhibitors of the polyamine pathway is α-difluoromethylornithine (DFMO), an inhibitor of ODC that is approved by FDA for the treatment of African sleeping sickness caused by the parasite *Trypanasoma brucei gambiense*. DFMO has also been a subject of various clinical trials as a chemopreventive agent. The inhibitors of AdoMetDC methylglyoxal*bis*(guanylhydrazone) (MGBG) and 4-amidinoindan-1-one-2´-amidinohydrazone (CGP48664A) have been a subject various

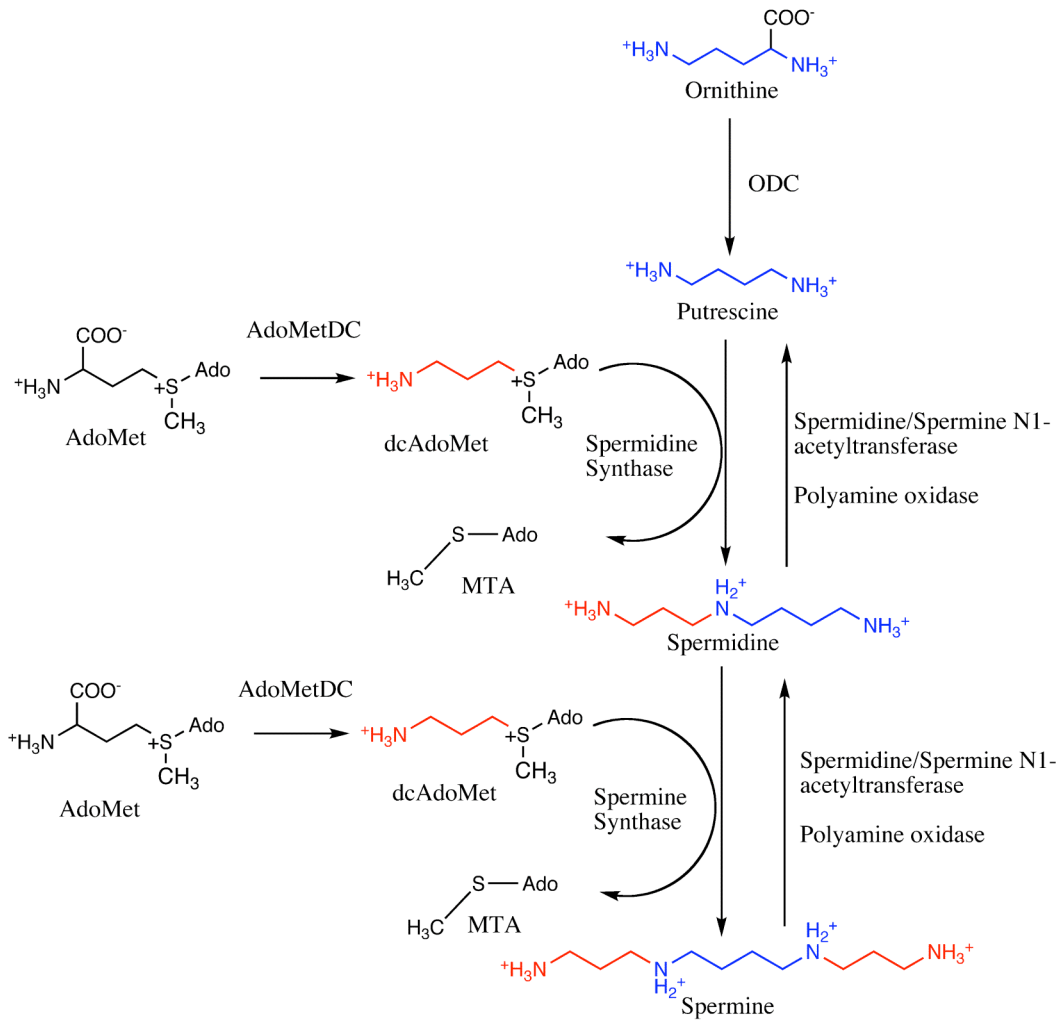

Figure 1.1 Overview of the polyamine biosynthetic and catabolic pathway

clinical trials. The compounds N^1,N^{11}-di(ethyl)norspermine (BE-3-3-3) and an unsaturated variant of N^1,N^{12}-di(ethyl)spermine (CGC-11047) are polyamine analogs that are inducers of SSAT and spermine oxidase. These compounds are currently in Phase II clinical trials in multiple cancers. The compounds mentioned above provide the proof of principle that the inhibitors of the polyamine pathway have potential therapeutic applications.

Section 1.4. S-Adenosylmethionine Decarboxylase

Decarboxylation reactions in enzymes usually depend on a pyridoxal-5´-phosphate (PLP) or a pyruvoyl group for the reaction. AdoMetDC belongs to a small class of enzymes that depend on a pyruvoyl group for the decarboxylation process. Other examples of pyruvoyl group dependant decarboxylases are histidine decarboxylase and aspartate decarboxylase respectively (*15, 16*).

The pyruvoyl group in AdoMetDC is generated from a serine residue in a self-cleavage reaction. In humans, the processing reaction happens spontaneously and there might be other factors involved for processing in different species. The mechanism of autoprocessing in human AdoMetDC is shown in Figure 1.2. The cleavage occurs between the residues Glu67 – Ser 68. The backbone of the serine residue attacks the adjacent carbonyl carbon of Glu67 to generate a five-member ring oxyoxazolidine intermediate. The intermediate collapses to form an ester intermediate. The basic residue His243 abstracts a proton from the Cα carbon of Ser68 resulting in the cleavage of the ester intermediate to two chains. The subunit containing the N-terminal part of the uncleaved chain is called the β subunit and the subunit containing the C-terminal part is called the α subunit. The N-terminus of the α subunit has a newly formed dehydroalanine residue that is tautomerized to form an imine, which is further hydrolyzed to form the pyruvoyl group.

The pyruvoyl group acts as a cofactor in the decarboxylation process. The substrate AdoMet binds to the enzyme by making a Schiff base to the active site puruvoyl group (Figure1.3). The decarboxylation reaction proceeds with the pair of electrons from the leaving group delocalized into the pyruvoyl group. The acidic residue Cys82 protonates the Cα carbon of the substrate to generate the imine intermediate. The imine is further hydrolyzed to release the product dcAdoMet and regenerate the pyruvoyl group for further rounds of catalysis. It has also been observed that the incorrect protonation (on the pyruvoyl group) of the intermediate would result in the transamination of the pyruvoyl group resulting in a dead enzyme. Activity assays of human AdoMetDC have indicated that on an average, the enzyme performs 4-5 turnover reactions before being transaminated (*17*).

The polyamine putrescine is known to regulate the activity of AdoMetDC by affecting the rates of autoprocessing and decarboxylation respectively. However, the effect of putrescine on AdoMetDC are species specific. Putrescine activates the autoprocessing reactions in humans. Putrescine activates the decarboxylation reaction in humans, *Trypanosoma brucei, Trypanosoma cruzi,* and *Caenorhabditis elegans*. In *Neurospora crassa*, putrescine is essential for the decarboxylation but there is no effect on the processing reaction (*18-21*).

The crystal structure of human AdoMetDC with the methyl ester of AdoMet (MeAdoMet) and putrescine bound has been determined previously (*22*). The crystal structure reveals the active site and the binding pocket of putrescine in the enzyme. Putrescine binds 16 – 20 Å from the active site (Figure 1.4) and makes extensive interactions with the enzyme. Human AdoMetDC exists as a dimer and biochemical studies reveal positive cooperativity in putrescine and substrate binding to the dimeric form of the enzyme (Figure 1.5).

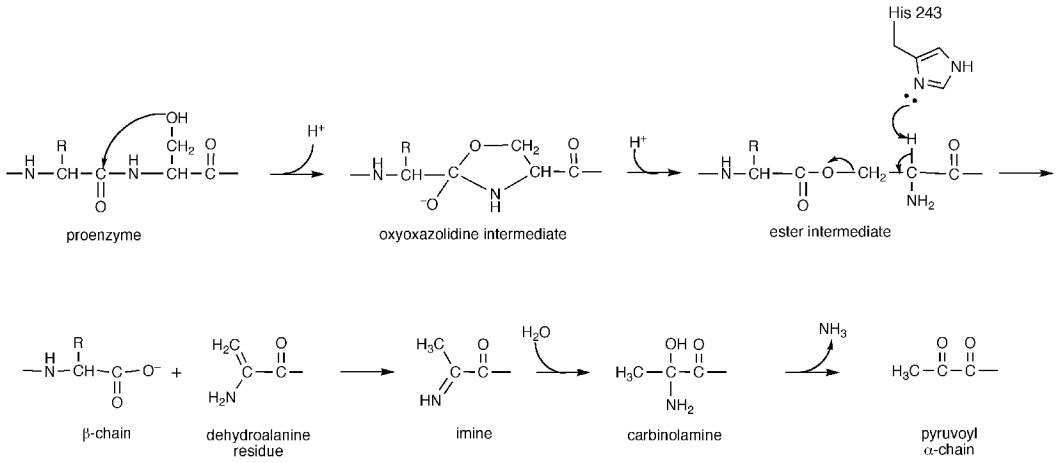

Figure 1.2. Mechanism of pyruvoyl group formation in AdoMetDC.

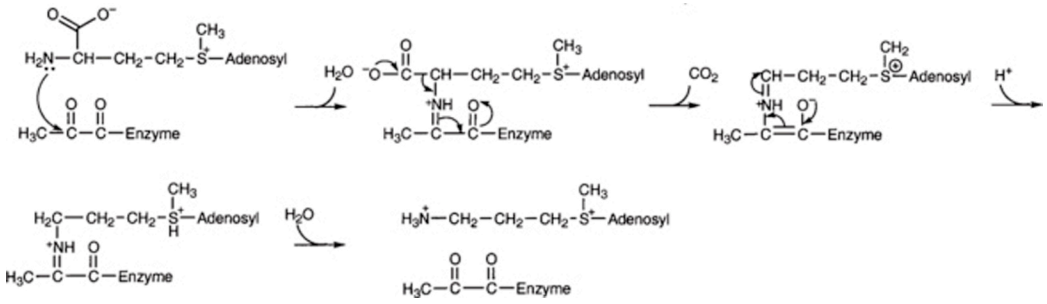

Figure 1.3. Mechanism of decarboxylation of AdoMetDC.

The crystal structure of human AdoMetDC provides an opportunity to investigate the regulation of the enzyme and rationally design inhibitors to the active site. The subsequent chapters 2-4 describe insights obtained by X-ray crystallography, biochemical analysis, and molecular modeling into regulation, substrate specificity, and inhibitor design of human AdoMetDC respectively. Chapter 5 describes the structural details of processing and complex formation in *Thermotoga maritima* AdoMetDC.

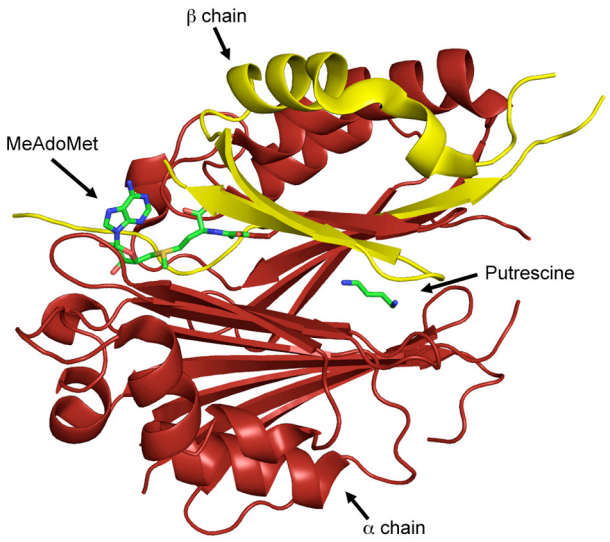

Figure 1.4. Monomeric form of processed human AdoMetDC. The α and β subunits are colored brown and yellow respectively. Putrescine and MeAdoMet are shown as sticks.

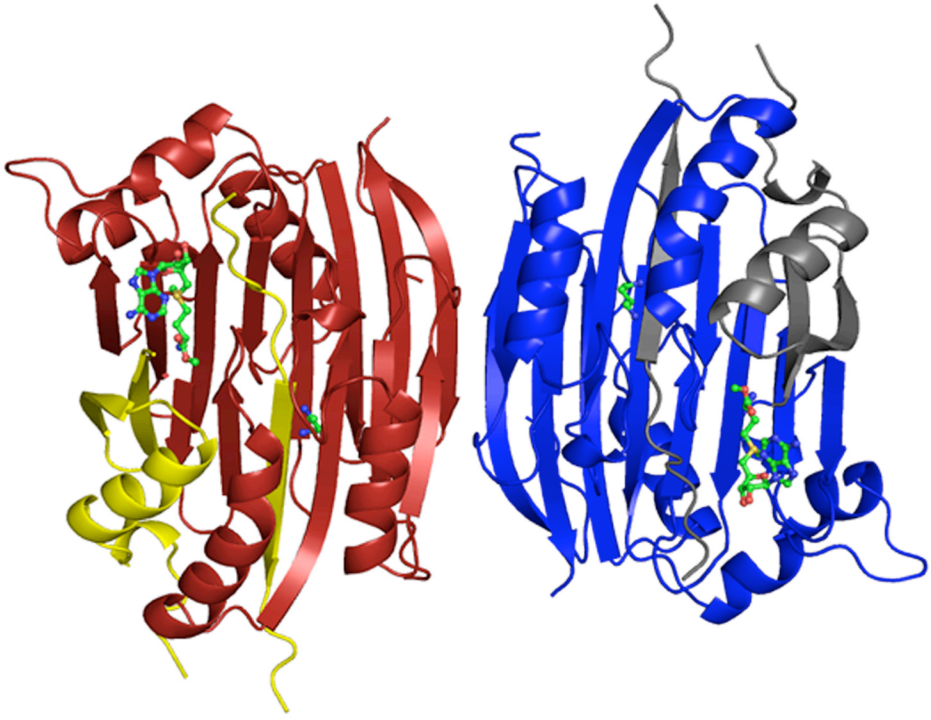

Figure 1.5. Dimeric form of human AdoMetDC viewing down the 2-fold axis. Putrescine and MeAdoMet are shown in ball and stick.

Section 1.5. Acknowledgements

The material in the following chapters focuses on the structural aspects of a collaborative project comprising of five research groups on the design of AdoMetDC inhibitors. The biochemical analysis was done in Prof. Anthony Pegg's laboratory in the Milton S. Hershey Medical Center of the Pennsylvania State University. The synthesis of the inhibitors was done in the laboratory of Prof. John A. Secrist III at the Southern Research Institute. The molecular modeling is supervised by Prof. Wayne C. Guida of the H. Lee Moffitt Cancer Center & Research Institute. Dr. William Waud from the Southern Research Institute supervises the *in vivo* cytotoxicity, growth and polyamine assays as well as the effect of AdoMetDC inhibitors on tumours in mice.

REFERENCES

1. Whittle, P. J., and Blundell, T. L. (1994) Protein structure--based drug design, *Annu Rev Biophys Biomol Struct 23*, 349-375.
2. Blundell, T. L., Sibanda, B. L., Montalvao, R. W., Brewerton, S., Chelliah, V., Worth, C. L., Harmer, N. J., Davies, O., and Burke, D. (2006) Structural biology and bioinformatics in drug design: opportunities and challenges for target identification and lead discovery, *Philos Trans R Soc Lond B Biol Sci 361*, 413-423.
3. Babine, R. E., and Abdel-Meguid, S. S., (Eds.) (2004) *Protein Crystallography in Drug Discovery*, Vol. 20, WILEY-VCH Verlag GmbH & Co. KGaA.
4. Flower, D. R., (Ed.) (2002) *Drug Design: Cutting Edge Approaches*, The Royal Society of Chemistry.
5. Eswar, N., Marti-Renom, M. A., Webb, B., Madhusudhan, M. S., Eramian, D., Shen, M., Pieper, U., and Sali, A. (2007) Comparative Protein StructureModeling with MODELLER, in *Current Protocols in Protein Science*, pp 2.9.1-2.9.31, Wiley, John & Sons, Inc.
6. Sali, A., and Blundell, T. L. (1993) Comparative protein modelling by satisfaction of spatial restraints, *J. Mol. Biol. 234*, 779-815.
7. Casero, R. A., Jr., and Marton, L. J. (2007) Targeting polyamine metabolism and function in cancer and other hyperproliferative diseases, *Nat Rev Drug Discov 6*, 373-390.
8. Gerner, E. W., and Meyskens, F. L., Jr. (2004) Polyamines and cancer: old molecules, new understanding, *Nat Rev Cancer 4*, 781-792.
9. Feuerstein, B. G., Williams, L. D., Basu, H. S., and Marton, L. J. (1991) Implications and concepts of polyamine-nucleic acid interactions, *J Cell Biochem 46*, 37-47.

10. Frydman, B., Westler, W. M., and Samejima, K. (1996) Spermine Binds in Solution to the TpsiC Loop of tRNA(Phe): Evidence from a 750 MHz (1)H-NMR Analysis, *J Org Chem 61*, 2588-2589.

11. Frydman, L., Rossomando, P. C., Frydman, V., Fernandez, C. O., Frydman, B., and Samejima, K. (1992) Interactions between natural polyamines and tRNA: an 15N NMR analysis, *Proc Natl Acad Sci U S A 89*, 9186-9190.

12. Hobbs, C. A., Paul, B. A., and Gilmour, S. K. (2003) Elevated levels of polyamines alter chromatin in murine skin and tumors without global changes in nucleosome acetylation, *Exp Cell Res 290*, 427-436.

13. Ha, H. C., Sirisoma, N. S., Kuppusamy, P., Zweier, J. L., Woster, P. M., and Casero, R. A., Jr. (1998) The natural polyamine spermine functions directly as a free radical scavenger, *Proc Natl Acad Sci U S A 95*, 11140-11145.

14. Kurata, H. T., Marton, L. J., and Nichols, C. G. (2006) The polyamine binding site in inward rectifier K+ channels, *J Gen Physiol 127*, 467-480.

15. Gallagher, T., Rozwarski, D. A., Ernst, S. R., and Hackert, M. L. (1993) Refined structure of the pyruvoyl-dependent histidine decarboxylase from Lactobacillus 30a, *J Mol Biol 230*, 516-528.

16. Albert, A., Dhanaraj, V., Genschel, U., Khan, G., Ramjee, M. K., Pulido, R., Sibanda, B. L., von Delft, F., Witty, M., Blundell, T. L., Smith, A. G., and Abell, C. (1998) Crystal structure of aspartate decarboxylase at 2.2 Å resolution provides evidence for an ester in protein self-processing, *Nat. Struct. Biol. 5*, 289-293.

17. Xiong, H., Stanley, B. A., and Pegg, A. E. (1999) Role of cysteine-82 in the catalytic mechanism of human *S*-adenosylmethionine decarboxylase, *Biochemistry 38*, 2462-2470.

18. Beswick, T. C., Willert, E. K., and Phillips, M. A. (2006) Mechanisms of allosteric regulation of *Trypanosoma cruzi* S-adenosylmethionine decarboxylase, *Biochemistry 45*, 7797-7807.

19. Ndjonka, D., Da'dara, A., Walter, R. D., and Luersen, K. (2003) Caenorhabditis elegans S-adenosylmethionine decarboxylase is highly stimulated by putrescine but exhibits a low specificity for activator binding, *Biol Chem 384*, 83-91.

20. Ekstrom, J. L., Tolbert, W. D., Xiong, H., Pegg, A. E., and Ealick, S. E. (2001) Structure of a human *S*-adenosylmethionine decarboxylase self-processing ester intermediate and mechanism of putrescine stimulation of processing as revealed by the H243A mutant., *Biochemistry 40*, 9495-9504.

21. Willert, E. K., Fitzpatrick, R., and Phillips, M. A. (2007) Allosteric regulation of an essential trypanosome polyamine biosynthetic enzyme by a catalytically dead homolog, *Proc Natl Acad Sci U S A 104*, 8275-8280.

22. Tolbert, D. W., Ekstrom, J. L., Mathews, I. I., Secrist, J. A. I., Kapoor, P., Pegg, A. E., and Ealick, S. E. (2001) The structural basis for substrate specificity and inhibition of human *S*-adenosylmethionine decarboxylase, *Biochemistry 40*, 9484-9494.

CHAPTER 2

STRUCTURAL BASIS FOR PUTRESCINE ACTIVATION OF HUMAN *S*-ADENOSYLMETHIONINE DECARBOXYLASE[1]

Section 2.1. Introduction

S-Adenosylmethionine decarboxylase (AdoMetDC) is a critical enzyme in the polyamine biosynthetic pathway (*1, 2*) and depends on a pyruvoyl group for the decarboxylation reaction (*3-5*). It is synthesized as a proenzyme that undergoes an apparent autocatalytic processing reaction to generate the pyruvoyl group from an internal serine residue. The enzyme converts *S*-adenosylmethionine (AdoMet) to *S*-adenosyl-5′-(3-methylthiopropylamine) (dcAdoMet). The propylamine group from the product is transferred to putrescine to form spermidine, or spermidine to form spermine. Putrescine is generated by the decarboxylation of ornithine by ornithine decarboxylase (ODC). Polyamine levels are highly regulated in the cell and are closely linked to normal cell growth and division. Both ODC and AdoMetDC are regulated through multiple mechanisms, catalyze reactions in the earlier stages of polyamine biosynthesis, and their reaction products are committed to polyamine biosynthesis. Consequently, these enzymes are the focus of inhibitor design, for both anticancer and antiparasitic agents (*6, 7*). α-Difluoromethylornithine is a suicide inhibitor of ODC and is approved by the Food and Drug Administration for the treatment of African sleeping sickness. Two inhibitors of AdoMetDC, methylglyoxal *bis*(guanylhydrazone) and 4-amidinoindan-1-one-2′-amidinohydrazone (CGP48664A), have been the subject of several clinical trials (*8-16*). Although neither compound is approved for clinical use, the polyamine biosynthetic pathway remains an attractive target for both cancer and antiparasitic chemotherapy.

---

[1] Reproduced with permission from Bale S, Lopez MM, Makhatadze G; Fang QI; Pegg AE, and Ealick SE. (2008). *Biochemistry* 47:13404-13417. Copyright 2008 American Chemical Society

All AdoMetDCs currently characterized are pyruvoyl enzymes but they can be divided into two classes. Class 1 enzymes are present in bacteria and archaea and class 2 enzymes are present in eukaryotes (*5, 17*). The human AdoMetDC proenzyme contains 334 amino acid residues. The processing reaction generates the α- (67 amino acids) and β-subunits (266 amino acids) with the pyruvoyl group at the N-terminus of the β-subunit (*18*). Only a small fraction of the total AdoMet pool is in the decarboxylated form and AdoMetDC activity is very highly regulated according to the need for polyamine synthesis (*3, 19, 20*). An important part of this regulation in mammalian cells and some other eukaryotes with class 2 AdoMetDCs, but not in plants, is the activation of the enzyme by putrescine (*3, 19-21*). Activation of the mammalian enzyme occurs at two stages: the rate of processing of the proenzyme is stimulated and the decarboxylase activity is increased in the presence of putrescine (*22, 23*). These factors provide a link between the availability of putrescine and the production of dcAdoMet, which is the other substrate of spermidine synthase. This allows the very efficient conversion of putrescine into spermidine without increasing the steady state pool of dcAdoMet. Mammalian cells therefore have spermidine content greatly in excess of putrescine and c.1-2% of the AdoMet is in the form of dcAdoMet (*20, 24, 25*). AdoMetDCs from fungi and several protozoal parasites have also been shown to be activated by putrescine (*20, 22, 26, 27*), but this activation may occur only at the level of the stimulation of activity (*28, 29*).

Structural studies of human AdoMetDC have indicated that the functional form of human AdoMetDC is an $(\alpha\beta)_2$ dimer with one active site and one pyruvoyl cofactor per protomer (*23, 30, 31*). The putrescine binding site is located between two central β-sheets of the enzyme, away from the active site and near the dimer interface (Figure 2.1 A). One end of putrescine is directly hydrogen bonded to Asp174, Glu15 and

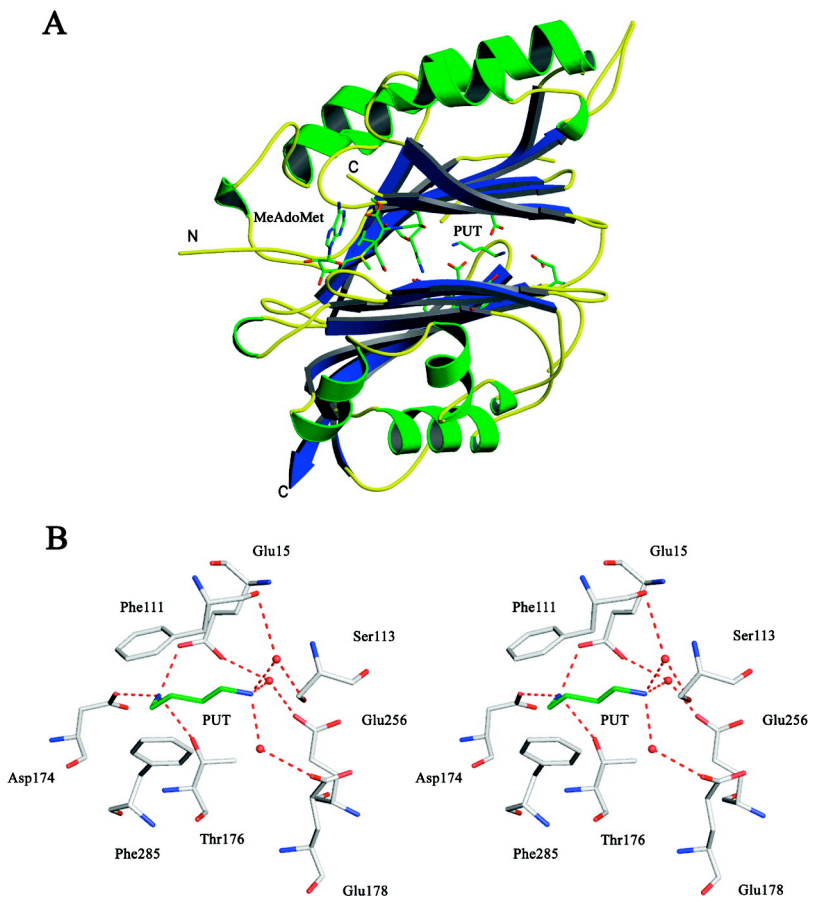

Figure 2.1. Putrescine binding site of human AdoMetDC. (A) Ribbon diagram of AdoMetDC showing the putrescine binding site and the active site with MeAdoMet bound (from pdb 1I7B). (B) Stereoview of interactions of putrescine with the enzyme. Putrescine carbon atoms are colored green. Water molecules are shown as red spheres and hydrogen bonds are shown as dashed lines.

Thr176. The other end is hydrogen bonded through water molecules to Glu178, Glu15, Glu256 and Ser113. The aliphatic chain of putrescine stacks against Phe285 and Phe111 (Figure 2.1 B). The putrescine molecule is linked to the active site by several buried charged residues. Mutations of residues in the putrescine binding site modulate the effects of putrescine (*32*). Studies using site-directed mutagenesis of the human and *T. cruzi* AdoMetDCs have identified multiple residues whose alteration abolished the activation (*22, 29, 32-34*). These include Asp174 in the human enzyme, which is conserved in all the known putrescine-stimulated AdoMetDCs and is not

present in other class 2 AdoMetDCs such as those from plants, which are not putrescine activated (*33, 35*).

Apart from these studies, there is virtually no information on the binding of putrescine to human AdoMetDC or the changes brought about by this binding. To obtain further insights into the mechanism of putrescine activation, we undertook structural studies of human AdoMetDC and putrescine binding mutants D174N, E178Q and E256Q, with (+Put) and without (-Put) bound putrescine. We have also studied the biochemical properties of the putrescine free enzymes using UV-CD spectroscopy, analytical ultracentrifugation and isothermal titration calorimetry (ITC). The crystal structures showed no global structural changes but revealed a local rearrangement of four aromatic residues near the putrescine binding site, Phe285, Phe315, Tyr318 and Phe320, and a conformational change in the loop 312-320. Biophysical studies confirmed one putrescine binding site per protomer and showed positive cooperativity between the two binding sites within the dimer. Additionally, the D174N mutant did not bind putrescine and the E178Q and E256Q mutants bind putrescine weakly with no cooperativity. Our findings demonstrate that putrescine activates AdoMetDC primarily through positioning of active site residues and electrostatic effects relayed to the active site largely through hydrogen bonding.

Section 2.2. Materials and Methods

Cloning and Expression. The constructs for expression of human AdoMetDC and mutants were modified from those described previously (*18, 32-34*) to place the $(His)_6$ tag at the carboxyl end of the protein replacing the C-terminal –QQQQQS sequence. Briefly, primers 5'-d(ATTAAAGAGGAGAAATTAACTATGGAAGCTGCACATTT-TTTC)-3' with a Bser I site (underlined) and 5'-(GTGGTGGGATTCACTCTGCTGTTG-TTGCTG)-3' with a BamH I site (underlined) were used as the sense and antisense primers in a PCR

reaction using pQE-SAMDC as a template. The product was digested with Bser I and BamH I and ligated into plasmid pQE-C145S (*36*), which encodes the C-terminal $(His)_6$–tag, that had been digested with the same enzymes. *E.coli* strain BL21(DE3) containing the AdoMetDC wild type plasmid or plasmid for the mutant proteins was grown at 30 °C overnight in a 2 x YT media containing 100 mg/mL ampicillin. The protein expression was induced by addition of 1 mM isopropyl-1-thio-β-D-galactopyranoside. Cells were harvested after 4 h and resuspended in 50 mM sodium phosphate pH 8.0, 200 mM NaCl, 2.5 mM putrescine and 0.1 mM phenylmethylsulphonyl fluoride. The cells were lysed using a French pressure cell. The wild type AdoMetDC and mutants were purified using a Ni-NTA (Qiagen) affinity column under native conditions in the presence of 2.5 mM putrescine. Fractions containing the desired protein were combined and concentrated by ammonium sulfate precipitation (80%). The pellet was dissolved and dialyzed against 50 mM phosphate, 200 mM NaCl, 1 mM ethylenediaminetetraacetic acid (EDTA) and 1 mM tris(2-carboxyethyl)phosphine (TCEP) and loaded onto a Sephacryl S-200 HR equilibrated in the same buffer and connected to an AKTA (Pharmacia) chromatography system. The eluted pure protein was concentrated by ammonium sulfate precipitation (80%), dissolved and dialyzed against 50 mM sodium phosphate pH 7.5, 1 mM TCEP, and 1 mM EDTA. The concentrated protein was kept at –80 °C. The purified protein correctly processed into a 31 kDa α subunit and a 7.5 kDa β subunit as judged by SDS-PAGE electrophoresis. The protein concentration was calculated spectrophotometrically using the extinction coefficient ε_{280} = 39,400 M^{-1} cm^{-1}. Corrections for light scattering were taken into account (*37*).

CD spectroscopy. The CD experiments were performed using a Jasco J-715 automatic recording spectrapolarimeter. Spectra were recorded at 20 °C in 10 mM phosphate pH 7.5, 0.2 mM EDTA and 0.2 mM TCEP in the absence and presence of

putrescine. Near-UV CD spectra were recorded in a 1 cm rectangular quartz cell. The protein concentration was 15 μM. The Far-UV CD spectra were recorded in a 1 mm cylindrical quartz cell. The protein concentration was 2.5 μM. The putrescine concentration was 4 fold higher than the wild type or 40-fold higher than the variant proteins to ensure that the proteins were saturated with putrescine. The molar ellipticity, [Θ], was calculated as:

$$[\Theta] = \frac{\Delta\Theta \cdot Mw}{10 \cdot l \cdot c} \qquad (1)$$

where *Mw* is the mean molecular mass of amino acid residues in AdoMetDC (115 Da), *c* is the protein concentration in mg/ml and *l* is the optical pathlength in centimeters.

Analytical Ultracentrifugation. Equilibrium sedimentation experiments were performed using a Beckman XL-A analytical ultracentrifuge with an AN-60Ti rotor, operating at 4 °C. Samples were loaded into two-sector cells and spun at three different speeds (12,000, 15,000 and 20,000 rpm). The absorbance at 280 nm, A, was recorded as a function of the radial position, r. Equilibrium was considered to be attained when replicate scans separated by 6 h were indistinguishable. The data sets for each protein were globally fitted according to a model in which single species are present in solution:

$$A = I + A_o \cdot \exp \frac{(M \cdot (r^2 - r_o^{\,2}))}{\left(\frac{2 \cdot R \cdot T}{(1 - \rho \cdot \nu) \cdot \omega^2}\right)} \qquad (2)$$

where I is the baseline offset constant, M is the molecular weight of the species present in solution, ν is the partial specific volume (0.749 cm^3/g) calculated as described in (*38*), ω is the angular velocity, R is the gas constant in erg/(mol•K), T is

the temperature in Kelvin and ρ is the density of the solvent (1 g/cm^3). The goodness of the fit was assessed by the quality of the residuals.

Isothermal Titration Calorimetry. The ITC experiments were performed using a VP-ITC titration microcalorimeter (MicroCal, Inc.). The procedure for these experiments has been described previously (*39*). In brief, the experiments were performed by injecting 3-10 μl of putrescine with concentrations ranging between 0.7 and 16 mM into the sample cell containing the protein solution. The protein concentration varied between 12 and 87 μM, depending on the magnitude of the heat effects observed. The buffer used was 50 mM phosphate pH 7.5, 1 mM EDTA and 1 mM TCEP. Dilution effects were taken into account by injecting the putrescine solution into the buffer. The heat of the reaction after each injection, q_i, was obtained by integrating the peak after the injection using the ORIGIN software provided by the manufacturer. The binding isotherms were fitted to a single set of sites (as described previously, (*40*)), model 1 in which 2 molecules of putrescine bind to the dimeric protein according to scheme 1 as shown below.

$$M_2 + 2 \cdot L \xleftrightarrow{K} M_2L_2$$

The heat of the reaction, Q, is defined as follows:

$$Q = \Delta H \cdot \frac{A - \sqrt{A^2 - 4 \cdot n \cdot [L]_T \cdot [M]_T}}{2 \cdot [M]_T} \qquad (3)$$

where $A = [M]_T + n \cdot [L]_T + (1/K)$ and $[M]_T$ is the total protein concentration expressed per monomer, $[L]_T$ is the total putrescine concentration, n is the stoichiometry of the interaction, ΔH is the enthalpy of binding and K is the equilibrium constant.

Putrescine binding to wild type AdoMetDC was also fitted according to model 2 (scheme 2 shown below) (*41*).

$$M_2 + L \xleftrightarrow{K_1} M_2L \xleftrightarrow{K_2} M_2L_2$$

The heat of the reaction expressed per mol of protein relates to the thermodynamic parameters as follows:

$$Q = \frac{K_1 \cdot [L] \cdot \Delta H_1 + K_1 K_2 \cdot [L]^2 \cdot (\Delta H_1 + \Delta H_2)}{(1 + K_1 \cdot [L] + K_1 \cdot K_2 \cdot [L]^2)} \quad (4)$$

ΔH_1 and ΔH_2 are the enthalpies of binding the first and second putrescine molecule, respectively. ΔH_1 and ΔH_2 are both expressed per mol of monomer. K_1 and K_2 are the apparent binding constants under the approximation that the free putrescine concentration is equal to the total concentration.

The populations of each species in equilibrium were calculated as:

$$\frac{[M_2]}{[M_T]} = \frac{1}{(1 + K_1 \cdot [L] + K_1 \cdot K_2 \cdot [L]^2)} \quad (5)$$

$$\frac{[M_2 L]}{[M_T]} = \frac{K_1 \cdot [L]}{(1 + K_1 \cdot [L] + K_1 \cdot K_2 \cdot [L]^2)} \quad (6)$$

$$\frac{[M_2 L_2]}{[M_T]} = \frac{K_1 \cdot K_2 \cdot [L]^2}{(1 + K_1 \cdot [L] + K_1 \cdot K_2 \cdot [L]^2)} \quad (7)$$

Fits to equations 3 and 4 were done using nonlinear fitting routine NLREG (http://www.nlreg.com/), as described previously (*42*).

Putrescine Analysis. Putrescine was released from bound protein by treatment with perchloric acid and determined by reverse-phase HPLC using post-column derivatization with o-phthalaldehyde and fluorescence detection (*43*).

Crystallization Conditions. The protein was buffer exchanged into 10 mM N-(2-hydroxyethyl)piperazine-N´-2-ethanesulfonic acid, pH 7.5, 200 mM NaCl and 1 mM dithiothreitol (DTT) using Bio-Rad buffer exchange chromatography columns. For crystallization, the concentration of the protein was maintained at 10 mg/mL for

the E178Q(-Put) mutant and at 5 mg/mL for the D174N(-Put) and E256Q(-Put) mutant. The crystals were grown using the hanging drop method at 22 °C in 13-16% polyethylene glycol 8000, 100 mM tris(hydroxymethyl)aminomethane, pH 7.5-8.5, 10 mM DTT. The crystals grew to a maximum size of 0.2 mm × 0.15 mm × 0.1 mm in 2-3 days. For the complexes of the mutants with MeAdoMet, each of the mutants was incubated with 4-6 molar excess of MeAdoMet for 24 h prior to crystallization. To obtain structures of the mutants with putrescine bound, the E178Q and E256Q mutant proteins were incubated with 4-6 M excess of putrescine for 2 h prior to crystallization.

Data Collection and Processing. The data for the D174N(-Put), E178Q(-Put) and E256Q(-Put) were collected at the A1 station of the Cornell High Energy Synchrotron Source (CHESS) using a ADSC Quantum 210 detector. Data for D174N(-Put) and E256Q(-Put) were collected over 180° with a 1° oscillation angle and 30 s exposure time per image at a crystal to detector distance of 175 mm. Data for the E178Q(-Put) were collected over 110° with a 1° oscillation angle and 60 s exposure time per image at a crystal to detector distance of 185 mm. The data for the putrescine free mutant complexes with MeAdoMet and E178Q(+Put) and E256Q(+Put) were collected at NE-CAT beamlines 24-ID-C and 24-ID-E, respectively, at the Advanced Photon Source (APS). Data were collected over a range of 160° - 360° with a 1 s exposure time and a 1° oscillation range. The crystal to detector distance varied between 200 – 280 mm. The data for the wild type AdoMetDC(-Put) were collected at a home source using a Rigaku R-AXIS IV^{++} detector and CuKα radiation from a Rigaku RU-300 rotating anode generator. Data were collected over 140° with a 0.5º oscillation angle and 20 min exposure per oscillation with a crystal to detector distance of 180 mm. The crystals were sequentially transferred to solutions with 2%, 5%, 8%, 15% and 18% glycerol with 1-

2 min equilibration between each step. The crystals were flash frozen under liquid nitrogen for the MeAdoMet complexes and putrescine bound mutants and the crystals were directly flash frozen under a liquid nitrogen stream for putrescine free mutants and AdoMetDC(-Put). The data were indexed, integrated and scaled using the HKL2000 program suite (*44*). The data collection statistics are summarized in Table 2.1 and 2.2 respectively.

Structure Determination and Refinement. All the structures were determined by molecular replacement using CNS (45). The structure of AdoMetDC(+Put)/MeAdoMet (PDB ID 1I7B), minus pyruvoyl group, putrescine, MeAdoMet and water molecules, was used as the search model. The model building for the E178Q(-Put) structure was done using the program O (46). The model building for the rest of the structures was done using the program COOT (47). The refinement process included successive rounds of simulated annealing, minimization, B-factor refinement, calculation of composite omit maps, difference Fourier maps and model building. After a few rounds of refinement, the improved difference F_o-F_c Fourier map was used to identify ligands. The ligand was then added to the model followed by another round of refinement and picking of water molecules. The parameter and the topology files for MeAdoMet were generated using the HIC-Up server (48). The difference F_o-F_c Fourier map was also used to identify conformational changes of residues in the putrescine binding site as well as the active site. The final refinement statistics are given in Table 2.3 and 2.4 respectively. A difference distance matrix program was used to identify conformational changes in the backbone of the protein structure (49, 50).

Section 2.3. Results

Studies were carried out with wild type AdoMetDC and three mutants of the protein in which acidic residues that hydrogen bond with putrescine (Figure 2.1 B)

Table 2.1. Data collection statistics for AdoMetDC mutants and complexes

	D174N (-Put)	E256Q (-Put)	E178Q (-Put)	D174N(-Put) /MeAdoMet	E256Q(-Put) /MeAdoMet
Wavelength (Å)	0.9764	0.9764	0.9766	0.9795	0.9795
Space Group (Å)	C2	C2	C2	C2	C2
a (Å)	90.60	90.71	90.57	99.22	94.44
b (Å)	55.24	55.90	56.26	50.60	50.08
c (Å)	74.22	74.33	74.05	68.82	70.17
β (°)	109.64	109.84	109.73	104.95	105.00
Resolution (Å)	1.84	1.88	1.98	1.70	2.00
Total reflections	88255	71106	53478	122776	54248
Unique reflections	27642	27282	21433	35113	18180
Redundancy	3.2(2.8)	2.6(2.3)	2.5(2.2)	3.5(2.5)	2.9(2.7)
% completeness	92.1(73.8)	96.7(87.0)	89.8(89.4)	96.3(78.0)	84.0(72.6)
I/σ	15.9(2.2)	16.0(2.0)	14.4(2.0)	15.4(2.2)	9.9(3.3)
Rsym*	6.4(39.0)	4.9(39.6)	7.1(43.8)	8.3(32.8)	10.7(25.6)
Matthews coef. ($Å^3$/Da)	2.28	2.31	2.32	2.18	2.09
Solvent content (%)	45.1	45.9	45.9	42.5	40.1

Values in parenthesis are for the highest resolution shell.
* $R_{sym}=\Sigma\Sigma_i|I_i - \langle I\rangle|/\Sigma\langle I\rangle$, where $\langle I\rangle$ is the mean intensity of the N reflections with intensities I_i and common indices *h,k,l*.

Table 2.2. Data collection statistics for AdoMetDC mutants and complexes.

	E178Q(-Put) /MeAdoMet	AdoMetDC (-Put)	E178Q (+Put)	E256Q (+Put)
Wavelength (Å)	0.9795	1.5418	0.9792	0.9792
Space Group (Å)	C2	C2	C2	C2
a (Å)	100.15	90.57	91.60	92.35
b (Å)	51.07	55.54	54.49	53.54
c (Å)	68.95	74.31	74.58	74.71
β (°)	105.40	109.66	109.45	109.09
Resolution (Å)	1.97	2.35	2.10	1.75
Total reflections	73956	41261	69216	123289
Unique reflections	23589	14524	19713	34072
Redundancy	3.1(2.5)	2.8(2.6)	3.5(2.8)	3.6(3.0)
% completeness	98.6(91.1)	99.1(95.7)	96.8(79.8)	97.7(89.6)
I/σ	15.0(3.4)	13.9(2.0)	34.4(6.2)	30.1(4.6)
Rsym*	8.0(23.8)	9.1(46.8)	3.7(12.2)	4.2(15.8)
Matthews coef. ($Å^3$/Da)	2.22	2.30	2.29	2.28
Solvent content (%)	43.5	45.5	45.3	45.0

Values in parenthesis are for the highest resolution shell.
* $R_{sym}=\Sigma\Sigma_i|I_i - \langle I\rangle|/\Sigma\langle I\rangle$, where $\langle I\rangle$ is the mean intensity of the N reflections with intensities I_i and common indices *h,k,l*

Table 2.3. Refinement statistics for AdoMetDC mutants and complexes.

	D174N (-Put)	E256Q (-Put)	E178Q (-Put)	D174N(-Put)/ MeAdoMet	E256Q(-Put)/ MeAdoMet
Resolution (Å)	1.84	1.88	1.98	1.70	2.00
R-factor[a]	0.241	0.226	0.208	0.214	0.217
R-free[b]	0.278	0.254	0.243	0.239	0.245
No of non-H atoms					
Protein	2424	2428	2433	2468	2470
Ligand	8	8	12	28	28
Water	182	153	109	176	201
B-factors					
Protein ($Å^2$)	48.5	47.8	38.6	32.7	35.9
Ligand ($Å^2$)	83.6	67.3	56.6	30.1	38.1
rms deviations					
bonds (Å)	0.007	0.010	0.006	0.013	0.024
angles	1.4	1.4	1.3	1.6	1.8
dihedrals	25.8	25.7	25.4	27.7	28.6
Ramachandran plot					
Most favored region (%)	89.6	90.1	91.2	90.5	90.0
Additional favored region (%)	8.8	9.5	7.3	7.6	9.6
Generously allowed region (%)	0.4	0.4	0.4	1.5	0.0
Disallowed region (%)	1.2	0.0	0.0	0.4	0.4

[a]R-factor = $\Sigma_{hkl}||F_{obs}|-k|F_{cal}||/\Sigma_{hkl}|F_{obs}|$, where F_{obs} and F_{cal} are observed and calculated structure factors, respectively. In [b]R-free the sum is extended over a subset of reflections (5%) that were excluded from all stages of refinement

Table 2.4. Refinement statistics for AdoMetDC mutants and complexes.

	E178Q(-Put)/ MeAdoMet	AdoMetDC(-Put)	E178Q (+Put)	E256Q (+Put)
Resolution (Å)	1.97	2.35	2.10	1.75
R-factor[a]	0.205	0.222	0.219	0.230
R-free[b]	0.228	0.283	0.249	0.241
No of non-H atoms				
Protein	2484	2456	2503	2500
Ligand	28	8	14	6
Water	222	110	142	220
B-factors				
Protein ($Å^2$)	29.6	52.3	40.5	31.9
Ligand ($Å^2$)	40.4	87.2	58.9	28.6
rms deviations				
bonds (Å)	0.014	0.006	0.023	0.040
angles	1.6	1.3	1.6	2.1
dihedrals	27.4	24.3	25.6	26.2
Ramachandran plot				
Most favored region (%)	90.9	86.2	90.8	91.2
Additional favored region (%)	8.0	12.3	8.5	8.8
Generously allowed region (%)	1.1	1.5	0.7	0.0
Disallowed region (%)	0.0	0.0	0.0	0.0

[a]R-factor = $\Sigma_{hkl}||F_{obs}|-k|F_{cal}||/\Sigma_{hkl}|F_{obs}|$, where F_{obs} and F_{cal} are observed and calculated structure factors, respectively. In [b]R-free the sum is extended over a subset of reflections (5%) that were excluded from all stages of refinement

were altered to the corresponding amides. The proteins were dialyzed extensively to remove bound putrescine. Direct analysis of the protein preparations confirmed that they contained <0.001mol putrescine/mol protein.

Far-UV and Near-UV CD. Far-UV CD spectroscopy was used to assess the effect of substitutions and putrescine binding on the secondary structure of the protein. Figure 2.2 A shows the Far-UV CD spectra for the wild type AdoMetDC and mutants. In all cases the spectra show a minimum at 218 nm and a maximum at 195 nm, typical of proteins with significant β-sheet content. The difference in ellipticity among the proteins is within the experimental error indicating that these single amino acid substitutions did not perturb the secondary structure of AdoMetDC. Figure 2.2 A inset shows the effect of putrescine binding on the wild type AdoMetDC secondary structure. It can be seen that the holo protein has overall the same secondary structure as the apo form. The small difference observed might be due to contributions of the aromatic residues which interact with putrescine (Phe111, Phe285, Tyr318, Phe315 and Phe320) (*23, 30, 31*).

Near-UV CD is very sensitive to the environment of aromatic side chains and therefore to the tertiary structure of the protein. Figure 2.2 B shows the near-UV CD spectra for the AdoMetDC wild type and variant proteins. The overall shapes of the spectra are similar with a minimum at 278 nm and a maximum at 256 nm. The small difference in absolute values observed among proteins is probably due to slightly different orientation of the aromatic residues caused by the substitutions. Putrescine has a small effect on the near-UV CD for the wild type and E256Q proteins (Figures 2.2 C and D, respectively). Under saturated conditions of putrescine, the ligand causes a small increase in ellipticity, probably due to a more rigid environment of the aromatic residues. On the other hand, no change in ellipticity was observed for E178Q and D174N, respectively (Figures 2.2 E and F, respectively).

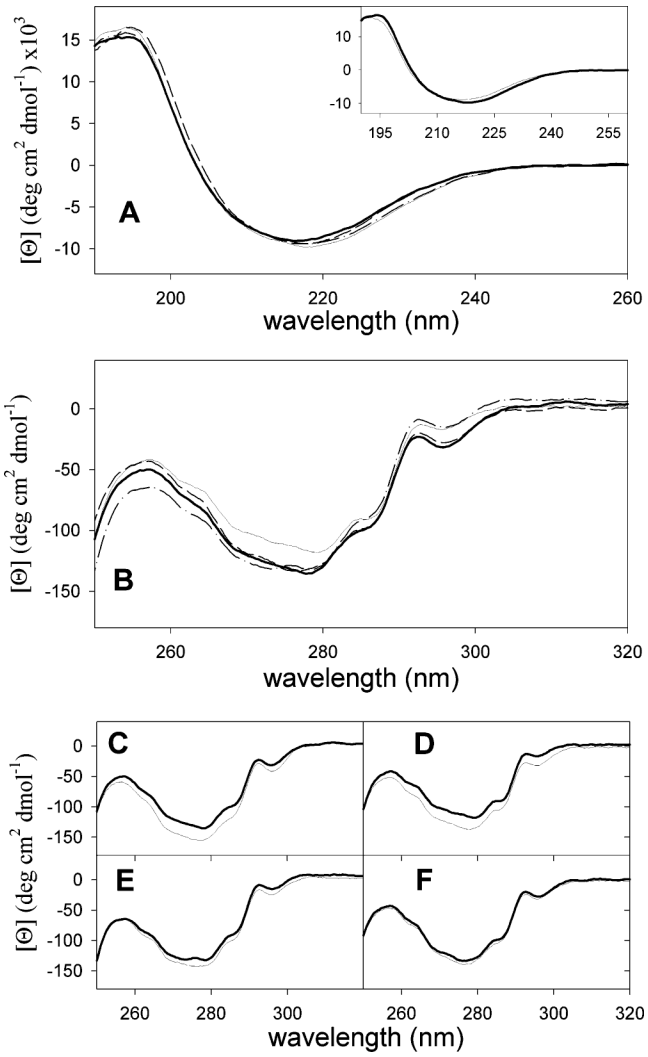

Figure 2.2. (A) Effect of mutations on the Far-UV CD spectra for human wild type AdoMetDC (thick solid line), E256Q (thin solid line), D174N (dashed line) and E178Q (dashed-and-dotted line). Inset: Effect of putrescine on the Far-UV CD spectra: wild type protein in the absence (thick solid line) and presence (thin solid line) of putrescine. (B) Effect of mutations on the Near-UV CD spectra for wild type AdoMetDC (thick solid line), E256Q (thin solid line), D174N (dashed line) and E178Q (dashed-and-dotted line). Effect of putrescine on the Near-UV CD spectra: wild type AdoMetDC (C), E256Q (D), E178Q (E) and D174N (F) in the absence (thick solid line) and presence (thin solid line) of putrescine.

This is expected for D174N as the substitution abolishes putrescine binding to the protein (see later Results).

Analytical Ultracentrifugation of the AdoMetDC Proteins. The X-ray structure of the human wild type AdoMetDC shows that the protein crystallizes as a dimer (*18, 23*). To assess if this is the functional unit in solution and if the putrescine or mutations affect the oligomerization state of the protein, sedimentation equilibrium experiments were performed at three different speeds. For each protein the data were globally fitted according to different oligomeric models. In all cases, the experimental data were best fitted according to a model with single species in equilibrium (equation 2 in Materials and Methods) and a molecular weight of a dimer. Figure 2.3 shows representative data for the wild type AdoMetDC. The molecular weight obtained from the global fit was 77.2 +/-0.3 kDa in very good agreement with the theoretical one (76.8 kDa).

Putrescine Binding to AdoMetDC Characterized by ITC. In the ITC experiments, the heat released upon putrescine binding to the proteins was measured. Figure 2.4 A shows representative heat effects for putrescine binding to wild type AdoMetDC at 15 °C. The heat of binding is proportional to the enthalpy and degree of binding and thus allows model-dependent estimates of the enthalpy (ΔH), the binding constant (K) and the stoichiometry (*n*). Figure 2.4 B shows the binding isotherm in which the heat effect is plotted as a function of putrescine concentration. The experimental data were fitted according to equation 3 (in Materials and Methods), which considers independent and non interactive binding sites (scheme 1). The *n* parameter was kept constant as 1 molecule of putrescine per monomer of wild type AdoMetDC. It can be seen that the fit to model 1 does not represent the experimental data. The binding isotherm was then fitted according to equation 4 (in Materials and Methods), which considers two interactive ligand binding sites per dimeric protein, according to the model shown in scheme 2. The fitted parameters are summarized in Table 2.5. We observed that the second putrescine molecule binds with significantly

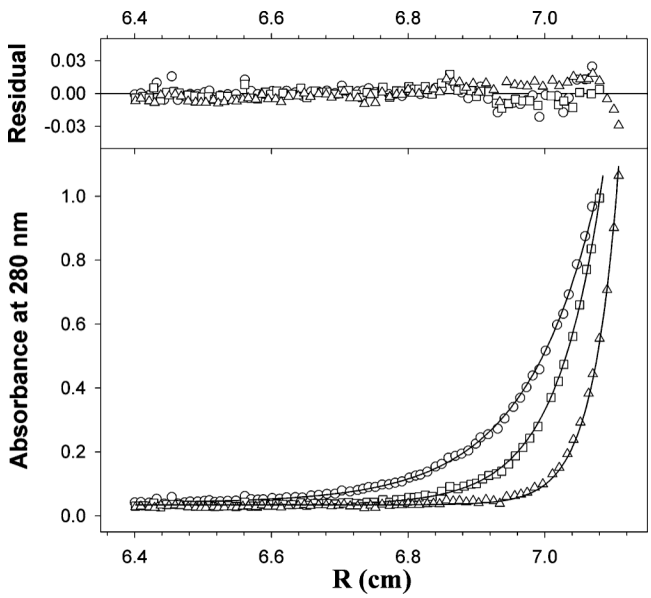

Figure 2.3. Equilibrium sedimentation analysis of human AdoMetDC. Representative traces for the wild type AdoMetDC at 12,000 (circles), 15,000 (squares) and 20,000 rpm (triangles). Solid lines represent the global fit according to equation 2. The molecular weight obtained from the fit was (77.2 ±0.1) kDa.

higher affinity to the dimeric protein than the first one. We found that $K_2 > K_1/4$ which implies that putrescine binding to the wild type AdoMetDC protein has positive cooperativity. The cooperativity in a two-site system can be characterized by

$$\Delta\Delta G = -R \cdot T \cdot \ln\left(4 \cdot K_2 / K_1\right) \quad (8)$$

We observe that ΔΔG is very significant (Table 2.5) if we compare it to the ΔG for the total process from the apo to the holo forms. The ΔG for this process is calculated as

$$\Delta G = -R \cdot T \cdot \ln\left(K_1 \cdot K_2\right) \quad (9)$$

Figure 2.4 C shows the changes in the population of the different species in equilibrium as a function of the putrescine concentration according to equations 5, 6

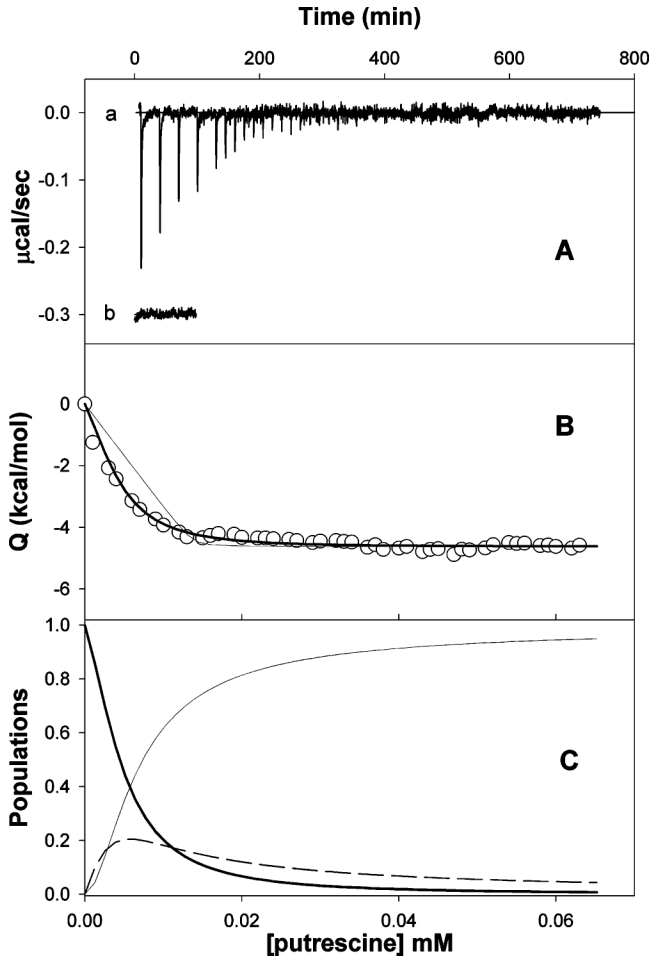

Figure 2.4. Putrescine binding to wild type AdoMetDC by ITC. (A) Representative isothermal titration calorimetry experiment at 15 °C. Heat effects are recorded as a function of time during 45 successive 3 µL injections of 0.70 mM solution of putrescine into the cell containing 0.0138 mM protein (a) or buffer (b). Buffer conditions were 50 mM sodium phosphate pH 7.5, 1 mM EDTA, 1 mM TCEP. (B) Cumulative heat effect corresponding to the titration in panel A (o) as a function of putrescine concentration. The thin line is the fit of the experimental data to equation 3. The thick line is the fit of the experimental data to equation 4 with the parameters listed in Table 3. (C) Populations present in solution as a function of putrescine concentration: $[M_2]/[M_T]$ (thick solid line), $[M_2L]/[M_T]$ (dashed line) and $[M_2L_2]/[M_T]$ (thin solid line) calculated according to equations 5, 6 and 7, respectively.

Table 2.5. Thermodynamic parameters for putrescine binding to the AdoMetDC proteins from the ITC experiments at 15 °C[a].

Protein	K_1	K_2	ΔH1	ΔH2	ΔG	$\Delta\Delta G^{coop}$
AdoMetDC(-Put)	$9x10^4$	$3.4x10^5$	-5.8	1.2	-13.8[b]	-1.55[c]
E256Q(-Put)	$1.0x10^4$	-	-6.1	-	-10.3[b]	NA
E178Q(-Put)	$2.0x10^3$	-	-1.2	-	-8.7[b]	NA
D174N(-Put)	NE	-	NE	-	NE	NA

[a] The binding constants are expressed in M^{-1}, the enthalpies are expressed in kcal per mol of monomer and free energies are expressed in kcal/mol. The error in the enthalpies and binding constants is ~15%. Note that for E256Q and E178Q, $K_1=K_2=K$ and ΔH1=ΔH2; NA: not applicable; NE - no heat effect was observed for D174N. [b] calculated according to equation (9); [c] calculated according to equation (8)

and 7 in Materials and Methods. We observe that the M_2L concentration is never higher than 20% of the total protein and the high cooperativity favors the binding of the second putrescine molecule (M_2L_2). The stoichiometry of the interaction is consistent with the crystal structure of the human AdoMetDC protein which shows that each monomer is able to bind one molecule of putrescine (*23, 30, 31*).

Figure 2.5 shows the putrescine binding isotherms for the AdoMetDC mutant proteins at 15 °C. One obvious conclusion can be drawn from these results: the putrescine binding to the D174N variant does not show any significant heat effect (Figure 2.5 C), strongly suggesting that AdoMetDC-D174N is no longer able to bind putrescine. To ensure that the lack of heat effect was due to lack of binding and not to a very small enthalpy of binding at that temperature or not enough protein concentration, experiments were performed at different temperature and different protein concentrations (results not shown). In all cases, titration of the D174N variant protein

with putrescine produced no significant heat effect under our experimental conditions. Thus, substitution of Asp174 by asparagine abolishes putrescine binding all together.

However, the putrescine binding to the E256Q and E178Q variant proteins shows significant heat effects different from that with wild type AdoMetDC. The isotherms for the E256Q and E178Q can be fitted according to equation 3 (model 1, Figures 2.5 A and 2.5 B). The fitted parameters are summarized in Table 2.5. It is obvious from these results that the mechanisms of putrescine interaction with the human AdoMetDC wild type protein and the E256Q, E178Q and D174N mutant proteins are very different. Substitution of Glu178 or Glu256 by glutamine not only abolishes the positive cooperativity for the binding of the second molecule of putrescine to these proteins, but also dramatically decreases the putrescine binding affinity as compared to K_1 for the wild type protein (Table 2.5).

Crystal Structures of Putrescine Free AdoMetDC. Crystal structures of AdoMetDC(-Put), D174N(-Put), E178Q(-Put) and E256Q(-Put) were obtained. Difference Fourier maps (F_o-F_c) and composite omit maps clearly show that putrescine was absent in these structures. Instead the putrescine binding site in the AdoMetDC(-Put) and D174N(-Put) and E256Q(-Put) mutants contains four additional water molecules (Figure 2.6 A). The nitrogen atom of putrescine closer to the active site is replaced with a water molecule (W_A). This water molecule makes hydrogen bonds to water molecules W_B and W_C, which in turn are hydrogen bonded to Glu256 and Ser113, respectively. A fourth water molecule (W_D) is present roughly at the center of the putrescine binding site and hydrogen bonds to W_A. Asp174 is found in various conformations in the putrescine free structures and is not hydrogen bonded to any conserved water molecule. The structure of the E178Q(-Put) mutant shows a ligand

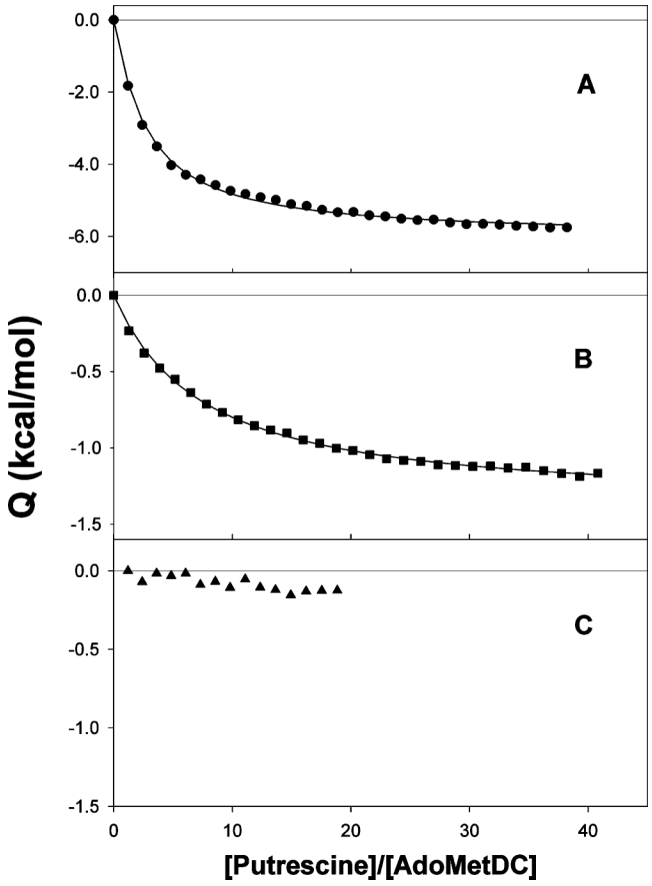

Figure 2.5. Dependence of the heat effect of putrescine binding to AdoMetDC-E256Q (A), AdoMetDC-E178Q (B) and AdoMetDC-D174N (C) as a function of the ratio putrescine/protein. Solid lines are the best fit to equation 3 with the parameters in Table 2.5.

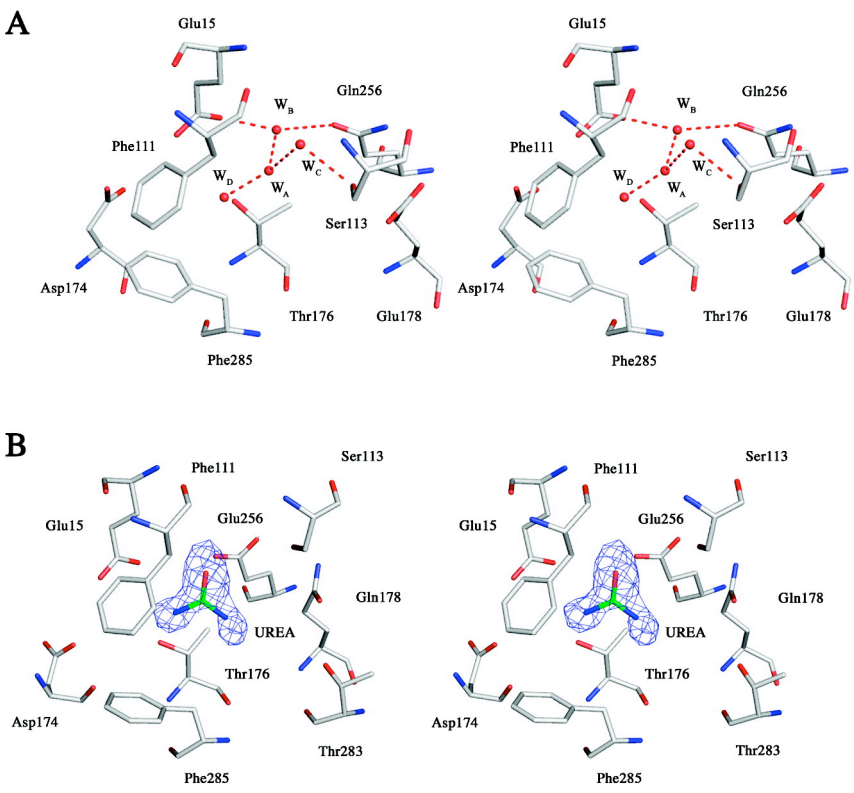

Figure 2.6. Putrescine binding site in the putrescine free mutants. (A) Stereoview of putrescine binding site in the E256Q(-Put) mutant. Water molecules are shown as red spheres and hydrogen bonds are shown as dashed lines. (B) Stereoview of the putrescine binding site in the E178Q(-Put) mutant. The density maps show a planar ligand comprised of four atoms bound in the putrescine binding site. A molecule of urea was modeled into the density. The difference F_o-F_c Fourier map is calculated omitting urea and is contoured at 4.0 σ. The hydrogen bonds are omitted for clarity.

bound in the putrescine binding site. Based on the electron density, which is triangular and flat, a molecule of urea was modeled into the putrescine binding site. The carbonyl oxygen of urea occupies the same position as the putrescine amino group closer to the active site and W_A, and is hydrogen bonded to the enzyme through water molecules. A stereoview of the ligand bound in the putrescine binding site of the E178Q(-Put) mutant is shown in Figure 2.6 B.

Three regions of the AdoMetDC show differences in the putrescine free structures relative to the putrescine bound structures: residues 171-173, 301-304 and

315-320 (Figure 2.7). In addition the side chains of Phe285, Ser 312 and Met314 show different conformation in the putrescine free structures. Loop 171-173 is adjacent to Asp174, which is required for putrescine binding. Four aromatic residues, Phe285, Phe315, Tyr318 and Phe320, are repositioned in the putrescine free structures mostly through changes in the χ_1 torsion angles plus lateral shifts (Figure 2.8). The repositioning is associated with a 1.5 to 3 Å shift in loop 312-318 and causes the putrescine binding site to become more solvent exposed. The biochemical relevance of loop 301-304 is unclear because it is far away from both the putrescine binding site and the active site.

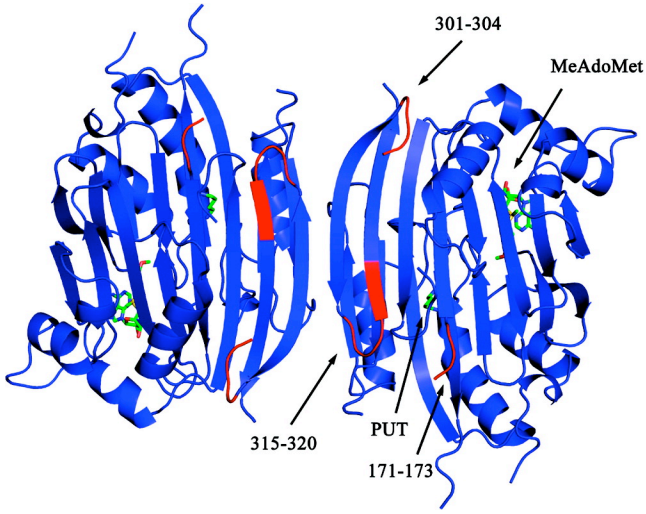

Figure 2.7. Dimeric form of AdoMetDC. Putrescine and MeAdoMet bound in the active site are shown as sticks. There is no overall change in the secondary structure. The loops undergoing conformational upon putrescine binding are colored red and labeled.

Crystal Structures of the Putrescine Free AdoMetDC/MeAdoMet Complexes. Complexes of putrescine free mutants with MeAdoMet were prepared to determine the effects of the absence of putrescine on the conformation of the substrate and active site residues. Difference Fourier maps showed MeAdoMet bound in the active site of all three mutants covalently linked to the pyruvoyl cofactor through a Schiff base. The

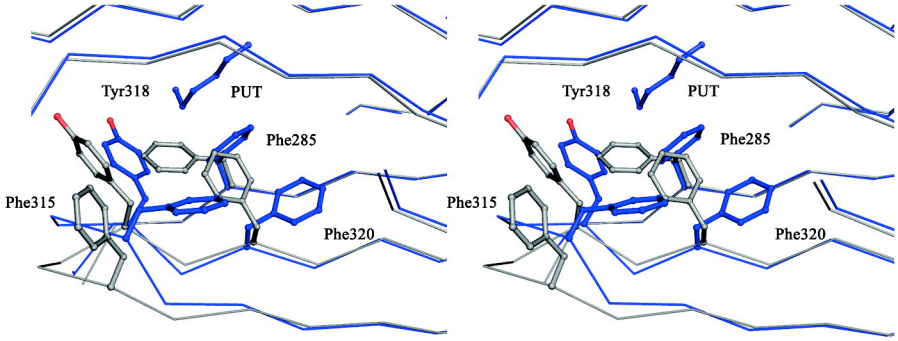

Figure 2.8. Stereoview of the changes in the conformation of aromatic side chains occurring due to putrescine binding. AdoMetDC(+Put) is shown in blue and AdoMetDC(-Put) is shown in gray. The conformational shift in loop Phe320-Ser312 as an effect of the changes in the aromatic side chains is clearly seen.

MeAdoMet conformation and the active site are essentially the same as for the complex of wt-AdoMetDC with MeAdoMet (*30*). The 2´ and 3´ oxygen atoms of the ribose each make a hydrogen bond to the carboxylate group of Glu247. The adenine base stacks between Phe7 and Phe223 with an overall *syn* conformation. All three mutant complexes, including E178Q, showed the same four conserved water molecules in the putrescine binding site. The mutant complexes also showed the same reorganization of the four aromatic residues Phe285, Phe315, Tyr318 and Phe320 and the conformational change in loop 312-320 seen without putrescine and substrate analog.

Structure of Mutants with Added Putrescine. Structures of E178Q and E256Q were determined after the addition of putrescine. The structure of D174N with putrescine was not determined because biochemical studies reported here show that this mutant does not bind putrescine. For both E178Q(+Put) and E256Q(+Put) addition of putrescine resulted in a reversal of the conformational changes in Phe285, Phe315, Tyr318 and Phe320 and the 312-320 loop seen in the putrescine free structures (Figure 2.8). The putrescine molecule is in the same position as observed in all previously reported human AdoMetDC structures (*23, 30, 31*). In both structures the aliphatic chain of putrescine stacks against Phe111 and Phe285, with the latter

residue involved in repositioning the aromatic residues for the putrescine free structures.

In the E256Q(+Put) mutant, one end of putrescine makes direct hydrogen bonds to Glu15, Asp174 and Thr176 while the other end makes water mediated hydrogen bonds to Glu178 and Gln256 as previously observed (*23, 30, 31*). The E178Q(+Put) mutant structure shows some interesting differences. One end of the putrescine molecule makes direct hydrogen bonds to Glu15, Asp174 and Thr176 and the other end of the putrescine makes a water mediated hydrogen bond with Glu256; however, there is no bridging water molecule between putrescine and Gln178. Additionally, compared to all other AdoMetDC structures, there is a conformational change in residues Glu11, Lys80, Ser229 and His243 in E256Q(+Put), which link the putrescine binding site and the active site (Figure 2.9). The χ_1 torsion angle of His243, which is important for both the processing and decarboxylation reactions, changes from -63° to 90°. In the alternate conformation the side chain is pointed away from both the pyruvyl cofactor and Ser229. Residues Lys80 and Glu11 also undergo conformational changes and are hydrogen bonded to each other through Ser254 and a water molecule. The other significant change in E256Q(+Put) is the transformation of the disordered loop 291-299 into a short α-helix. This helix is located at the dimer interface and interacts across the twofold axis with the same helix from the other protomer. The closest contact between the two helices is at the sulfur atoms of Cys292, which are 3.6 Å apart.

Section 2.4. Discussion

Putrescine Binding to AdoMetDC and Mutants. Activation of the AdoMetDC autoprocessing and decarboxylation reactions is species dependent. The regulation of the polyamine biosynthetic pathway by putrescine in certain species is poorly understood and a thorough understanding of the regulation of polyamine levels might

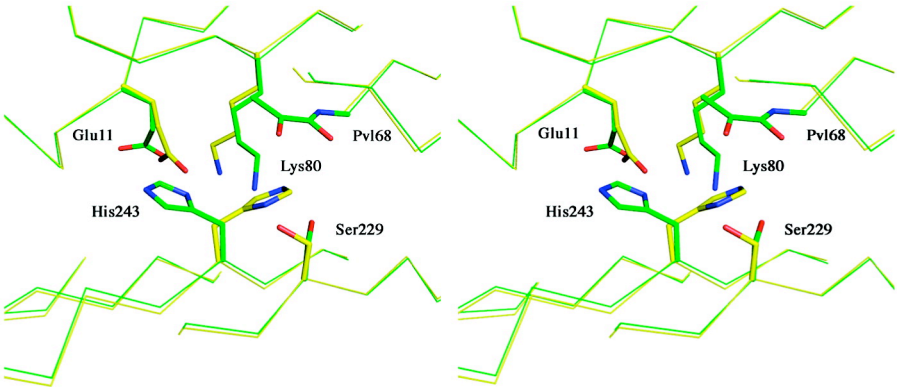

Figure 2.9. Stereoview of the comparison of the catalytic residues His243, Glu11, Lys80 and Ser229 in E256Q(+Put) and E256Q(-Put) mutants. E256Q(+Put) has carbon atoms colored in green and E256Q(-Put) has carbon atoms colored yellow.

provide an alternate route for inhibiting the pathway. However, the activation of autoprocessing and decarboxylation processes of human AdoMetDC by putrescine and other diamines is well known and studied (*23*). The rate of activation of the enzyme is highest by putrescine when compared to other diamines. The only previous direct measurements of putrescine binding to AdoMetDC were carried out with the *T. cruzi* enzyme (*29*). The K_d, which was determined by ultrafiltration and by fluorescence change measurements, was 150-180 μM. This is more than an order of magnitude greater than the values measured here by ITC for the human enzyme but, as described below, it has been shown recently that a much more active enzyme that is not putrescine-activated is formed by a heterodimer between *T. cruzi* AdoMetDC and a structurally homologous regulatory protein (*51*). Although Asp174 appears to be a key residue in binding for both enzymes since mutation to valine in *T. cruzi* (*29*) or asparagine in human (Table 2.5) abolished binding, it appears that there is little similarity in the activation of the parasite and mammalian enzymes. Our value is much closer to that which would be expected on the basis of the amount of putrescine needed for enzyme activation (K_a of c. 20 μM) (*3, 19-21*) or processing (K_a c. 50 μM) (*23*). The latter value may be increased due to competition for binding by nucleic

acids in the reticulocyte lysates used for studying processing in coupled transcription/translation systems.

The tight binding of putrescine to human AdoMetDC is also consistent with the difficulty in removing putrescine from the enzyme. This requires extensive dialysis and it is noteworthy that all of the previously published structures of the protein contain a bound putrescine even though it was not added to the buffers used for crystallization. The current results using ITC confirm that there is only one putrescine binding site in the human AdoMetDC αβ protomer and rules out postulated models in which two putrescine molecules bring about the changes in AdoMetDC activity (*19, 34, 52*). The previously unrecognized cooperative binding of putrescine to mammalian AdoMetDC is likely to explain the complex kinetics for activation previously reported (*52*). Furthermore, the ITC data confirm that in solution, the putrescine molecule binds in the site identified by the crystal structure. Mutation of Asp174, which interacts directly with the putrescine, totally abolished binding, highlighting the effect of the hydrogen bond from this residue upon putrescine binding. Mutations of Glu178 and Glu256, which both interact indirectly via a water molecule, greatly reduced the affinity for putrescine. Potato AdoMetDC, which is not activated by putrescine, is generally quite similar to the human structure but is an αβ monomer (*35*). In this structure, several amino acid substitutions in the putrescine binding pocket (Asp174 to valine, Phe111 to arginine, Leu13 to arginine and Phe285 to histidine) introduce side chains that mimic the role of putrescine in the human enzyme. Thus, dimerization and putrescine activation may be linked.

Structure of the Putrescine Binding Site with and without Putrescine. Previous structural studies clearly identified the putrescine binding site in human AdoMetDC (*23, 30, 31*). Putrescine is bound between the two central β-sheets of the enzyme at a distance of 15 to 20 Å from the active site. The putrescine amino group farther from

the active site is directly hydrogen bonded to Asp174, Glu15 and Thr176. The closer amino group is hydrogen bonded through water molecules to Glu178, Glu15, Glu256 and Ser113. The carbon chain of putrescine stacks against Phe285 and Phe111. The crystal structure also shows that there is only one molecule of putrescine bound per monomer.

Previously reported structures provided insights into the mechanism of putrescine activation of human AdoMetDC (*23*). On the basis of these studies, the mechanism of putrescine activation was believed to be due to two reasons. First, putrescine binds inside the β-sandwich region through charge neutralization of acidic residues and hydrophobic interactions to aromatic residues and it was proposed that stability of the β-sandwich is necessary for the correct orientation of residues for the autoprocessing reaction. Second, there is a hydrogen bonding network from the putrescine binding site to His243, which plays a critical role in the autoprocessing mechanism and in the decarboxylation processes through electrostatics and hydrogen bonding.

The crystal structures of the putrescine free enzyme and mutants provide newer insights into the putrescine binding site. The putrescine binding site is solvent accessible from one side and in the absence of putrescine the site is filled with water molecules. The comparison of crystal structures of putrescine free and putrescine bound AdoMetDC structures showed no significant changes in the secondary structure. The Far-UV CD experiments have also shown that there is no significant change in the secondary structure of AdoMetDC and the mutants upon putrescine binding, supporting the crystal structures. These observations suggest that putrescine has little effect in stabilizing the secondary structure of the enzyme as previously thought.

Conformational Changes upon Putrescine Binding. Difference distance matrix analysis (*49, 50*) showed significant changes in the Cα positions of residues 171-173, 301-304, 312-320. Asp174 is required for putrescine binding and residues 171-173 are near the entrance of the putrescine binding site. Consequently, these residues appear to serve as a gate to the putrescine binding site. In addition repositioning of the aromatic residues Phe285, Phe315, Tyr318 and Phe320 and the loop containing residues 312-320 further opens the putrescine binding site (Figure 2.8). In the absence of putrescine, the site is filled with water, more open and more solvent accessible. Binding of putrescine displaces two water molecules and Phe285 moves towards the aliphatic portion of the putrescine molecule, followed by closing off of the entrance thus shielding the putrescine from the solvent. These changes result in closer contacts between the protein side chains and an enhancement of electrostatic effects. The near-UV CD experiments showed a small effect for the wt-AdoMetDC and the E256Q mutant, which is due to the change in the aromatic side chain positions. This finding is in agreement with the change in the orientation of Phe285, Phe315, Tyr318 and Phe320 observed upon putrescine binding.

Positive Cooperativity of Putrescine Binding. Human AdoMetDC is a homodimer with two active sites and two putrescine binding sites. ITC studies showed positive cooperativity of putrescine binding for WT-AdoMetDC while no cooperativity was observed for the mutants (Table 2.6). Loop 312-320, which undergoes a shift upon putrescine binding, is at the dimer interface (Figure 2.10 A). The main contacts between this loop and the twofold related protomer occur between the residues Ser312-Ser312′, Met314-Cys310′, Phe315-Arg307′ and Gln311-Gln311′, where the prime designates residues in the twofold related protomer. The effect of putrescine binding and conformational changes in the loop provide a possible mechanism by which changes in one putrescine binding site are relayed through the

dimer interface to the putrescine binding site in the other monomer. Not consistent with this argument is that the E178Q and E256Q mutants bind putrescine but do not show cooperativity even though the same conformational changes are observed upon putrescine binding for loop 312-320 and the four aromatic residues, suggesting that other factors are involved.

Table 2.6. Effects of putrescine on AdoMetDC and mutants.

	Processing (-Put)	Processing[a] (+Put)	Decarboxyl-ation (-Put)	Decarboxyl-ation[b] (+Put)	Cooperativity in Put binding
WT	1	5-8	1	4	yes
D174N	1	NA	1	NA	NA
E178Q	1	1	4	1	none
E256Q	1	1	1	1	none

[a] Activation measured at 1 mM Put (*23*)

[b] Activation measured at 0.2 mM Put (*32*)

Structural Insights into Putrescine Stimulation of AdoMetDC Activity.

Structural comparisons suggest no global conformational changes upon putrescine binding to AdoMetDC; however, several local conformational changes are observed. This suggests that the primary effect of putrescine is electrostatic and that this effect is transmitted to the active site though hydrogen bonding (Figure 2.10 B). Binding of putrescine introduces two positive charges into a binding pocket that contains three conserved acidic residues. Glu178 and Glu256, are hydrogen bonded through water to the putrescine amino group closer to the active site and are near Lys80, which is disordered in most AdoMetDC structures. Lys80 is also near Glu11 and His243, two residues important for both autoprocessing and catalysis. Through this network the pK_a of His243 would increase in the presence of putrescine and decrease in the

absence. His243 is proposed as the base for proton abstraction needed for the cleavage of the ester intermediate (*23, 33*). It may also play a role in the decarboxylation reaction but this cannot be assessed using mutants since the autoprocessing step is essential for activity. The side chain of Glu11 is positioned to assist in protonation/deprotonation of the His243. Glu11 is an essential residue for the activation by putrescine although it plays no direct role in putrescine binding. Mutation of Glu11 to glutamine abolishes putrescine activation of processing (*34*) and mutation to aspartate causes putrescine to be an inhibitor of processing (*23*). Mutation E11K prevents processing completely (*34*). Mutation E11Q greatly reduces AdoMetDC activity (*34*) and reduces the stimulation by putrescine by 60%. The E11D change reduces activity of the processed enzyme by about 4-fold and putrescine activation by about 50% (unpublished). The mutant K80A has only about 10% activity and is stimulated by putrescine only at very high concentrations with a K_a of 400 μM. Similarly, the processing of this mutant is much slower than wild type and is putrescine activated but requires much higher levels of putrescine (K_a of c. 1 mM). Combination of the K80A/E11D mutation abolishes the inhibitory effect on processing of this mutation and the K80A and K80A/E11D mutants have identical responses to putrescine (unpublished). ITC binding results show that the D174N mutant protein does not bind putrescine. Asp174 hydrogen bonds to the putrescine amino group away from the active site and initiates the conformational changes that close the putrescine binding site and shield it from the solvent. The E178Q and E256Q mutants bind putrescine but show no stimulation of processing. Both glutamate/glutamine residues interact through water with putrescine and also participate in the hydrogen bonding network that links the putrescine binding site and active site. The negative charge appears to be key for influencing active site electrostatics and its absence blocks the effects of putrescine.

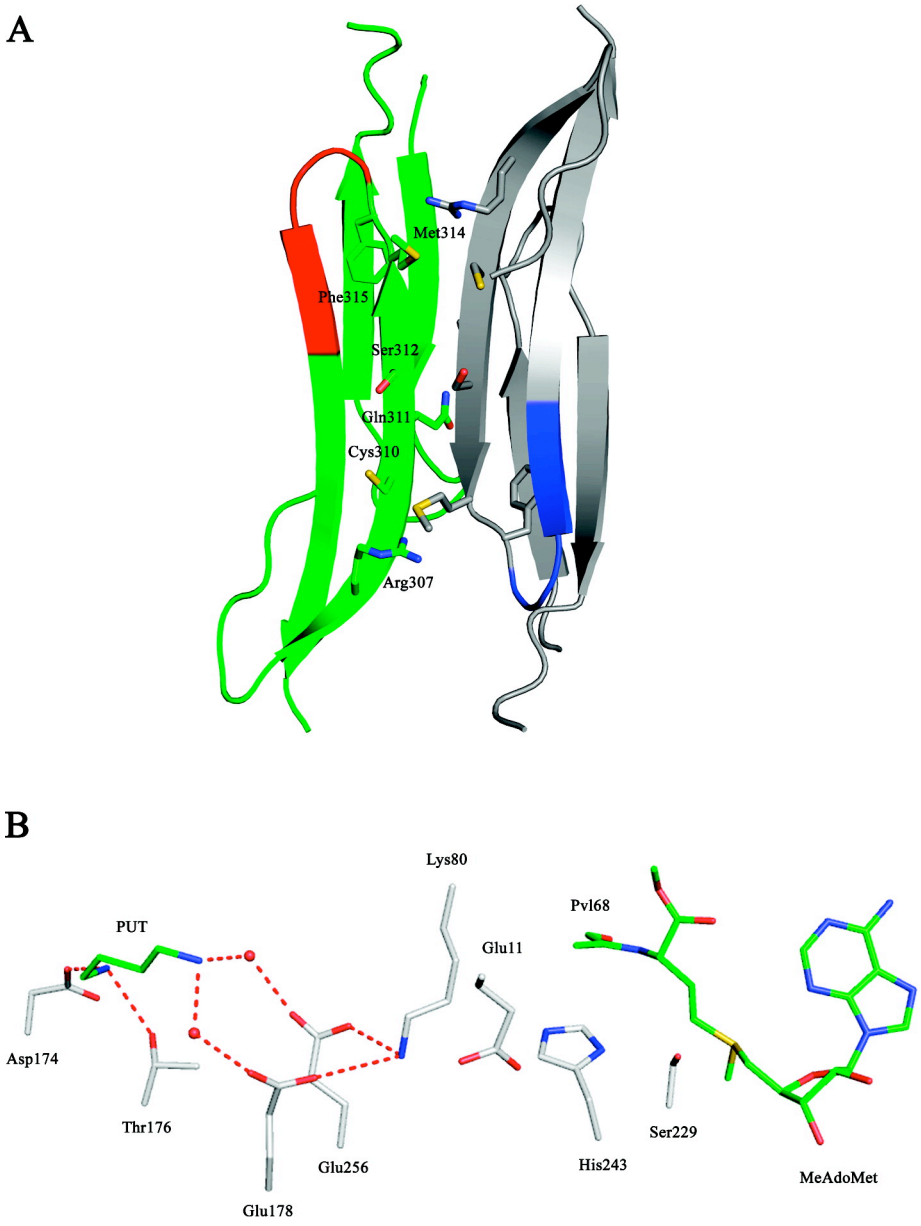

Figure 2.10. (A) Dimer interface of AdoMetDC. The monomers are colored green and gray respectively. The loop 315-320 is colored red one monomer and blue in the other. The residues at the interface are shown in sticks. (B) Charge network between the putrescine binding site and the active site. Putrescine, MeAdoMet and the active site pyruvoyl group carbon atoms are colored green. Water molecules are shown as red spheres and hydrogen bonds are shown as dashed lines.

In contrast the E178Q mutant has decarboxylation activity in the absence of putrescine comparable to wild type with putrescine, while the decarboxylation activity

of the E256Q mutant is not simulated by putrescine. These results are consistent with a proposed model of charge relay through Lys80 to Glu11 to His243 resulting from putrescine binding.

Another possibility is that putrescine utilizes electrostatic interactions to correctly position active site residues. Evidence for a structural switch comes from the structure of the E256Q(+Put), which shows conformational changes in Glu11, Lys80, Ser229 and His243. The largest change occurs in His243, which rotates about its χ_1 torsion angle by about 150 degrees. In this conformation the side chain is pointed away from both the pyruvoyl cofactor and Ser229. Previous biochemical data shows that the catalytic activity of the E256Q(-Put) mutant is far lower than the wild type enzyme and is not stimulated by the addition of putrescine (*32*), suggesting this positioning of residues represents a low activity state in which putrescine is unable to influence the correct positioning of active site residues. The structure E178Q(+Put) lacks a bridging water molecule between putrescine and Gln178, resulting in no activation of the E178Q(-Put) mutant by putrescine.

Implications for Other AdoMetDCs: The effect of putrescine varies among species. Class 1a and 1b enzymes have a fold that is similar to both the N-terminal and C-terminal halves of the class 2 protomer; however, class 1 AdoMetDCs do not have a putrescine binding site and are not stimulated by putrescine. Class 2a AdoMetDCs include the plant enzymes and have a fold very similar to the class 1a protomer but are monomeric rather than dimeric (*35*). The class 2a enzymes contain a buried cluster of charged residues that is reminiscent of the putrescine binding site found in human AdoMetDC; however, the pocket is filled by two arginine residues that are not present in any class 2b enzyme. Class 2a AdoMetDCs are not stimulated by putrescine but have constitutive processing and decarboxylation activities similar to those of the putrescine activated human AdoMetDC.

Multiple sequence alignments show that all of the key active residues are conserved in the class 2a and class 2b AdoMetDCs as are the residues that connect the buried charged cluster. Class 2a and 2b are distinguished in part by the nature of the buried cluster. Within class 2b there are two subclasses. The first is represented by human AdoMetDC and is distinguished by a conserved Lys80. Within this group the three acidic residues in the putrescine binding site are conserved. The four aromatic residues are not entirely conserved; however, these residues are always aromatic or large hydrophobic residues. The second subclass includes apicomplexan parasites and is distinguished by the substitution of isoleucine in place of Lys80. A hydrophobic residue would interrupt the electrostatic transfer of charge and suggests that putrescine stimulates this group of AdoMetDCs by a different mechanism than that of human AdoMetDC. Studies on the *Trypanosome brucei* AdoMetDC showed that putrescine stimulates the decarboxylation reaction; however, the activity was about 1000-fold lower than the activity of the human AdoMetDC (*51*). Recently, Phillips and coworkers showed that formation of a heterodimer between AdoMetDC and a structurally homologous but inactive regulatory protein resulted in decarboxylation rates comparable to human AdoMetDC (*51*). Furthermore, the heterodimeric *T. brucei* AdoMetDC was not stimulated by addition of putrescine. No structures are available for this group of AdoMetDCs and the mechanism of stimulation remains to be determined.

Regulating polyamine levels by controlling the enzymes in the polyamine biosynthetic pathway is a promising target for cancer and anti-parasitic therapy (*6, 7*). Our results suggest that an alternate approach to inhibiting AdoMetDC would be to target the putrescine binding site. Compounds binding to this site that mimic the effects of some of the mutants described above may prevent processing or significantly block activity.

REFERENCES

1. Tabor, C. W., and Tabor, H. (1984) Methionine adenosyltransferase (*S*-adenosylmethionine synthetase) and *S*-adenosylmethionine decarboxylase, *Advan. Enzymol. Related Areas Mol. Biol. 56*, 251-282.
2. Pegg, A. E. (1986) Recent advances in the biochemistry of polyamines in eukaryotes, *Biochem. J. 234*, 249-262.
3. Pegg, A. E., Xiong, H., Feith, D., and Shantz, L. M. (1998) *S*-adenosylmethionine decarboxylase: structure, function and regulation by polyamines, *Biochem. Soc. Trans. 26*, 580-586 526.
4. Li, Y. F., Hess, S., Pannell, L. K., Tabor, C. W., and Tabor, H. (2001) In vivo mechanism-based inactivation of *S*-adenosylmethionine decarboxylases from *Escherichia coli*, *Salmonella thyphimurium*, and *Saccharomyces cerevisiae*, *Proc. Natl. Acad. Sci. USA 98*, 10578-10583.
5. Hackert, M. L., and Pegg, A. E. (1997) Pyruvoyl-dependent enzymes, in *Comprehensive Biological Catalysis* (Sinnott, M. L., Ed.), pp 201-216, Academic Press, London.
6. van Poelje, P. D., and Snell, E. E. (1990) Pyruvoyl-dependent enzymes., *Ann. Rev. Biochem. 59*, 29-59.
7. Wallace, H. M., Fraser, A. V., and Hughes, A. (2003) A perspective of polyamine metabolism, *Biochem. J. 376*, 1-14.
8. Mihich, E. (1963) Current Studies with Methylglyoxal-Bis(Guanylhydrazone), *Cancer Res. 23*, 1375-1389.
9. Regenass, U., Mett, H., Stanek, J., Mueller, M., Kramer, D., and Porter, C. W. (1994) CGP 48664, a new *S*-adenosylmethionine decarboxylase inhibitor with broad spectrum antiproliferative and antitumor activity, *Cancer Res. 54*, 3210-3217.

10. Eskens, F. A., Greim, G. A., van Zuylen, C., Wolff, I., Denis, L. J., Planting, A. S., Muskiet, F. A., Wanders, J., Barbet, N. C., Choi, L., Capdeville, R., Verweij, J., Hanauske, A. R., and Bruntsch, U. (2000) Phase I and pharmacological study of the weekly administration of the polyamine synthesis inhibitor SAM 486A (CGP 48 664) in patients with solid tumors. European Organization for Research and Treatment of Cancer Early Clinical Studies Group, *Clin. Cancer Res. 6*, 1736-1743.

11. Zhou, H., Choi, L., Lau, H., Bruntsch, U., Vries, E. E., Eckhardt, G., Oosterom, A. T., Verweij, J., Schran, H., Barbet, N., Linnartz, R., and Capdeville, R. (2000) Population pharmacokinetics/toxicodynamics (PK/TD) relationships of SAM486A in phase I studies in patients with advanced cancers, *J. Clin. Pharmacol. 40*, 275-283.

12. Paridaens, R., Uges, D. R. A., Barbet, N., Choi, L., Seeghers, M., van der Graaf, W. T. A., and Groen, J. J. M. (2000) A phase I study of a new polyamine biosynthesis inhibitor, SAM486A, in cancer patients with solid tumours, *Br. J. Cancer 83*, 594-601.

13. Siu, L. L., Rowinsky, E. K., Hammond, L. A., Weiss, G. R., Hidalgo, M., Clark, G. M., Moczygemba, J., Choi, L., Linnartz, R., Barbet, N. C., Sklenar, I. T., Capdeville, R., Gan, G., Porter, C. W., Von Hoff, D. D., and Eckhardt, S. G. (2002) A phase I and pharmacokinetic study of SAM486A, a novel polyamine biosynthesis inhibitor, administered on a daily-times-five every-three-week schedule in patients with Advanced solid malignancies, *Clin. Cancer Res. 8*, 2157-2166.

14. van Zuylen, L., Eskens, F., Bridgewater, J., Sparreboom, A., Sklenar, I., Planting, A., Choi, L., Mueller, C., Capdeville, R., Ledermann, J., and Verweij, J. (2000) The Polyamine Synthesis Inhibitor SAM486A in

Combination, with 5-FU/LV in Metastatic Colorectal Cancer (MCC): Results of a Phase I and Pharmacokinetic Study., *Proc. Am. Soc. Clin. Oncol. 36*, 751.

15. Pless, M., Belhadj, K., Kern, W., Dumontet, C., Chemnitz, J., Menssen, H. D., Herrmann, R., Barbet, N. C., and Capdeville, R. (2000) Clinical Efficacy of SAM486A, a Novel Polyamine Biosynthesis Inhibitor, in Patients with Refractory or Relapsed Non-Hodgkin's Lymphoma., *Proc. Am. Soc. Clin. Oncol. 36*, 62.
16. Millward, M. J., Joshua, A., Kefford, R., Aamdal, S., Thomson, D., Hersey, P., Toner, G., and Lynch, K. (2005) Multi-centre Phase II trial of the polyamine synthesis inhibitor SAM486A (CGP48664) in patients with metastatic melanoma, *Invest. New Drugs 23*, 253-256.
17. Toms, A. V., Kinsland, C., McCloskey, D. E., Pegg, A. E., and Ealick, S. E. (2004) Evolutionary links as revealed by the structure of *Thermotoga maritima* S-adenosylmethionine decarboxylase, *J. Biol. Chem. 279*, 33837-33846.
18. Ekstrom, J. E., Matthews, I. I., Stanley, B. A., Pegg, A. E., and Ealick, S. E. (1999) The crystal structure of human *S*-adenosylmethionine decarboxylase at 2.25 Å resolution reveals a novel fold, *Structure 7*, 583-595.
19. Stanley, B. A. (1995) Mammalian *S*-adenosylmethionine decarboxylase regulation and processing, in *Polyamines: Regulation and Molecular Interaction* (Casero, R. A., Ed.), pp 27-75, R. G. Landes Co., Austin, TX.
20. Pegg, A. E. (1984) *S*-adenosylmethionine decarboxylase: a brief review, *Cell Biochem. Function 2*, 11-15.
21. Pegg, A. E., and Williams-Ashman, H. G. (1969) On the role of *S*-adenosyl-L-methionine in the biosynthesis of spermidine by the rat prostate, *J. Biol. Chem. 244*, 682-693.

22. Beswick, T. C., Willert, E. K., and Phillips, M. A. (2006) Mechanisms of allosteric regulation of *Trypanosoma cruzi* S-adenosylmethionine decarboxylase, *Biochemistry 45*, 7797-7807.

23. Ekstrom, J. L., Tolbert, W. D., Xiong, H., Pegg, A. E., and Ealick, S. E. (2001) Structure of a human *S*-adenosylmethionine decarboxylase self-processing ester intermediate and mechanism of putrescine stimulation of processing as revealed by the H243A mutant., *Biochemistry 40*, 9495-9504.

24. Mamont, P. S., Danzin, C., Wagner, J., Siat, M., Joder-Ohlenbusch, A., and Claverie, N. (1982) Accumulation of decarboxylated *S*-adenosylmethionine in mammalian cells as a consequence of the inhibition of putrescine synthesis, *Eur. J. Biochem. 123*, 499-504.

25. Hibasami, H., Hoffman, J. L., and Pegg, A. E. (1980) Decarboxylated S-adenosylmethionine in mammalian cells, *J. Biol. Chem. 255*, 6675-6678.

26. Tekwani, B. L., Bacchi, C. J., and Pegg, A. E. (1992) Putrescine activated *S*-adenosylmethionine decarboxylase from *Trypanosoma brucei brucei*, *Mol. Biochem. Biochem. 117*, 53-61.

27. Persson, K., Aslund, L., Grahn, B., Hanke, J., and Heby, O. (1998) *Trypanosoma cruzi* has not lost its *S*-adenosylmethionine decarboxylase: characterization of the gene and the encoded enzyme, *Biochem. J. 333*, 527-537.

28. Hoyt, M. A., Williams-Abbott, L. J., Pitkin, J. W., and Davis, R. H. (2000) Cloning and expression of the *S*-adenosylmethionine decarboxylase gene of Neurospora crassa and processing of its product, *Mol. Gen. Genet. 263*, 664-673.

29. Clyne, T., Kinch, L. N., and Phillips, M. A. (2002) Putrescine activation of *Trypanosoma cruzi S*-adenosylmethionine decarboxylase, *Biochemistry 41*, 13207-13216.

30. Tolbert, D. W., Ekstrom, J. L., Mathews, I. I., Secrist, J. A. I., Kapoor, P., Pegg, A. E., and Ealick, S. E. (2001) The structural basis for substrate specificity and inhibition of human *S*-adenosylmethionine decarboxylase, *Biochemistry 40*, 9484-9494.

31. Tolbert, W. D., Zhang, Y., Cottet, S. E., Bennett, E. M., Ekstrom, J. L., Pegg, A. E., and Ealick, S. E. (2003) Mechanism of human *S*-adenosylmethionine decarboxylase proenzyme processing as revealed by the structure of the S68A mutant, *Biochemistry 42*, 2386-2395.

32. Stanley, B. A., Shantz, L. M., and Pegg, A. E. (1994) Expression of mammalian S-adenosylmethionine decarboxylase in *Escherichia coli*. Determination of sites for putrescine activation of activity and processing, *J Biol Chem 269*, 7901-7907.

33. Xiong, H., Stanley, B. A., Tekwani, B. L., and Pegg, A. E. (1997) Processing of mammalian and plant *S*-adenosylmethionine decarboxylase proenzymes., *J. Biol. Chem. 272*, 28342-28348.

34. Stanley, B. A., and Pegg, A. E. (1991) Amino acid residues necessary for putrescine stimulation of human *S*-adenosylmethionine decarboxylase proenzyme processing and catalytic activity, *J. Biol. Chem. 266*, 18502-18506.

35. Bennett, E. M., Ekstrom, J. L., Pegg, A. E., and Ealick, S. E. (2002) Monomeric *S*-Adenosylmethionine Decarboxylase from Plants Provides an Alternative to Putrescine Stimulation, *Biochemistry 41*, 14509-14517.

36. Liu, L., Xu-Welliver, M., Kanugula, S., and Pegg, A. E. (2002) Inactivation and degradation of O(6)-alkylguanine-DNA alkyltransferase after reaction with nitric oxide, *Cancer Res 62*, 3037-3043.

37. Winder, A. F., and Gent, W. L. (1971) Correction of light-scattering errors in spectrophotometric protein determinations, *Biopolymers 10*, 1243-1251.

38. Makhatadze, G. I., Medvedkin, V. N., and Privalov, P. L. (1990) Partial molar volumes of polypeptides and their constituent groups in aqueous solution over a broad temperature range, *Biopolymers 30*, 1001-1010.

39. Lopez, M. M., and Makhatadze, G. I. (2002) Isothermal titration calorimetry, *Methods Mol. Biol. 173*, 121-126.

40. Brokx, R. D., Lopez, M. M., Vogel, H. J., and Makhatadze, G. I. (2001) Energetics of target peptide binding by calmodulin reveals different modes of binding, *J. Biol. Chem. 276*, 14083-14091.

41. Indyk, L., and Fisher, H. F. (1998) Theoretical aspects of isothermal titration calorimetry, *Methods Enzymol 295*, 350-364.

42. Lopez, M. M., Yutani, K., and Makhatadze, G. I. (1999) Interactions of the major cold shock protein of *Bacillus subtilis* CspB with single-stranded DNA templates of different base composition, *J. Biol. Chem. 274*, 33601-33608.

43. Seiler, N., and Knödgen, B. (1980) High performance liquid chromatographic procedure for the simultaneous determination of the natural polyamines and their monoacetyl derivatives, *J. Chromatography 221*, 227-235.

44. Otwinowski, Z., and Minor, W. (1997) Processing of x-ray diffraction data collected in oscillation mode, *Methods Enzymol. 276*, 307-326.

45. Brünger, A. T., Adams, P. D., Clore, G. M., DeLano, W. L., Gros, P., Grosse-Kunstleve, R. W., Jiang, J. S., Kuszewski, J., Nilges, M., Pannu, N. S., Read, R. J., Rice, L. M., Simonson, T., and Warren, G. L. (1998) Crystallography &

NMR system: A new software suite for macromolecular structure determination, *Acta Crystallogr. D 54*, 905-921.

46. Jones, T. A., Zou, J.-Y., Cowan, S. W., and Kjeldgaard, M. (1991) Improved methods for the building of protein models in electron density maps and the location of errors in these models., *Acta Crystallogr. A 47*, 110-119.

47. Emsley, P., and Cowtan, K. (2004) Coot: model-building tools for molecular graphics, *Acta Crystallogr. D 60*, 2126-2132.

48. Kleywegt, G. J., and Jones, T. A. (1998) Databases in protein crystallography, *Acta Crystallogr. D 54*, 1119-1131.

49. Richards, F. M., and Kundrot, C. E. (1988) Identification of structural motifs from protein coordinate data: secondary structure and first-level supersecondary structure, *Proteins 3*, 71-84.

50. Schneider, T. R. (2004) Domain identification by iterative analysis of error-scaled difference distance matrices, *Acta Crystallogr. D 60*, 2269-2275.

51. Willert, E. K., Fitzpatrick, R., and Phillips, M. A. (2007) Allosteric regulation of an essential trypanosome polyamine biosynthetic enzyme by a catalytically dead homolog, *Proc. Natl. Acad. Sci. U. S. A. 104*, 8275-8280.

52. Dezeure, F., Gerhart, F., and Seiler, N. (1989) Activation of rat liver S-adenosylmethionine decarboxylase by putrescine and 2-substituted 1,4 butanediamines, *Int. J. Biochem. 21*, 889-899.

CHAPTER 3

ROLE OF THE SULFONIUM CENTER IN DETERMINING LIGAND SPECIFICTY OF HUMAN *S*-ADENOSYLMETHIONINE DECARBOXYLASE[2]

Section 3.1. Introduction

The polyamines putrescine, spermidine and spermine are aliphatic polycations that are critical for maintaining cell differentiation and proliferation (*1-3*). Elevated levels of polyamines are found in cancerous and tumor cell lines (*4, 5*). Thus, depleting polyamine levels by inhibition of the polyamine biosynthetic pathway is a promising approach for the treatment and prevention of cancer and also for the treatment of various parasitic diseases. *S*-adenosylmethionine decarboxylase (AdoMetDC) is a key enzyme in the polyamine biosynthetic pathway and depends on a pyruvoyl cofactor for the decarboxylation reaction (*6-9*). AdoMetDC catalyzes the decarboxylation of *S*-adenosylmethionine (AdoMet) to *S*-adenosyl-5′-(3-methylthiopropylamine) (dcAdoMet). The aminopropyl group from dcAdoMet is transferred to putrescine or spermidine to form spermidine or spermine, respectively. AdoMetDC catalyzes an early step in the pathway and dcAdoMet is completely committed to polyamine biosynthesis; thus, AdoMetDC is an attractive target for drug design.

The early inhibitors of AdoMetDC included the potent competitive inhibitor methylglyoxal *bis*guanylhydrazone (MGBG) (*10*). Clinical studies on this compound were hampered by an unexpected mitochondrial toxicity unrelated to its inhibition of AdoMetDC. An MGBG analogue, 4-amidinoindan-1-one-2′-amidinohydrazone (CGP48664A) showed promise in multiple phase I and phase II clinical trials (*11-18*). Irreversible (or slowly reversible) substrate analogue inhibitors, which form a Schiff

[2] Reproduced with permission from Biochemistry, submitted for publication. Unpublished work copyright 2009 American Chemical Society.

base with the active site pyruvoyl group, have also been synthesized but are limited by their nonspecific activity towards cellular aldehydes and ketones (*19*). *In vitro* assays showed that a positive charge at the position of the sulfonium ion is essential for ligand binding and inhibition (*20*). Thioether and sulfoxide substrate analogues, which lack the positive charge, showed no activity. Alternately, replacement of a sulfur atom with a nitrogen atom, which is protonated at physiological pH and retains the positive charge, resulted in AdoMetDC inhibition. This is consistent with the observation that *S*-adenosylhomocysteine (SAH) is not a substrate for AdoMetDC (*21*).

Previously, the structure of AdoMetDC and its complexes with inhibitors 5′-deoxy-5′-[*N*-methyl-N-(3-hydrazinopropyl)amino]adenosine (MHZPA), 5′-deoxy-5′-[*N*-methyl-*N*-[(2-aminooxy)ethyl]amino]adenosine (MAOEA), the methyl ester of AdoMet (MeAdoMet), MGBG and CGP48664A were determined (*22*). MGBG and CGP48664A act as competitive inhibitors of the enzyme and stack between Phe7 and Phe223, and form hydrogen bonds with Glu247, Ser229 and the backbone amide of Leu65. The substrate analogues MHZPA, MAOEA and MeAdoMet have positive charges at the sulfonium ion position and covalently bind to the enzyme acting as slowly reversible inhibitors. The adenine base of these inhibitors stacks between Phe7 and Phe223, the glycosidic bond adopts an unusual *syn* conformation, and both ribose hydroxyl groups hydrogen bond to Glu247. The requirement for a positive charge in substrate analogues remained puzzling because no negatively charged amino acid side chain was located nearby.

We chose to investigate the basis of the ligand specificity of AdoMetDC using crystallography, quantum chemical calculations and stopped-flow kinetic experiments. We determined crystal structures of the enzyme co-crystallized with 5′-deoxy-5′-(dimethylsulfonio)adenosine (MMTA) and 5′-deoxy-5′-(*N*-dimethyl)amino-8-

methyladenosine (DMAMA). The energy difference between the *syn* and *anti* conformation of the ligands in solution and in the active site of the enzyme was obtained using quantum chemical calculations. Stopped-flow kinetic experiments were carried out to investigate the importance of Phe7 and Phe223, two residues located near the positive charge. Our results show that ligand specificity in human AdoMetDC is mainly due to cation-π interactions and to electrostatic interactions between N3 of adenine and the sulfonium ion, which stabilizes the *syn* conformation.

Section 3.2. Materials and Methods

Materials. The syntheses of MMTA and DMAMA were previously reported (23) and the compounds were the gift of Dr. Jack Secrist at Southern Research Institute.

*Protein Expression and Purification. T*he plasmid encoding the enzyme was cloned into a pQE30 vector and transformed into JM109 strain *E. coli* cells. An overnight culture of 10 mL was grown in LB media at 37 °C with 100 mg/mL ampicillin for resistance and then introduced into larger cell cultures of 1 L volume containing 100 mg/mL ampicillin. The cells were grown until they reached an $O.D_{600}$ of 0.6 and then induced with 100 mg/L isopropyl-1-β-D galactopyranoside. The temperature was reduced to 15 °C and the cells were allowed to grow and express the protein overnight. The cells were harvested by centrifugation and washed using a wash buffer containing 20 mM Na_2HPO_4, pH 7.0, 500 mM NaCl, 2.5 mM putrescine, 0.02% polyoxyethyleneglycol dodecyl ether (Brij-35) and 10 mM imidazole and stored at -80 °C. The frozen cell pellet was resuspended in the wash buffer and lysed using a French press at 1500 psi. The cellular debris was separated from the lysate by centrifugation at 12000 g. Talon metal affinity resin was equilibrated with the wash buffer and the protein was bound to the resin by gently spinning the lysate and the resin together for 1.5 h. The resin was loaded onto a column and washed with the

wash buffer 15-20 times the column volume. The washing was continued with the wash buffer containing 25 mM imidazole. The protein was eluted with the wash buffer containing 100 - 200 mM imidazole. The elute was concentrated to around 10 mL and passed through a Sephadex G-75 column pre-equilibrated with 10 mM *N*-(2-hydroxyethyl)piperazine-*N′*-2-ethanesulfonic acid (HEPES), pH 7.5, 2.5 mM putrescine, 5 mM DTT, 0.1 mM ethylene diamine tetraacetic acid (EDTA), 0.02 % Brij-35 and 300 mM NaCl. The fractions containing the protein were identified by UV peaks at 280 nm and collected. The protein was concentrated to 10 mg/mL and stored at -80 °C.

Crystallization. The protein was buffer exchanged into 10 mM HEPES, pH 7.5, 200 mM NaCl and 1 mM DTT using Bio-Rad buffer exchange chromatography columns. The protein was incubated separately with a 4-6 molar excess of MMTA and DMAMA for 24 h prior to crystallization. The crystals were grown using the hanging drop method at 22 °C in 13-16% polyethylene glycol 8000, 100 mM tris(hydroxymethyl)aminomethane, pH 8.0-9.0 and 10 mM DTT. Crystals appeared overnight and were stable for 1-2 weeks but deteriorated after that.

*Data Collection and Processing. T*he crystals were sequentially transferred to solutions containing the well solution with 2%, 5%, 8%, 15% and 18% glycerol with 1-2 min equilibration between each step. The crystals were flash frozen under liquid nitrogen before being placed in the liquid nitrogen stream. The data for the complex of AdoMetDC with MMTA were collected at NE-CAT beamline 8-BM at the Advanced Photon Source using a ADSC Quantum 315 detector (Area Detector Systems Corporation). Data were collected over a rotation range of 200º with an oscillation range of 1º and 60 s exposure per frame with a detector to crystal distance of 320 mm. The data for the complex of DMAMA were collected at the NE-CAT beamline 24-ID-C. Data were collected over a rotation range of 200º with an

oscillation range of 1º and 1 s exposure per frame with a detector to crystal distance of 250 mm. The data for the complexes were indexed, integrated and scaled using the HKL2000 program suite (*24*). The data collection statistics for both complexes are summarized in Table 3.1.

*Structure Determination and Refinement. T*he structures of the complexes were determined by molecular replacement with CNS (*25*) using the structure of the AdoMetDC/MeAdoMet complex (PDB code 1I7B) as the search model. Model building for the complex of MMTA was performed using the program O (*26*). The model building for the complex of DMAMA was performed using the program Coot (*27*). The initial model obtained from molecular replacement was adjusted using composite omit maps and refined using successive rounds of simulated annealing, minimization, B-factor refinement, generation of new composite omit maps, difference Fourier maps and model building. After a few rounds of refinement, the positions and the conformations of the ligand molecules were identified using the improved difference Fourier maps and composite omit maps. The ligands were included in the models and water molecules were added based on the peaks in the difference Fourier maps. The parameter and the topology files for the ligands were generated using the HIC-Up server (*28*). The difference maps also showed density for a molecule of putrescine bound in each of the structures. The final refinement statistics for both complexes are given in Table 3.2.

*Quantum Mechanical Calculations. T*he quantum chemical calculations on the cation-π interactions were performed using Jaguar version 6.0 or 6.5 (Schrödinger). The X-ray structure of MMTA bound to AdoMetDC was employed for these calculations and single point energy calculations were performed using the LMP2/6-31G** method on the following: $(CH_3)_3S^+$ (from MMTA) plus two benzene rings (from Phe7 and Phe223); $(CH_3)_3S^+$ (from MMTA) plus one benzene ring (from

Phe223); $(CH_3)_3S^+$ (from MMTA) plus one benzene ring (from Phe7); $(CH_3)_3S^+$ alone; benzene alone; $(CH_3)_2S$ (from MMTA) plus two benzene rings (from Phe223 and

Table 3.1. Data Collection Statistics for AdoMetDC Complexes

	AdoMetDC + MMTA	AdoMetDC + DMAMA
Wavelength (Å)	0.9795	0.9795
Space Group (Å)	C2	C2
a (Å)	93.85	99.45
b (Å)	49.54	50.02
c (Å)	70.00	68.69
β	105.03	105.32
Resolution (Å)	2.24	1.81
Total/Unique reflections	56742/15123	107489/29093
Redundancy[a]	3.9(4.0)	3.7(2.5)
% complete	95.1(99.4)	95.8(73.5)
I/σ	8.9(4.26)	17.7(3.4)
R_{sym}[b]	10.5(31.7)	7.9(21.5)
Matthews no.	2.05	2.19
Solvent content	38.9	42.9

[a]Values for the highest resolution shell are given in parentheses.
[b]$R_{sym} = \Sigma\Sigma_i \left| I_i - \langle I \rangle \right| / \Sigma \langle I \rangle$, where $\langle I \rangle$ is the mean intensity of the N reflections with intensities I_i and common indices h,k,l.

Table 3.2. Refinement Statistics for AdoMetDC Complexes

	AdoMetDC+MMTA	AdoMetDC+DMAMA
Resolution (Å)	2.24	1.81
R factor[a]	0.226	0.193
R_{free}[b]	0.274	0.218
No of non-H atoms		
Protein	2405	2439
Ligand	21	22
Water	76	234
B-factors		
Protein (Å^2)	32.6	29.3
Ligand (Å^2)	43.1	22.8
Putrescine (Å^2)	35.0	47.7
rms deviations		
bonds (Å)	0.006	0.008
angles (°)	1.3	1.3
dihedrals (°)	25.1	25.3
Ramachandran plot		
Most favored region (%)	90.7	92.0
Additional favored region (%)	8.5	6.9
Generously allowed region (%)	0.8	0.8
Disallowed region (%)	0.0	0.4

[a]R factor = $\Sigma_{hkl}||F_{obs}|-k|F_{cal}||/\Sigma_{hkl}|F_{obs}|$, where F_{obs} and F_{cal} are observed and calculated structure factors respectively.
[b]For R_{free}, the sum is extended over a subset of reflections (5%) excluded from all stages of refinement.

Phe7); $(CH_3)_2S$ alone. The level of theory for the calculations is sufficient to account for the polarization effect and hence cation-π interactions (*29*).

The energies and conformations of MMTA and 5′-deoxy-5′-methyl thioadenosine (MTA) in solution were determined starting with the NMR structure of AdoMet in solution (*30*) and truncating the molecule to MMTA or MTA. The *syn* conformation was obtained by adjusting the O-C1′-N9-C4 torsion angle. The structures were subjected to geometry optimization using the B3LYP/6-31G* density functional method and the SCRF implicit aqueous solvation model available in Jaguar. The single point energy of the geometry optimized structures was then obtained using the Local Moller-Plesset second-order perturbation (LMP2)/cc-PVTZ(-f) method with aqueous self-consistent reaction field (SCRF) solvation.

The energies of the *syn* and *anti* conformations of MMTA in complex with the enzyme were determined using the MMTA complex as the basis. The truncated model for the *syn* conformation consisted of MMTA and residues Phe223 and Phe7. Backbone atoms of the adjacent residues were also included in the calculations. In addition, an acetate moiety derived from Glu247 was included. Hydrogen atoms were added to the model. Constrained geometry optimization was performed at the Hartree-Fock (HF)/6-31G** level and the single point energy was then calculated at the LMP2//6-31G** level. All atoms were constrained during the geometry optimization except the adenine ring, the ribose C1′ atom and the ribose hydroxyl groups. The *anti* conformation was generated from this truncated model by adjusting the O-C1′-N9-C4 torsion angle to -140° followed by geometry optimization as described above. The partial charges after geometry optimization were obtained for each of atom.

Stopped-Flow Experiments. The stopped-flow experiments were performed using a KinTek Stopped-Flow apparatus (Model SF-2004, KinTek Corp., Austin, TX). Experiments were carried out at 25 °C in 10 mM HEPES, pH 7.5, 200 mM NaCl, and

1 mM DTT. The time dependence of binding was measured by monitoring changes in the intrinsic protein fluorescence. An excitation wavelength of 298 nm (rather than the excitation maximum of ~280 nm) was used to avoid problems associated with inner filtering caused by increasing the ligand concentration. Emission was observed using a band-pass filter centered at 340 nm (± 10 nm). All reported concentrations refer to the final value after rapidly mixing ligand with enzyme at a ratio of 1:1 (v/v). The final enzyme concentration was 25 μM for the WT protein, F7A and E247A mutants and 100 μM for the F223A mutant. AdoMet was mixed with enzyme in at least a 4-fold excess in order to maintain pseudo-first order conditions. Linear and nonlinear regression of the data were performed using GraFit 5 (Erithacus Software, Horley, Surrey, UK).

Figure Preparation. Structural figures were generated using Pymol (*31*).

Section 3.3. Results

Cocrystallization of AdoMetDC with Ligands. The enzyme was cocrystallized in the presence of SAH, MMTA, DMAMA and MTA. The crystallization experiments show that only MMTA and DMAMA bound to the enzyme in the crystal while MTA and SAH did not. Cocrystallization experiments for MTA and SAH were performed at increased concentrations and incubation times to increase the possibility of binding at the active site; however, no active site density was observed.

*Crystal Structure of AdoMetDC with MMTA. T*he overall fold of AdoMetDC is a four-layer αββα sandwich as previously described (*32*). AdoMetDC autoprocessing results in an α subunit with an N-terminal pyruvoyl group and a smaller β subunit (*32, 33*). One molecule of putrescine is bound between the β sheets for each monomer and is located about 15-20 Å from the active site.

In the crystal structure of AdoMetDC with MMTA, loops containing residues 1-4, 22-26, 165-172, 288-299, 328-334 were disordered and were excluded from the

model. MMTA ribose forms hydrogen bonds to Glu247; the O2′ - Oε2 distance is 3.2 Å and the O3′ - Oε1 distance is 2.7 Å. The sulfonium sulfur atom is 4.4 Å from the center of Phe233 ring and the closest contact of sulfur atom with Phe223 is 3.9 Å (Cε1). The methylene carbon atom adjacent to the sulfonium ion of MMTA is 4.4 Å from the center of Phe7 and 3.6 Å from the Cε2 carbon of Phe7. The glycosidic bond of MMTA adopts a *syn* conformation and the adenine ring stacks between Phe223 and Phe7. The stereoview of the electron density for MMTA in the active site is shown in Figure 3.1.

Crystal Structure of AdoMetDC with DMAMA. In the structure of AdoMetDC with DMAMA the loops containing the residues 1-3, 24-26, 165-173, 288-299, 328-334 were missing in the crystal structure. The ribose makes two hydrogen bonds to Glu247 with the O2′- Oε2 distance being 2.9 Å and the O3′- Oε1 distance being 2.6 Å. The nitrogen is 4.7 Å from the center of Phe223 and 4.2 Å from the Cε1 atom of Phe223. The methylene carbon atom adjacent to the nitrogen atom is at a distance of 4.3 Å from the center of Phe7 and 3.7 Å from the Cε2 carbon of Phe7. The adenosine moiety of DMAMA is in a *syn* conformation with the adenine base stacking between Phe7 and Phe223. A stereoview of the electron density for DMAMA in the active site is shown in Figure 3.2.

Quantum Mechanical Calculations. The LMP2/6-31G** energies from the quantum mechanical calculations are shown in Table 3.3. The calculated gas phase binding energy of $(CH_3)_3S^+$ between two benzene rings in the same geometrical orientations as Phe7 and Phe223 is -5.09 kcal/mol. On the other hand, the binding energy of $(CH_3)_2S$ between two benzene rings in the same geometrical orientations as Phe7 and Phe223 is only -0.60 kcal/mol. These calculations suggest that the cation-π interaction provides an addition stabilization of approximately -4.5 kcal/mol. Similar calculations suggest that the binding energy of $(CH_3)_3S^+$ to Phe223 is -3.15 kcal/mol

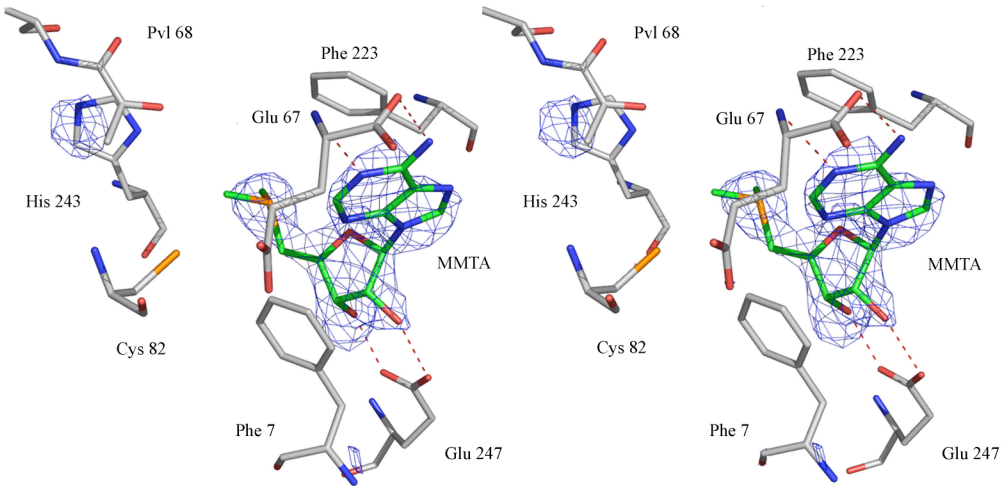

Figure 3.1. Stereoview of the complex of MMTA with AdoMetDC. The difference F_o-F_c Fourier density is contoured at 2.5σ. The carbon atoms of the ligand are colored green. The hydrogen bonds are shown as red dashed lines.

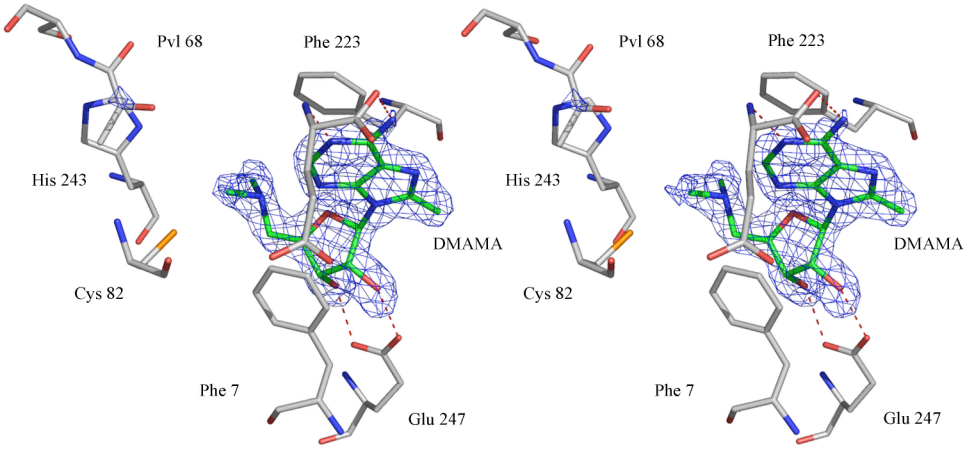

Figure 3.2. Stereoview of the complex of DMAMA with AdoMetDC. The difference F_o-F_c Fourier density is contoured at 4σ. The carbon atoms of the ligand are colored green. The hydrogen bonds are shown as red dashed lines.

and the binding energy to Phe7 is -3.41 kcal/mol.

The *ab initio* energy of the *syn* conformation of MMTA in the complex with Phe223, Phe7 and Glu247 is -3039.28899965619 hartrees and the energy of the *anti* conformation is -3039.26998403002 hartrees. Thus, the energy difference between

the *syn* and *anti* conformations of MMTA in the active site is -11.93 kcal/mol favoring the *syn* conformation. This would represent the stabilization of the *syn* conformation caused primarily by Phe223 and Phe7.

We also investigated the conformational energetics of MMTA and MTA in aqueous solution using quantum chemical calculations. The results are in agreement with the experimental results described by Markham et al. (30) These compounds prefer an anti conformation in aqueous solution. The LMP2/cc-PVTZ(-f) //B3LYP/6-31G* calculated energy difference between the anti and syn conformations was 1.06 kcal/mol for MMTA and 0.88 kcal/mol for MTA favoring the anti conformation in each case.

Table 3.3. Quantum Chemical Energies of Residues / Ligands

	Energy in hartrees
Benzene	-231. 47989407141
$(CH_3)_2S$	-477.13908367149
$(CH_3)_2S$ + Phe223 + Phe 7	-940.10191861550
$(CH_3)_3S+$ + Phe223	-748.08525375049
$(CH_3)_3S+$ + Phe7	-748.08567703979
$(CH_3)_3S+$	-516.60034059742
$(CH_3)_3S+$ + Phe223 + Phe 7	-979.57032658617

Stopped-Flow Experiments. An intrinsic fluorescence change was observed when AdoMetDC was rapidly mixed with AdoMet. However, when SAH was mixed with AdoMetDC, there was no significant change other than that determined to be due to photobleaching (compared to a control minus SAH). This indicates that SAH binding is much weaker and/or produces no discernable conformational change. The

signal when MMTA was mixed with AdoMetDC was also too weak to measure the kinetics of the binding reaction.

Kinetic data of AdoMet binding to WT AdoMetDC along with the F223A, F7A and E247A mutants were collected. For WT, F7A and E247A the data were best fit to a double exponential equation

($F=A_1e^{-l1t} + A_2e^{-l2t} + C$) to yield the observed rates (*l1* and *l2*) and amplitudes (A_1 and A_2) of the two phases at each concentration of AdoMet. The concentration dependence of the fast and slow phases are plotted in Figure 3. The fast phase exhibited a linear concentration dependence, and did not saturate. The slow phase was approximately hyperbolic and saturated at relatively low concentrations. The data are best described by a minimal model of two sequential steps:

$$E + S \underset{k_{-1}}{\overset{k_1}{\leftrightarrow}} EX \underset{k_{-2}}{\overset{k_2}{\leftrightarrow}} EA$$

According to this model, the fast phase of the reaction occurs at an observed rate approximately equal to the sum of all four intrinsic rate constants (*34*):

$$\lambda_1 \sim k_1[S] + k_{-1} + k_2 + k_{-2}$$

A linear fit of the fast phase (AdoMet binding to WT enzyme) results in a $k_1 = 0.136 \pm 0.005\ \mu M^{-1}s^{-1}$, $k_{-1} = 33 \pm 2\ s^{-1}$ and $k_2 + k_{-2} = 3.7 \pm 0.2\ s^{-1}$. Therefore, the dissociation constant (K_d) for AdoMet binding to AdoMetDC can be estimated to be 242 ± 17 μM from the ratio of k_{-1}/k_1.

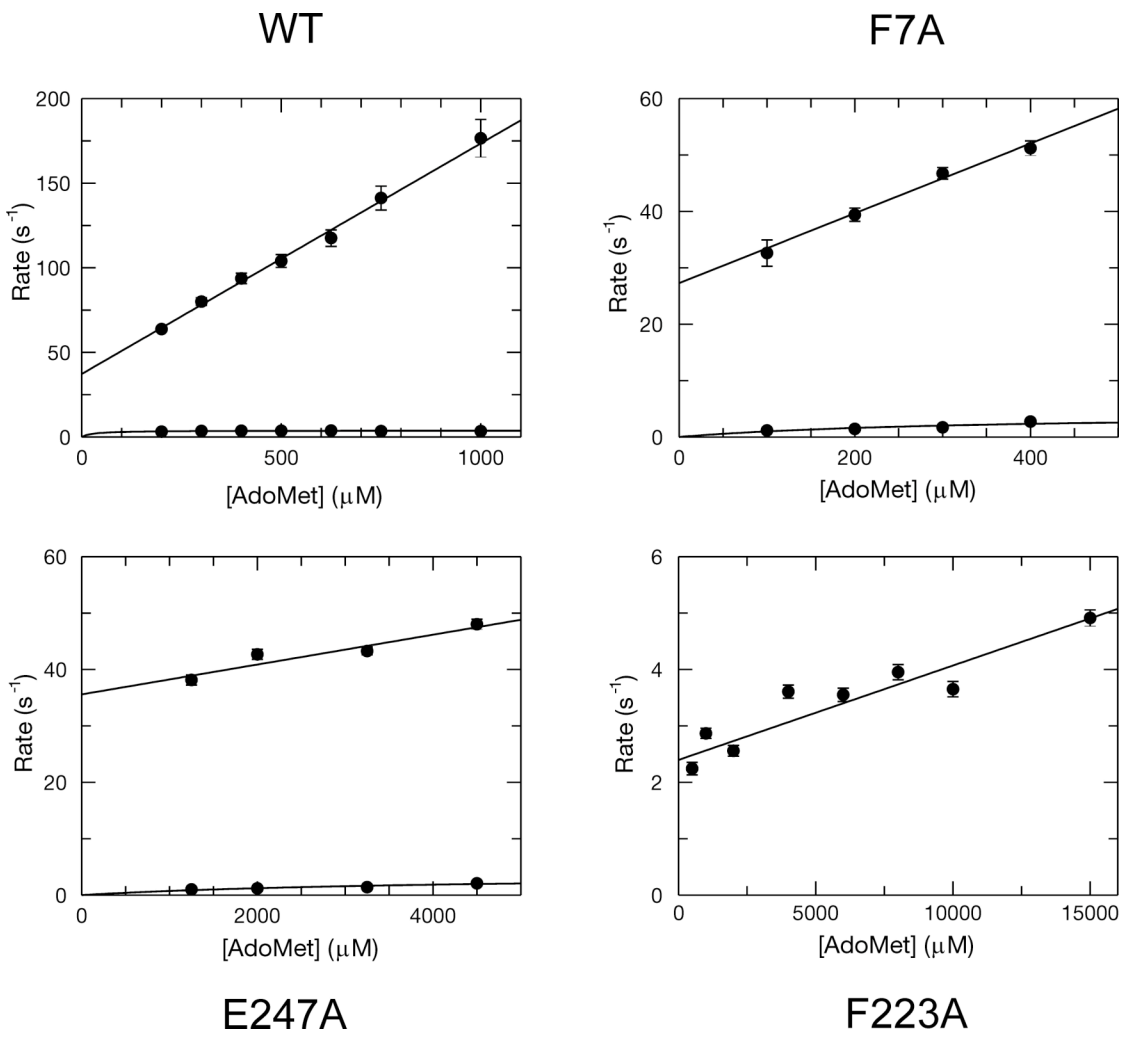

Figure 3.3. Plots of observed rate vs. [AdoMet] for the WT, F223A, F7A and E247A mutants. The linear concentration dependence of the observed rates was fit using a line which allowed for the definition of k_1 and k_{-1}. A hyperbolic fit of the slow phase defined the sum of k_2 and k_{-2}, except in the case of F223A, where the kinetics were monophasic and indicative of a more simple one step binding model. In this case the slope of the best fit line defines the k_1 and the y-intercept defines the k_{-1} directly.

For the F7A and E247A mutants, the data were analyzed in a similar fashion except that a lower overall signal change caused photobleaching to become a significant component of the data. Therefore, the decrease due to photobleaching was corrected by using data from a control reaction where substrate was omitted (resulting in a linear decrease in fluorescence). After correction, the kinetic parameters were

obtained as for the WT enzyme. The values of k_{-1} and $k_2 + k_{-2}$ were similar for both the mutants but the value of the second order rate constant for substrate binding (k_1) changed significantly. Based upon the values of k_1 and k_{-1}, the K_d for the F7A mutant was 370 ± 60 μM and the K_d for the E247A mutant was 12.2 ± 3.6 mM.

The fluorescence change seen upon mixing AdoMet with the F223A mutant was best fit using a single exponential equation. The concentration dependence of the observed rate varied linearly with a slope (k_1) of $1.7 \pm 0.3 \times 10^{-4}$ $\mu M^{-1}s^{-1}$ and a y-intercept (k_{-1}) of 2.4 ± 0.2 s^{-1} yielding a K_d of 14 ± 3 mM. Generally, the values measured here follow the same trend as the steady state kinetic parameters (k_{cat} and K_m) obtained previously (*22*). A comparison of K_d values for AdoMet binding to WT, F223A, F7A, and E247A mutants reveals that the importance of residues for substrate binding follows the order F223A ~ E247A >> F7A > WT.

Section 3.4. Discussion

Cation-π Interactions and Ligand Specificity of AdoMetDC. Cation-π interactions are ubiquitous in nature and aid in protein stability, ligand recognition, catalysis and ion channel function (*35, 36*). In the gas phase, the binding energy of cations to aromatic groups ranges from 10-40 kcal/mol which places the cation-π interaction among the strongest noncovalent forces (*35, 37*). The magnitude of the cation-π interaction depends on the geometry, distance and the nature of the cation and the aromatic group. In biological systems, the bulk of these interactions are seen with the amino acid side chains of proteins. Aromatic amino acids such as tryptophan, tyrosine and phenylalanine interact with positive charged amino acids such as lysine and arginine. The energetics of these interactions have been studied both experimentally and theoretically (*38, 39*). In a few cases, ligand recognition by an enzyme is attributed completely to the cation-π interaction (*40*). It has been shown that AdoMetDC binds substrate analogues only if they have a positive charge at the

sulfonium position (*20*). MHZPA and MAOEA, which do not contain a sulfonium center, have an ammonium group that is protonated at physiological pH. The inability to form MTA and SAH complexes in cocrystallization experiments is consistent with this observation.

The results reported here suggest that cation-π interactions play a primary role in determining substrate specificity. The crystal structure of AdoMetDC with MMTA shows that the sulfonium center is at a favorable distance and geometry for a cation-π interaction with Phe223. The positive charge of the sulfonium ion is distributed to the adjacent methyl and the methylene groups (Figure 3.4). The methylene group of MMTA is at a favorable distance and geometry for a cation-π interaction with Phe7. The quantum chemical calculations suggest the stabilization of a $(CH_3)_3S^+$ group in the active site is primarily due to its interaction with Phe223 and Phe7. Other ligands with a positive charge such as MHZPA, MAOEA, MeAdoMet and DMAMA show similar interactions with Phe223 and Phe7 (Figure 3.5). The magnitude of stabilization obtained due to the cation-π interaction is approximately -4.5 kcal/mol. The interaction may be weakened from its maximum value by distribution of positive charge to adjacent carbon and hydrogen atoms and because of non-ideal geometry.

The cation-π interaction as a theme for sulfonium recognition was debated by Markham *et al.* based on a survey of the crystal structures of AdoMet with various enzymes (*30*). The survey which spanned 20 crystal structures showed that the sulfonium of AdoMet interacts with negatively charged atoms and aromatic amino acids in very few cases. In glycine-*N*-methyltransferase (PDB code 1xva) and *HhaI* DNA methylase (PDB code 1hmy), the sulfonium interacts with negatively charged carboxylate atoms (*41, 42*). There are only two cases in the survey where the sulfonium ion has a close contact with an aromatic group. The sulfonium ion of AdoMet is 3.2 Å from the methylene carbon atom of Trp41 in *HhaI* DNA methylase

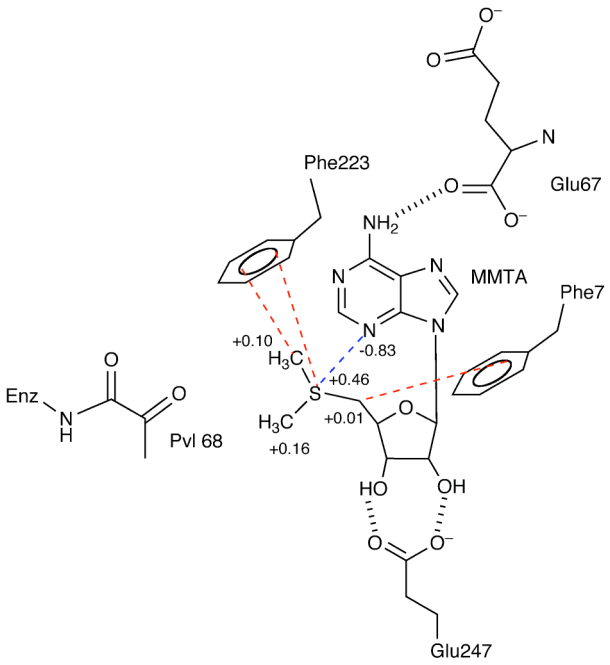

Figure 3.4. Schematic diagram of the key interactions MMTA makes in the active site of AdoMetDC. The adenine base stacks in the *syn* conformation aided by aromatic stacking interactions to Phe7 and Phe223. The N6 of the adenine base hydrogen bonds to the backbone carbonyl of Glu67. The sulfonium ion and the terminal methyl group have a cation-π interaction with Phe223 (shown in red) and the partially positively charged methylene group adjacent to sulfonium interacts with Phe7. The N3 atom is partially negative charged and interacts with the sulfonium. The partial charges on the relevant atoms are indicated. The ribose makes two hydrogen bonds to Glu247.

(PDB code 1hmy) and in the structure of AdoMetDC with MeAdoMet bound (PDB code 1I7B) the sulfonium ion is located 4.1 Å from the center of Phe223. The survey concluded that in a broader picture, cation-π interactions are not a recurring theme for sulfonium recognition. However, the uniqueness of the AdoMet decarboxylation reaction in this study may explain the importance of cation-π interaction for AdoMetDC, which further is supported by theoretical calculations and stopped-flow kinetic experiments.

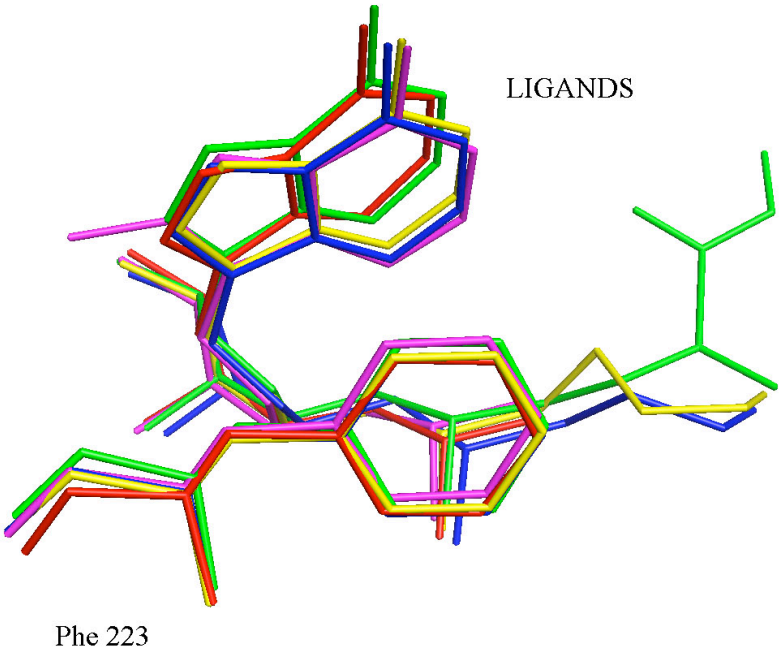

Figure 3.5. The superposition of the complexes of AdoMetDC showing the geometry of the cation-π interaction between the positive sulfonium / nitrogen with Phe223. The color coding for the complexes is as follows; MMTA, red; DMAMA, magenta; MeAdoMet, green; MAOEA, blue; MHZPA, yellow.

Stabilization of the syn Conformation by AdoMetDC. The conformational preference of AdoMet in solution and gas phase was studied by Markham *et al.* (*30*). According to the NMR studies, AdoMet prefers an *anti* conformation about the glycosidic bond in solution and a *syn* conformation in vacuum. The energy difference between the *anti* and *syn* conformations in solution was calculated to be -34 kcal/mol based on the modeling studies using NMR constraints. This energy difference was calculated based on molecular mechanics without polarization effects and it is likely that the actual difference is less negative (*23*). The crystal structure of AdoMetDC

with MeAdoMet, MHZPA and MAOEA reported previously showed that the enzyme binds the ligands in the energetically unfavorable *syn* conformation (*22*).

The crystal structures of AdoMetDC with MMTA and DMAMA also show that the adenosine moiety binds in a *syn* conformation. The quantum chemical calculations for MMTA in a truncated model of the enzyme with only Phe7, Phe223 and Glu247 included suggest that the *syn* conformation of the ligand is stabilized by ~12 kcal/mol compared to hypothetical *anti* conformation, which has never been observed in an AdoMetDC complex. The actual energy difference is likely to be greater than the above value since the *anti* conformation places the six-membered ring of the adenine in close proximity to Asn224 and Pro225. Moreover, the amino group on the adenine ring is in close proximity and makes hydrogen bonds to Glu67 in the *syn* conformation but forms no appreciable interactions with the enzyme in the *anti* conformation.

The *syn* conformation of the adenine base is primarily stabilized by stacking interactions with Phe7 and Phe223 and hydrogen bonds of the ribose to Glu247. The N3 atom of the adenine base carries a partial negative charge and interacts favorably with the sulfonium ion. This electrostatic effect further contributes in stabilizing the *syn* conformation of the ligand. The preference of AdoMetDC to bind ligands in the *syn* conformation was recently exploited in the design of substrate analogues with enhanced affinity. Substitution at the C^8 position on the adenine base favored the *syn* conformation resulting a 5-18 fold increase in potency compared to the unsubstituted compounds (*23*).

Insights into Inhibitor Design. The design of substrate analogue inhibitors for AdoMetDC benefit from the presence of a positive charge required for the cation-π interaction. Unlike MAOEA and MHZPA, MMTA shows competitive inhibition because it lacks an amino terminus required to form a Schiff base with the active site

pyruvoyl group. Studies on MMTA also show that the ribose, adenine base and the positive charge are sufficient for inhibition of AdoMetDC. The schematic diagram showing all of the stabilizing interactions of MMTA in the active site is shown in Figure 3.4.

The MMTA analog, DMAMA shows that the replacement of the sulfur by nitrogen also yields a competitive inhibitor because the nitrogen is protonated at physiological pH. DMAMA has a methyl substitution at the 8-position which should favor the *syn* conformation in solution and improve the binding to AdoMetDC (*23*). Because MMTA and DMAMA lack hydrazino or oxyamino groups, which react nonspecifically with cellular aldehydes and ketones, and because further evolution of their structures are possible, MMTA and DMAMA, with IC_{50} values of 15 μM and 600 nM (*23*), respectively, are promising lead compounds for inhibitor design.

REFERENCES

1. van Poelje, P. D., and Snell, E. E. (1990) Pyruvoyl-dependent enzymes., *Ann. Rev. Biochem. 59*, 29-59.
2. Wallace, H. M., Fraser, A. V., and Hughes, A. (2003) A perspective of polyamine metabolism, *Biochem. J. 376*, 1-14.
3. Casero, R. A., Jr., Celano, P., Ervin, S. J., Applegren, N. B., Wiest, L., and Pegg, A. E. (1991) Isolation and characterization of a cDNA clone that codes for human spermidine/spermine N^1-acetyltransferase, *J. Biol. Chem. 266*, 810-814.
4. Gerner, E. W., and Meyskens, F. L., Jr. (2004) Polyamines and cancer: old molecules, new understanding, *Nat Rev Cancer 4*, 781-792.
5. Pegg, A. E., and Feith, D. J. (2007) Polyamines and neoplastic growth, *Biochem Soc Trans 35*, 295-299.
6. Hackert, M. L., and Pegg, A. E. (1997) Pyruvoyl-dependent enzymes, in *Comprehensive Biological Catalysis* (Sinnott, M. L., Ed.), pp 201-216, Academic Press, London.
7. Pegg, A. E., Xiong, H., Feith, D., and Shantz, L. M. (1998) *S*-adenosylmethionine decarboxylase: structure, function and regulation by polyamines, *Biochem. Soc. Trans. 26*, 580-586 526.
8. Tabor, C. W., and Tabor, H. (1984) Polyamines, *Annu. Rev. Biochem. 53*, 749-790.
9. Tabor, C. W., and Tabor, H. (1984) Methionine adenosyltransferase (*S*-adenosylmethionine synthetase) and *S*-adenosylmethionine decarboxylase, *Advan. Enzymol. Related Areas Mol. Biol. 56*, 251-282.
10. Williams-Ashman, H. G., and Schenone, A. (1972) Methylglyoxal bis(guanylhydrazone) as a potent inhibitor of mammalian and yeast *S*-

adenosylmethionine decarboxylases, *Biochem. Biophys. Res. Commun. 46*, 288-295.

11. Regenass, U., Mett, H., Stanek, J., Mueller, M., Kramer, D., and Porter, C. W. (1994) CGP 48664, a new *S*-adenosylmethionine decarboxylase inhibitor with broad spectrum antiproliferative and antitumor activity, *Cancer Res. 54*, 3210-3217.
12. Eskens, F. A., Greim, G. A., van Zuylen, C., Wolff, I., Denis, L. J., Planting, A. S., Muskiet, F. A., Wanders, J., Barbet, N. C., Choi, L., Capdeville, R., Verweij, J., Hanauske, A. R., and Bruntsch, U. (2000) Phase I and pharmacological study of the weekly administration of the polyamine synthesis inhibitor SAM 486A (CGP 48 664) in patients with solid tumors. European Organization for Research and Treatment of Cancer Early Clinical Studies Group, *Clin. Cancer Res. 6*, 1736-1743.
13. Zhou, H., Choi, L., Lau, H., Bruntsch, U., Vries, E. E., Eckhardt, G., Oosterom, A. T., Verweij, J., Schran, H., Barbet, N., Linnartz, R., and Capdeville, R. (2000) Population pharmacokinetics/toxicodynamics (PK/TD) relationships of SAM486A in phase I studies in patients with advanced cancers, *J. Clin. Pharmacol. 40*, 275-283.
14. Paridaens, R., Uges, D. R. A., Barbet, N., Choi, L., Seeghers, M., van der Graaf, W. T. A., and Groen, J. J. M. (2000) A phase I study of a new polyamine biosynthesis inhibitor, SAM486A, in cancer patients with solid tumours, *Br. J. Cancer 83*, 594-601.
15. Siu, L. L., Rowinsky, E. K., Hammond, L. A., Weiss, G. R., Hidalgo, M., Clark, G. M., Moczygemba, J., Choi, L., Linnartz, R., Barbet, N. C., Sklenar, I. T., Capdeville, R., Gan, G., Porter, C. W., Von Hoff, D. D., and Eckhardt, S. G. (2002) A phase I and pharmacokinetic study of SAM486A, a novel

polyamine biosynthesis inhibitor, administered on a daily-times-five every-three-week schedule in patients with Advanced solid malignancies, *Clin. Cancer Res. 8*, 2157-2166.

16. van Zuylen, L., Eskens, F., Bridgewater, J., Sparreboom, A., Sklenar, I., Planting, A., Choi, L., Mueller, C., Capdeville, R., Ledermann, J., and Verweij, J. (2000) The Polyamine Synthesis Inhibitor SAM486A in Combination, with 5-FU/LV in Metastatic Colorectal Cancer (MCC): Results of a Phase I and Pharmacokinetic Study., *Proc. Am. Soc. Clin. Oncol. 36*, 751.
17. Pless, M., Belhadj, K., Kern, W., Dumontet, C., Chemnitz, J., Menssen, H. D., Herrmann, R., Barbet, N. C., and Capdeville, R. (2000) Clinical Efficacy of SAM486A, a Novel Polyamine Biosynthesis Inhibitor, in Patients with Refractory or Relapsed Non-Hodgkin's Lymphoma., *Proc. Am. Soc. Clin. Oncol. 36*, 62.
18. Millward, M. J., Joshua, A., Kefford, R., Aamdal, S., Thomson, D., Hersey, P., Toner, G., and Lynch, K. (2005) Multi-centre Phase II trial of the polyamine synthesis inhibitor SAM486A (CGP48664) in patients with metastatic melanoma, *Invest New Drugs 23*, 253-256.
19. Shantz, L. M., Stanley, B. A., Secrist, J. A., and Pegg, A. E. (1992) Purification of human *S*-adenosylmethionine decarboxylase expressed in *Escherichia coli* and use of this protein to investigate the mechanism of inhibition by the irreversible inhibitors, 5'-deoxy-5'-[(3-hydrazinopropyl)methylamino]adenosine and 5'{[(Z)-4-amino-2-butenyl]methylamino-5'-deoxyadenosine, *Biochemistry 31*, 6848-6855.
20. Pankaskie, M., and Abdel-Monem, M. M. (1980) Inhibitors of polyamine biosynthesis 8: Irreversible inhibition of mammalian *S*-adenosyl-L-methionine decarboxylase by substrate analogs, *J. Med. Chem. 23*, 121-127.

21. Pegg, A. E., and Jacobs, G. (1983) Comparison of inhibitors of S-adenosylmethionine decarboxylase from different species, *Biochem J 213*, 495-502.

22. Tolbert, D. W., Ekstrom, J. L., Mathews, I. I., Secrist, J. A. I., Kapoor, P., Pegg, A. E., and Ealick, S. E. (2001) The structural basis for substrate specificity and inhibition of human *S*-adenosylmethionine decarboxylase, *Biochemistry 40*, 9484-9494.

23. McCloskey, D. E., Bale, S., Secrist, J. A., Tiwari, A., Moss, T. H., Valiyaveettil, J., Brooks, W. H., Guida, W. C., Pegg, A. E., and Ealick, S. E. (2009) New Insights into the Design of Inhibitors of Human S-Adenosylmethionine Decarboxylase: Studies of Adenine C(8) Substitution in Structural Analogues of S-Adenosylmethionine, *J. Med. Chem*. 52, 1388-1407

24. Otwinowski, Z., and Minor, W. (1997) Processing of x-ray diffraction data collected in oscillation mode, *Methods Enzymol. 276*, 307-326.

25. Brünger, A. T., Adams, P. D., Clore, G. M., DeLano, W. L., Gros, P., Grosse-Kunstleve, R. W., Jiang, J. S., Kuszewski, J., Nilges, M., Pannu, N. S., Read, R. J., Rice, L. M., Simonson, T., and Warren, G. L. (1998) Crystallography & NMR system: A new software suite for macromolecular structure determination, *Acta Crystallogr. D 54*, 905-921.

26. Jones, T. A., Zou, J.-Y., Cowan, S. W., and Kjeldgaard, M. (1991) Improved methods for the building of protein models in electron density maps and the location of errors in these models., *Acta Crystallogr. A 47*, 110-119.

27. Emsley, P., and Cowtan, K. (2004) Coot: model-building tools for molecular graphics, *Acta Crystallogr. D 60*, 2126-2132.

28. Kleywegt, G. J., and Jones, T. A. (1998) Databases in protein crystallography, *Acta Crystallogr. D 54*, 1119-1131.

29. Mecozzi, S., West, A. P., and Dougherty, D. A. (1996) Cation-pi interactions in simple aromatics: Electrostatics provide a predictive tool, *J Am Chem Soc 118*, 2307-2308.

30. Markham, G. D., Norrby, P. O., and Bock, C. W. (2002) *S*-adenosylmethionine conformations in solution and in protein complexes: conformational influences of the sulfonium group, *Biochemistry 41*, 7636-7646.

31. DeLano, W. L. (2002), The PyMOL Molecular Graphics System, DeLano Scientific, San Carlos, CA.

32. Ekstrom, J. E., Matthews, I. I., Stanley, B. A., Pegg, A. E., and Ealick, S. E. (1999) The crystal structure of human *S*-adenosylmethionine decarboxylase at 2.25 Å resolution reveals a novel fold, *Structure 7*, 583-595.

33. Ekstrom, J. L., Tolbert, W. D., Xiong, H., Pegg, A. E., and Ealick, S. E. (2001) Structure of a human *S*-adenosylmethionine decarboxylase self-processing ester intermediate and mechanism of putrescine stimulation of processing as revealed by the H243A mutant., *Biochemistry 40*, 9495-9504.

34. Johnson, K. A. (1986) Rapid kinetic analysis of mechanochemical adenosinetriphosphatases, *Methods Enzymol. 134*, 677-705.

35. Ma, J. C., and Dougherty, D. A. (1997) The Cation-pi Interaction, *Chem. Rev. 97*, 1303-1324.

36. Gallivan, J. P., and Dougherty, D. A. (1999) Cation-pi interactions in structural biology, *Proc. Natl. Acad. Sci. U. S. A. 96*, 9459-9464.

37. Ruan, C., and Rodgers, M. T. (2004) Cation-pi interactions: structures and energetics of complexation of Na+ and K+ with the aromatic amino acids, phenylalanine, tyrosine, and tryptophan, *J Am Chem Soc 126*, 14600-14610.

38. Biot, C., Buisine, E., Kwasigroch, J. M., Wintjens, R., and Rooman, M. (2002) Probing the energetic and structural role of amino acid/nucleobase cation-pi interactions in protein-ligand complexes, *J. Biol. Chem. 277*, 40816-40822.

39. Biot, C., Buisine, E., and Rooman, M. (2003) Free-energy calculations of protein-ligand cation-pi and amino-pi interactions: from vacuum to proteinlike environments, *J Am Chem Soc 125*, 13988-13994.

40. Zacharias, N., and Dougherty, D. A. (2002) Cation-pi interactions in ligand recognition and catalysis, *Trends Pharmacol. Sci. 23*, 281-287.

41. Cheng, X., Kumar, S., Posfai, J., Pflugrath, J. W., and Roberts, R. J. (1993) Crystal structure of the HhaI DNA methyltransferase complexed with S-adenosyl-L-methionine, *Cell 74*, 299-307.

42. Fu, Z., Hu, Y., Konishi, K., Takata, Y., Ogawa, H., Gomi, T., Fujioka, M., and Takusagawa, F. (1996) Crystal structure of glycine N-methyltransferase from rat liver, *Biochemistry 35*, 11985-11993.

CHAPTER 4

NEW INSIGHTS INTO THE DESIGN OF INHIBITORS OF HUMAN *S*-ADENOSYLMETHIONINE DECARBOXYLASE: STUDIES OF ADENINE C^8 SUBSTITUTION IN STRUCTURAL ANALOGUES OF *S*-ADENOSYLMETHIONINE[3]

Section 4.1. Introduction

S-Adenosylmethionine decarboxylase (AdoMetDC) is a pyruvoyl dependent decarboxylase and a critical enzyme in the polyamine biosynthetic pathway, which is found in mammals, *Protista* and many other species (*1-4*). The polyamines putrescine, spermidine and spermine are essential for cell growth and play important roles in cell proliferation and differentiation (*5-7*). Polyamines have been found to be elevated in various types of cancer including non small cell lung cancer, prostate cancer, melanoma, and pancreatic cancer (*8, 9*). Polyamine levels in cells depend on the polyamine biosynthetic and catabolic pathways as well as on import and export of polyamines across the cellular membrane. Altering regulation of the key enzymes in the polyamine pathway is a therapeutic strategy for treatment of various types of cancers. AdoMetDC catalyzes the conversion of *S*-adenosylmethionine (AdoMet) to decarboxylated *S*-adenosylmethionine (dcAdoMet), which then donates the aminopropyl group to putrescine or spermidine to form spermidine and spermine, respectively. AdoMetDC is at a key branch point in the pathway and its action commits AdoMet to polyamine biosynthesis and removes it from the pool available for methyl transfer to a variety of substrates.

---

[3] Reproduced in part with permission from McCloskey DE, Bale S, Secrist III JA, Tiwari A, Moss III TH, Valiyaveettil J, Brooks WH, Guida WC, Pegg AE, Ealick SE. (2009) *J. Med. Chem.* 52(5) 1388-1407 Copyright 2009 American Chemical Society

Attempts to regulate polyamine levels have resulted in the development of inhibitors that target the biosynthetic enzymes ornithine decarboxylase (ODC) (*10*), AdoMetDC and the catabolic enzyme spermidine/spermine N^1-acetyltransferase (SSAT) (*11*). The best-known inhibitor of ODC is α-difluoromethylornithine (DFMO), which irreversibly inactivates the enzyme. The success of DFMO in cancer therapy has been limited as the cells compensate for the decreased synthesis of polyamines through increased cellular uptake of polyamines (*12*). DFMO is currently being investigated as a chemopreventive agent against carcinogenesis (*13-17*). The development of drugs to inhibit AdoMetDC (Figure 4.1 A) started with the competitive inhibitor methylglyoxal *bis*(guanylhydrazone) **1** (MGBG), which is similar to spermidine in structure (*18*). Use of MGBG **1** caused extreme toxicity in humans and many analogues of MGBG **1** were developed in attempts to decrease the toxicity. One such AdoMetDC inhibitor that resulted was 4-amidinoindan-1-one-2′-amidinohydrazone **2** (CGP48664A), which progressed into clinical trials as a cancer chemotherapeutic agent (*19*). Alternatively, inhibitors such as 5′-deoxy-5′-[(3-hydrazinopropyl)methylamino]adenosine **3** (MHZPA), 5′-deoxy-5′-[(3-hydrazinoethyl)methylamino]adenosine **4** (MHZEA) and 5′-[(2-aminooxyethyl)methylamino]-5′-deoxyadenosine **5** (MAOEA) that are structural analogues of the natural substrate were developed (Figure 4.1 B). These compounds inactivate AdoMetDC by forming a Schiff base to the active site pyruvoyl group (*20*). Another known nucleoside inhibitor of AdoMetDC is 5′-[[(*Z*)-4-amino-2-butenyl]methylamino]-5′-deoxyadenosine. This butenyl analogue was designed as an enzyme-activated irreversible inhibitor (*21*) but subsequent experiments showed that it acted via transamination of the pyruvate prosthetic group (*20*).

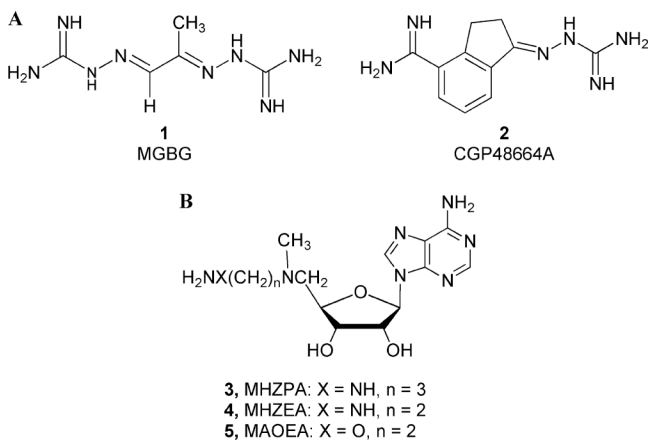

Figure 4.1: Previously described inhibitors of hAdoMetDC

The crystal structure of AdoMetDC and its S68A and H243A mutants were solved to aid understanding of the mechanisms of decarboxylation and autoprocessing (*22-24*). The crystal structures of AdoMetDC with inhibitors such as MAOEA **5**, MHZPA **3** and the methyl ester of *S*-adenosylmethionine (MeAdoMet) also have been solved previously (*25*). These structures show that the adenine base of the inhibitors assumes an unusual *syn* conformation within the active site. The preference for the unusual conformation has led us to develop new structural analogues of AdoMet with modifications on the adenine base and to investigate, through biochemical analysis, computational modeling, and analysis of crystal structures, whether these compounds would be more potent inhibitors of AdoMetDC than the unsubstituted parent compounds. Substitution at the 8-position of adenine is expected to result in ligands that favor the *syn* conformation in solution, and it was hoped that this would increase their ability to inhibit AdoMetDC. We now describe the synthesis of several series of structural analogues of AdoMet with 8-substituted adenine and present AdoMetDC inhibition data. We report the crystal structures of the AdoMetDC F223A mutant complexed with MeAdoMet and the wild-type protein complexed with several 8-substituted inhibitors.

Section 4.2. Materials and Methods

Target Synthesis. TLC analysis was performed on Analtech precoated (250 μm) silica gel GF plates. Melting points were determined on a Mel-Temp apparatus and are uncorrected. Purifications by flash chromatography were carried out on Merck silica gel (230-400 mesh). Evaporations were performed with a rotary evaporator, higher boiling solvents (dimethylformamide (DMF), pyridine) were removed *in vacuo* (<1 mm, bath to 35 °C). Products were dried *in vacuo* (<1 mm) at 22-25 °C over P_2O_5. The mass spectral data were obtained with a Varian-MAT 311A mass spectrometer in the fast atom bombardment (FAB) mode or with a Bruker BIOTOF II by electrospray ionization (ESI). ^{1}H NMR spectra were recorded on a Nicolet NT-300 NB spectrometer operating at 300.635 MHz. Chemical shifts in $CDCl_3$ and Me_2SO-d_6 are expressed in parts per million downfield from tetramethylsilane (TMS) and in D_2O chemical shifts are expressed in parts per million downfield from sodium 3-(trimethylsilyl)propionate-2,2,3.3-d_4 (TMSP). Chemical shifts (δ) listed for multiplets were measured from the approximate centers, and relative integrals of peak areas agreed with those expected for the assigned structures. UV absorption spectra were determined on a Perkin-Elmer Lambda 19 spectrometer by dissolving each compound in MeOH or EtOH, and diluting 10-fold with 0.1 N HCl, pH 7 buffer, or 0.1 N NaOH. Numbers in parentheses are extinction coefficients ($\varepsilon \times 10^{-3}$). Microanalyses were performed by Atlantic Microlab, Inc. (Atlanta, GA) or the Spectroscopic and Analytical Department of Southern Research Institute. Analytical results indicated by element symbols were within ±0.4% of the theoretical values, and where solvents are indicated in the formula, their presence was confirmed by ^{1}H NMR.

Chemical Synthesis. Our synthetic efforts relating to AdoMetDC date back many years, when we prepared an early series of related compounds that included

MHZPA **3** and MAOEA **5** (*26*). In our current research, we have prepared a series of compounds with various 8-substituents on an adenosine template having a chain extension at C-5′. These compounds fall into four broad categories with respect to the various substituents at C-5′, and synthetic schemes will be organized based upon these categories. For comparison purposes, we have included available compounds with an 8-H within the four categories. End groups of the C-5′ substituent such as an aminooxyalkyl will bind covalently and to a large extent irreversibly to the pyruvoyl group within the active site of the enzyme, while groups ending in an amide will not even bind reversibly to the pyruvoyl group. Amino end groups will bind covalently, but entirely reversibly, while a hydrazide group binds with some reversibility. In addition to these compounds we have prepared several compounds without a chain extension at C-5′, i.e., compounds that do not reach the vicinity of the pyruvate group within the binding site.

The syntheses of some of the 8-unsubstituted compounds date back to our earlier work (*26*), and these compounds dictated our initial synthetic approaches. We began by assuming that we needed to block the 2′- and 3′-hydroxyl groups, which we did with an isopropylidene group. Later, we discovered that it was possible to conduct the chemistry without blocking these two hydroxyl groups, and that the new schemes were superior to those that utilized a blocking-deblocking sequence. In situations where we had already prepared a target compound utilizing a blocked precursor, we did not go back and resynthesize the compound without using a blocking group, and the schemes below reflect that fact. Figure 4.2 presents the precursor nucleoside series **8** and **9** that we have used along with their syntheses.

Target compounds with an aminooxyalkylamino side chain at C-5′ were prepared using two different routes, as shown in Figure 4.3. In our original sequence, which utilized a 2′,3′-*O*-isopropylidene group for protection, we generated the

hydroxyalkylamino precursor **15** by displacement of a tosyl group with the requisite amine. Using N-hydroxyphthalimide, triphenylphosphine and DEAD (*27*) the aminooxy precursor **16** was produced and then converted to the desired target **5** under acidic conditions. Later we found that it was more effective to first generate the aminooxy precursors ethyl *N*-(2-bromoethoxy)ethanimidate (*28*) and ethyl N-(*N*-4-bromobutoxy)ethanimidate (*29*), which could be appended to C-5′ by halide displacement with a 5′-methylamino-5′-deoxynucleoside to produce product series **11** and **13**. Initially we carried out this displacement with an isopropylidene protecting group on the nucleoside, but subsequently determined that the reaction works as well or better without the protecting group. By the above means targets **12a-c** and **14a-f** were prepared.

All of the amides and hydrazides were made by similar procedures, as shown in Figure 4.4. The 5′-methylamino-5′-deoxynucleosides were treated with the appropriate ω-chloroester followed by treatment with either ammonia or hydrazine. If an isopropylidene group was involved, then it was removed with an acidic deprotection step. In this manner targets **17d-f**, **j-m**, with two different linker lengths and various 8-substitutions were prepared. Targets with an aminoalkylamino side chain at C-5′ were mainly prepared utilizing the displacement of a C-5′ leaving group with the asymmetrical amine (Figure 4.5). For example, treatment of **8a** with 3-methylaminoethylamine produced a mixture of **18f** and **19d**, which were separated to afford pure **18f**, our desired target. In the case where this procedure involved a starting material with an isopropylidene group, treatment with acid produced the desired final product. In early work, compounds **21c,d** were prepared by treatment of a 5′-methylamino-5′-deoxynucleoside with 3-bromopropylphthalimide followed by two deprotection steps.

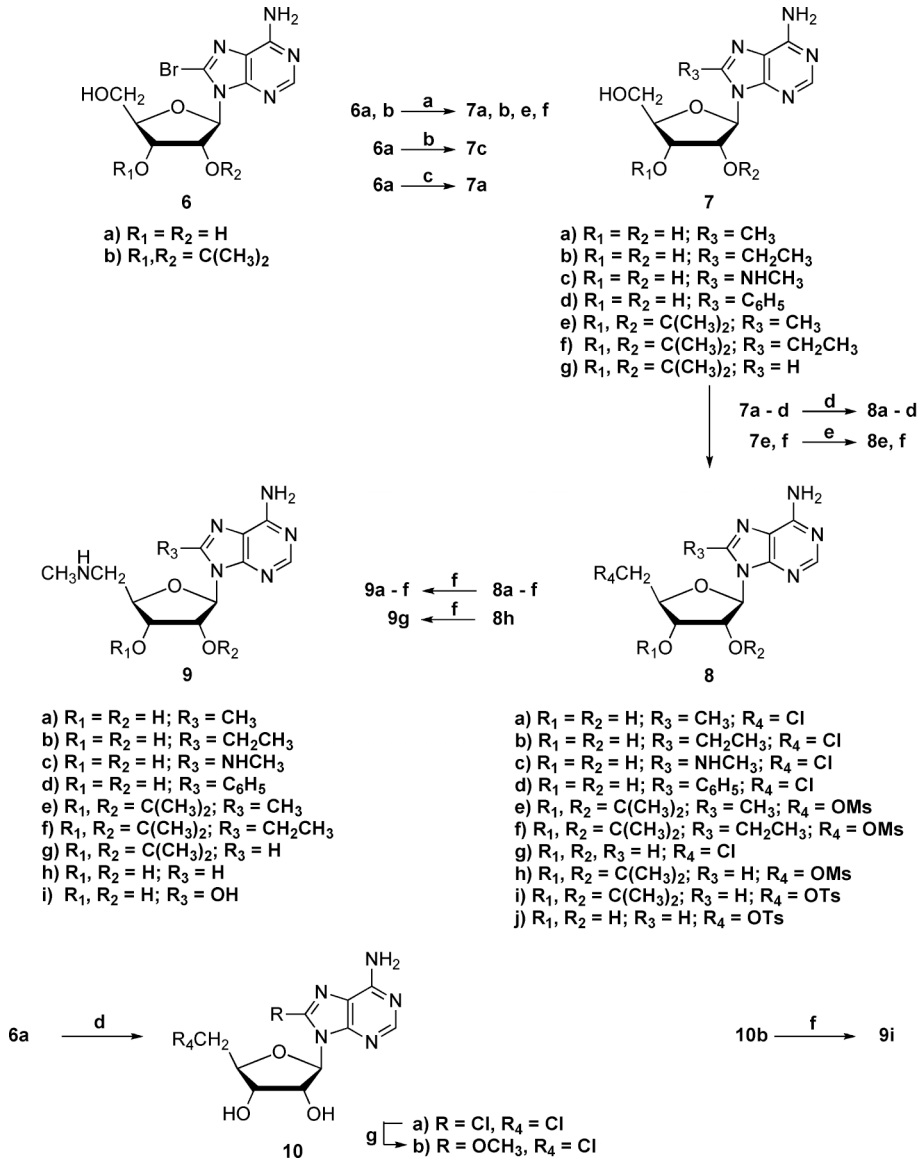

Figure 4.2 Synthetic scheme for new inhibitors – part I. (a) $(CH_3)_4Sn$ or $(CH_3CH_2)_4Sn$, HMDS/dioxane, NMP, $(Ph_3P)_4Pd$, 110 °C; (b) CH_3NH_2, MeOH, 110 °C; (c) $C_6H_5B(OH)_2$, K_2CO_3, $(Ph_3P)_4Pd$, 1,2-DME-H_2O (2:1), 90 °C; (d) $SOCl_2$, CH_3CN/pyridine, 0 °C-RT, NH_4OH, RT; (e) MsCl, pyridine, 0 °C; (f) 33% CH_3NH_2, EtOH, RT (9e,f,g) or 90 °C (9a-d); (g) NaOMe/MeOH, RT

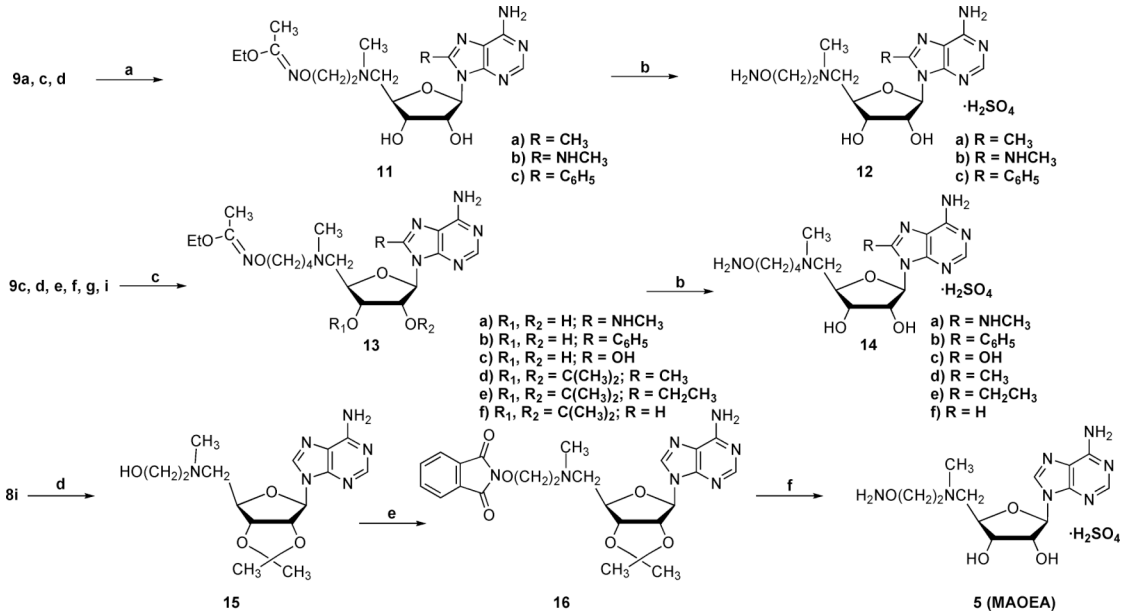

Figure 4.3 Synthetic scheme for new inhibitors – part II.
(a) $CH_3(OEt)C{=}NO(CH_2)_2Br$, DMF, DIEA, 50 °C; (b) 1 N H_2SO_4, RT; (c) $CH_3(OEt)C{=}NO(CH_2)_4Br$, DMF, DIEA, 50 °C; (d) 2-(methylaminoethanol), RT; (e) -hydroxyphthalimide, PPh_3, DEAD, THF, RT; (f) 1 N H_2SO_4, 60 °C.

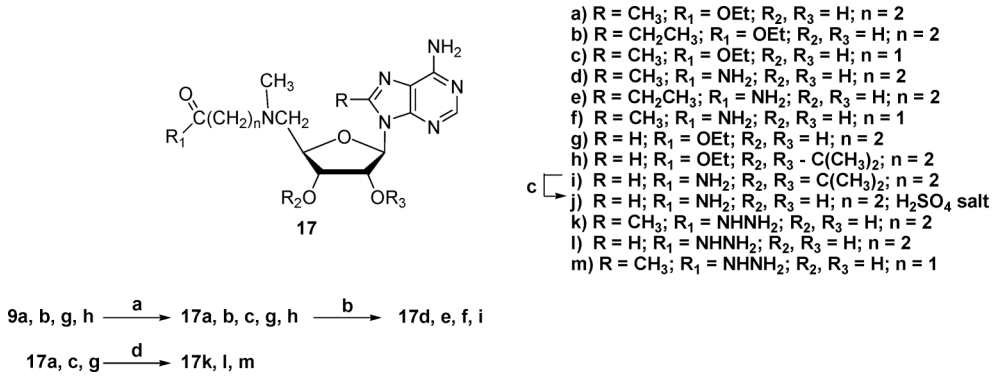

Figure 4.4 Synthetic scheme for new inhibitors – part III. (a) $Cl(CH_2)_nCO_2Et$ (n = 1 or 2), DMF, DIEA, 60 °C; (b) NH_3/MeOH, RT; (c) 1 N H_2SO_4, RT; (d) NH_2NH_2, H_2O, EtOH, reflux.

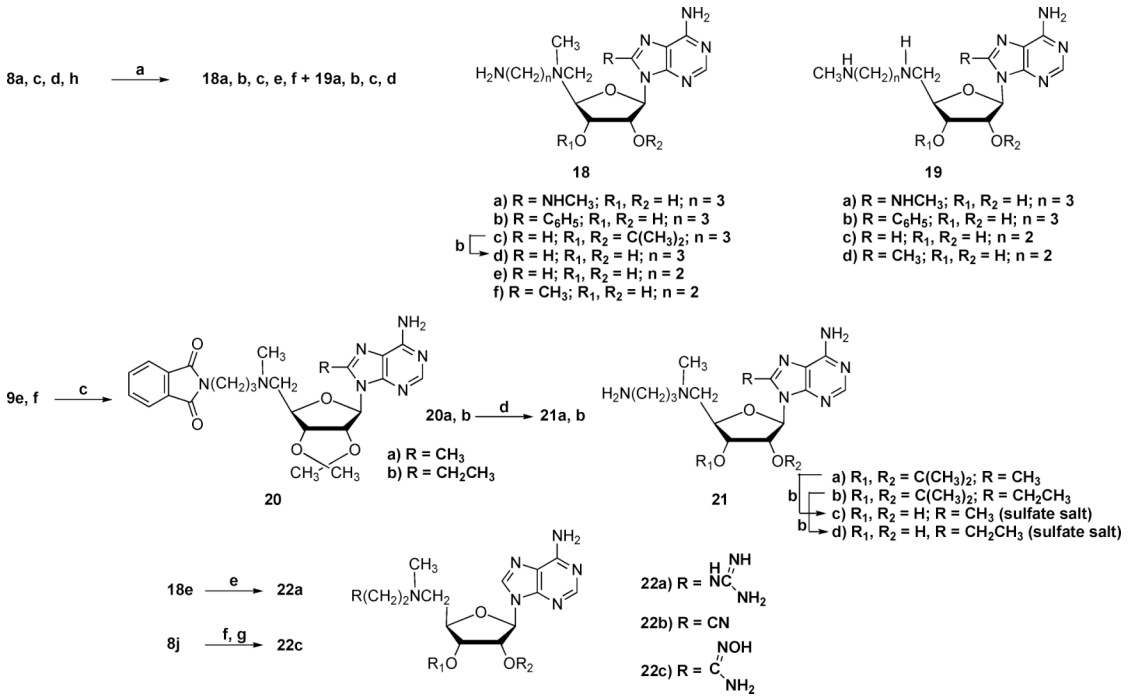

Figure 4.5 Synthetic scheme for new inhibitors – part IV. (a) $CH_3NH(CH_2)_nNH_2$ (n = 1 or 2), RT; (b) 1 N H_2SO_4, RT; (c) 3-bromopropylphthalimide, DMF, DIEA, 60 °C; (d) NH_2NH_2, H_2O, reflux; (e) 1H- pyrazole-1-carboxamidine · HCl, DMF, DIEA, RT; (f) 3-(methylamino)propionitrile, RT; (g) NH_2OH · HCl, MeOH, DMF, KOH, RT.

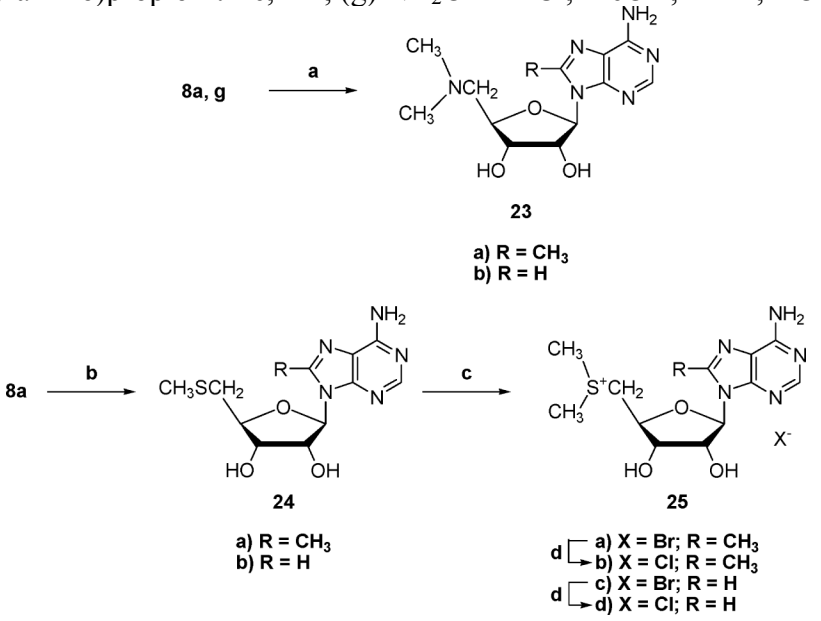

Figure 4.6 Synthetic scheme for new inhibitors – part V. (a) $(CH_3)_2NH$, 2 M solution in MeOH, 90 °C; (b) CH_3SNa, DMF, RT; (c) CH_3Br, Et_2O, HCO_2H, HOAc, RT; (d) IRA-400 (Cl) ion exchange resin.

Building on the aminoalkylamino side chain, reaction of **18e** with 1-carboxamidinopyrazole (*30*) produced the guanidine target **22a**. In a related sequence, the target amidoxime **22c** was prepared by treating **8j** with 3-(methylamino)propionitrile to produce the nitrile **22b** (*31*), which was treated with hydroxylamine hydrochloride under basic conditions.

The 5′-dimethylamino and 5′-dimethylsulfonio compounds **23a,b** and **25a-d** were prepared by routine methods (Figure 4.6). The dimethylamino group was introduced by displacement of a 5′-chlorine on **8a** or **8g** (*32*) with dimethylamine. The 5′-methylthio compounds **24a,b** were treated with methyl bromide to produce **25a** and **25c**. Ion exchange was utilized to prepare the chloride salts **25b** and **25d**. 8-Methyl-5′-methylthio nucleoside **24a** was prepared by displacement of the 5′-chlorine in **8a** with sodium thiomethoxide.

Protein Production. For crystallography of wild type and F223A mutant of human AdoMetDC (hAdoMetDC), plasmids in the pQE30 vector in *E. coli* were produced as described previously (*25*). This construct replaces the N-terminal methionine with MRGS$(H)_6$GS- for purification by immobilized metal affinity chromatography. A different plasmid also based on the pQE30 vector was used for the production of protein for the hAdoMetDC enzyme assays. In this plasmid, the $(H)_6$ tag was located at the carboxyl end replacing the terminal –QQQQQS. The position of the $(H)_6$ tag did not alter the activity of the purified enzyme.

The wild type hAdoMetDC was purified based on the protocol described by Ekstrom *et al*. (*22*). The plasmid encoding the enzyme is in the pQE30 vector and was transformed into JM109 strain *E. coli* cells. The cells were grown as an overnight culture in LB media at 37 °C and then introduced into larger cell cultures with both of the cultures containing 100 mg/mL ampicillin. The cells were grown until they reached an $O.D_{600}$ of 0.6 and then were induced with 100 mg/L isopropyl β-D-

thiogalactopyranoside (IPTG). The cells were allowed to grow overnight at 15 °C and were then harvested by centrifugation, washed using a wash buffer which contained 20 mM Na_2HPO_4, pH 7.0, 500 mM NaCl, 2.5 mM putrescine, 0.02% Brij-35 and 10 mM imidazole, and stored at -80 °C. The frozen cell pellet was thawed, suspended in the wash buffer, and lysed using a French press at 1500 psi. The cellular debris and the lysate were separated by centrifugation at 12000 g. Talon metal affinity resin was equilibrated with the wash buffer and then the lysate and the resin were gently spun together for 1.5 h. The resin was loaded onto a column and washed with a volume of wash buffer equivalent to 15-20 times the column volume. Next, the column was washed in the same manner with wash buffer containing 25 mM imidazole. The protein was then eluted with buffer containing 100-200 mM imidazole. The eluted protein solution was concentrated to around 10 mL and passed through a Sephadex G-75 column pre-equilibrated with 10 mM N-(2-hydroxyethyl)piperazine-N′-2-ethanesulfonic acid (HEPES), pH 7.5, 2.5 mM putrescine, 5 mM dithiothreitol (DTT), 0.1 mM ethylenediaminetetraacetic acid, 0.02 % Brij-35, and 300 mM NaCl. The buffer was run through the column and the fractions containing the protein were identified by UV absorbance at 280 nm. The protein was concentrated to ~ 10 mg/mL and stored at -80 °C. The purification of the F223A mutant was similar to that of the native enzyme.

Structure Determination. The protein was thawed on ice and buffer exchanged to 10 mM HEPES, pH 7.5, 200 mM NaCl and 1 mM DTT using Bio-Rad buffer exchange chromatography columns (Bio-Rad Laboratories, Hercules, CA 94547). The wild type protein was incubated with a 4-6 M excess of inhibitor for 24 h prior to crystallization. The F223A mutant was diluted to ~6 mg/mL and incubated with a 4-6 M excess of MeAdoMet for 24 h prior to crystallization. Crystals of both the native and the mutant complexes were grown using the hanging drop method at 22 °C in 13-

16% PEG 8000, 100 mM Tris, pH 8.0-9.0, and 10 mM DTT. Crystals appeared overnight and were stable for 1-2 weeks.

The data for the **12a** complex were collected at a home source with a Rigaku R-AxisIV^{++} image plate detector using Cu-K_α radiation from a Rigaku RU-300 rotating anode generator. The data for the **14e** complex were collected at NE-CAT beamline 8-BM at the Advanced Photon Source (APS) using a ADSC Q315 detector. Data for the **17f** complex were collected at NE-CAT beamline 24-ID-C using a ADSC Q315 detector. The data for AdoMetDC F223A with MeAdoMet and the complexes with **17d** and **21c** were collected at the F2, A1 and A1 stations of CHESS respectively, using an ADSC Q210 detector. The diffraction quality of the crystals strongly depended on cryoprotection conditions. The crystals were sequentially transferred to a solution containing the well solution with 2%, 5%, 8%, 15% and 18% glycerol with 1-2 min equilibration between each step. The data for all of the complexes were indexed, integrated and scaled using the HKL2000 (*33*) program suite. The data collection statistics are summarized in Table 4.1.

The structures of all of the complexes were determined by molecular replacement using the structure of native AdoMetDC with MeAdoMet bound (PDB 1I7B) as the search model, and the CNS program suite (*34*). The model building was done using the program O (*35*) or Coot (*36*). The conformations of the ligand molecules were determined using difference F_o-F_c and composite omit maps. The parameter and the topology files for the ligands were generated using the HIC-Up server (*37*). The difference maps also showed density for a molecule of putrescine bound in all of the structures. The refinement statistics of the complexes are given in Table 4.2.

Molecular Modeling. Determination of the conformational preference of ligands in the active site of AdoMetDC was carried out with Macromodel version 7.2

(*38*) available from Schrödinger, L. L. C. To make the computational studies tractable, the protein was truncated to a shell of atoms that included any residue that contained an atom within 20.0 Å of MeAdoMet located in the active site of AdoMetDC (from PDB 1I7B) and was used as the starting model for conformational searching/energy minimization. Removal of water molecules from this "docking shell" was followed by appropriate hydrogen treatment using Schrödinger's protein preparation utility that aids in the generation of appropriate ionic states and histidine tautomers for active site amino acids and minimizes the protein's potential energy gradient through a series of constrained energy minimizations. For the conformational searches, the appropriate ligand was added to the active site and, where appropriate, the covalent bond between the amino terminus of the ligand and the pyruvoyl group was formed.

The resulting structures were subjected to 50,000 mixed Monte Carlo MCMM/Low Mode conformational search steps (*39, 40*) allowing residues within a 5 Å shell surrounding the active site to move freely during each Monte Carlo/Low Mode step and subsequent energy minimization step of the search. All other protein atoms were constrained to their starting position. Residues His5, Glu67, Cys226 and Glu247 were also constrained to their starting position. The energy minimization step was considered to have converged when the energy gradient was less than 0.05 kJ / mol. The AMBER* force field (*41, 42*), with a distance dependent dielectric "constant" further attenuated by a factor of four was employed for the calculations, and the energy minimizations relied upon the TNCG minimization technique (*43*). The global minimum and low energy ensemble of structures within 15 kJ/mol of the global minimum (after convergence) were further refined by energy minimization until a gradient less than 0.01 kJ / mol was obtained with just the ligand allowed to move during this subsequent energy minimization procedure. All protein atoms during this

process were constrained to their starting position. The jobs were run with the nucleoside starting in both the *syn* and *anti* conformations for completeness. The AMBER* parameters for the sulfonium ion were adapted from Markham *et al*. (*44*).

The modeling of the terminal three atoms of **14e** was done using conformational searching with Macromodel version 7.2 as described above. Since the position of the rest of the ligand and the protein was determined to high accuracy by fitting to the electron density determined by X-ray diffraction, all of the protein and the ligand atoms except the last three non-hydrogen atoms and their attached hydrogens were fixed during the conformational search. Torsional rotation was allowed around the last two bonds of the C-5' extension during the conformational search. A visual survey of the five lowest energy structures, which spanned an energy range of 6.5 kJ/mol, showed that they were similar and the global minimum of the search was utilized to obtain the coordinates of the disordered terminal atoms of **14e**.

AdoMetDC Activity and Inhibition. AdoMetDC was assayed by measuring the release of $^{14}CO_2$ from *S*-adenosyl-L-[carboxy-^{14}C]methionine (Amersham Pharmacia Biotech, ~60 mCi/mmol) (*45*). Assay of 30 ng of C-terminal his-tagged AdoMetDC under these conditions results in ~7000 cpm with a background of 30, and an activity of ~1.5 pmol/min/ng protein. For determination of the abilities of compounds to inhibit AdoMetDC, the enzyme activity was determined in the presence of no inhibitor and at least 5 concentrations of each potential inhibitor. The enzyme concentation was 1 nM. The IC_{50} values were determined from curve fitting to plots of the inhibitor concentration versus the % inhibition of AdoMetDC.

Table 4.1. Data collection statistics for hAdoMetDC complexes.

	F223A + MeAdoMet	**WT + 12a**	**WT + 14e**	**WT + 17d**	**WT + 17f**	**WT + 21c**
Wavelength (Å)	0.9795	1.5418	0.9795	0.9790	0.9792	0.9771
Space Group (Å)	C2	C2	C2	C2	C2	C2
a (Å)	95.98	96.78	94.43	99.82	99.65	100.08
b (Å)	44.25	44.46	50.04	50.95	50.75	50.75
c (Å)	70.83	70.55	70.41	68.98	68.90	69.04
β	104.52	104.17	105.34	105.52	105.34	105.56
Resolution (Å)	2.62	2.43	1.83	1.84	1.91	1.86
Total/Unique reflections	23532/ 8160	26010 /10403	83134/ 26894	89749/ 28243	97188/ 25449	77769/ 27505
Redundancy	2.9(2.6)*	2.5 (1.9)	3.1(3.1)	3.2(2.6)	3.8(2.6)	2.8(2.5)
% complete	92.9(91.2)	93.6(86.8)	95.6(95.5)	97.6(94.1)	98.8(91.0)	98.7(96.8)
I/σ	13.3(2.0)	10.9(2.9)	13.5(2.7)	17.4(8.0)	16.6(3.9)	14.2(2.2)
R_{sym}	7.7(45.2)	9.0(33.8)	7.2(54.8)	6.0(14.0)	7.6(25.0)	7.1(39.1)
Matthews no	1.90	1.92	2.09	2.21	2.19	2.21
Solvent content (%)	34.1	34.8	39.7	43.2	42.9	43.2

* Values in parenthesis are for the highest resolution shell.
$R_{sym}=\Sigma\Sigma_i|I_i - \langle I\rangle| / \Sigma\langle I\rangle$, where $\langle I\rangle$ is the mean intensity of the N reflections with intensities I_i and common indices *h,k,l*.

Table 4.2. Refinement statistics for hAdoMetDC complexes.

	F223A + MeAdoMet	**WT + 12a**	**WT + 14e**	**WT + 17d**	**WT + 17f**	**WT + 21c**
Resolution (Å)	2.62	2.43	1.83	1.84	1.91	1.86
R-factor[a]	0.203	0.199	0.208	0.204	0.197	0.200
R-free[b]	0.280	0.247	0.231	0.237	0.208	0.232
No of non-H atoms						
Protein	2473	2419	2381	2489	2454	2470
Ligand	28	25	28	26	25	25
Water	79	73	137	222	212	217
B-factors						
Protein ($Å^2$)	41.3	31.5	29.6	26.8	28.2	32.4
Ligand ($Å^2$)	63.4	42.1	32.3	26.0	43.9	39.9
Putrescine ($Å^2$)	32.4	27.9	40.0	22.4	24.7	29.8
rms deviations						
Bonds (Å)	0.010	0.011	0.007	0.006	0.012	0.008
Angles (º)	1.4	1.4	1.3	1.3	1.4	1.3
Dihedrals (º)	24.9	25.2	25.3	25.3	25.8	25.2
Ramachandran plot						
Most favored region (%)	84.2	89.3	91.4	91.8	92.1	92.5
Additional favored region (%)	14.7	9.5	7.8	7.8	7.5	7.5
Generously allowed region (%)	0.8	0.8	0.4	0.4	0.4	0.0
Disallowed region (%)	0.4	0.4	0.4	0.0	0.0	0.0

[a]R-factor = $\Sigma_{hkl}||F_{obs}|-k|F_{cal}||/\Sigma_{hkl}|F_{obs}|$, where F_{obs} and F_{cal} are observed and calculated structure factors, respectively. In [b]R-free the sum is extended over a subset of reflections that were excluded from all stages of refinement.

Section 4.3. Results

Modeling of MeAdoMet in the active site of AdoMetDC. The crystal structures of AdoMetDC complexed with MeAdoMet or the inhibitors MHZPA **3** and MAOEA **5** have shown that the ligand binds with the adenine base in the unusual *syn* conformation (*25*). The active site residues of AdoMetDC with MeAdoMet bound are shown in Figure 4.7. However, NMR data, coupled with molecular modeling studies, suggest that in solution AdoMet assumes an *anti* conformation as an energy minimum (*44*). A survey of crystal structures in which AdoMet is bound showed that the substrate assumes a range of glycosidic torsion angles, but that the *anti* conformation is preferred (*44*). In order to explain the conformational preferences and the related energetics of ligand binding to AdoMetDC, the modeling of MeAdoMet in the active site of AdoMetDC was done. Since MeAdoMet is tethered to the active site of AdoMetDC through covalent bonding to the pyruvoyl group, docking involving positional and orientational sampling was not performed. Instead, a conformational search to locate the populated low energy conformations of AdoMet in the AdoMetDC active site was performed using the mixed Monte Carlo/Low Mode conformational search method within the MacroModel program (*38-40*). The conformational search started with AdoMet in either the *anti* or *syn* conformation and in each case the five lowest energy structures from the search exhibited a *syn* conformation for the adenine nucleoside. A superposition of the modeled structure with the crystal structure (Figure 4.7) indicates that the results of the conformational search match well with those observed crystallographically. Conformational searches were also done for AdoMet, 5′-deoxy-5′-(dimethylsulfonio)adenosine (MMTA), MHZPA **3**, and MAOEA **5** binding to AdoMetDC, and each yielded a *syn* conformation for the glycosidic bond (data not shown). The ribose makes key hydrogen bonds to Glu247 and the adenine base stacks between Phe7 and Phe223 and also makes hydrogen bonds to the

backbone amide and C-terminal carboxyl group of Glu67. These interactions together with π-π stacking of the adenine base with Phe223 and with Phe7 constrain the glycosidic bond to the *syn* conformation

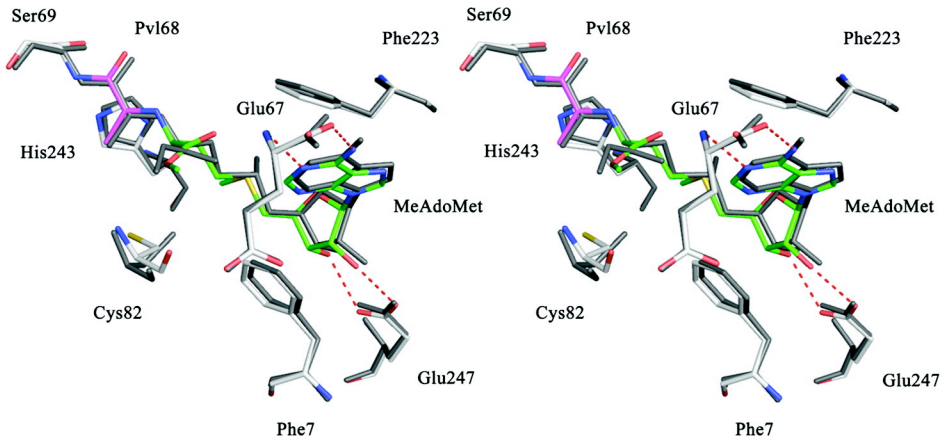

Figure 4.7 Comparison of the crystal structure of hAdoMetDC complexed with MeAdoMet to that of a structure derived from the modeling of the complex. The crystal structure has all atoms colored grey. For the model, the active site pyruvoyl group is shown in magenta and MeAdoMet carbon atoms are shown in green. MeAdoMet makes a Schiff base to the pyruvoyl group. The ribose makes two hydrogen bonds to Glu247 (shown as red dashed lines). The adenine base stacks between Phe223 and Phe7 in the unusual *syn* conformation. The hydrogen bonds between the adenine base and the backbone of Glu67 stabilize the *syn* conformation. The modeling result agrees well with the experimentally determined crystal structure.

Virtual mutations in the active site of AdoMetDC. Virtual mutations were made to study the effect of various residues on the conformation of the bound nucleoside. Conformational searching with MacroModel employing the AdoMetDC F223A and F7A single amino acid mutants, with MeAdoMet in the active site, resulted in a mixture of *syn* and *anti* conformations in the low energy ensemble. With each of the mutations, the global minimum was an *anti* conformation of the adenine base closely followed by a *syn* conformation with an energy difference of ~2 kJ/mol. The global minimum energy conformation of the ligand bound in the *anti*

conformation in the F223A mutant exhibits major changes compared to the 2nd lowest energy conformer which adopts the *syn* conformation. In the F223A binding site, the ribose of the global minimum energy structure is displaced and makes hydrogen bonds to Glu247 and Cys226 instead of to Glu247 alone (Figure 4.8 A). This change causes the ligand to twist back upon itself, the sulfonium stacks over the adenine base, and the adenine base makes three hydrogen bonds to Ser66. In the F7A binding site, the ligand assumes a similar conformation as with the F223A mutant. The Phe223 side chain undergoes a torsional change to accommodate the conformational change of the ligand and also stacks with the adenine base (Figure 4.8 B). The presence of the *anti* conformation in low energy structures of the ligand in the enzyme active site where virtual mutations have been made suggests the importance of the phenyl groups in maintaining the *syn* conformation of the ligand within the wild-type enzyme binding site. However, since we observed a *syn* conformation of the nucleoside as the 2nd lowest energy structure in our conformational search on the F223A mutant and since the relative energy of that structure compared to the global minimum (□E = 2.5 kJ/mol) is well within the error limit of our calculations, we were prompted to obtain the crystal structure of the F223A mutant complexed with MeAdoMet.

Structure of F223A Complexed with MeAdoMet. The structure of the F223A mutant is similar to that of the wild type protein (*22*). The human AdoMetDC protomer has a four layer αββα fold in which two β-sheets are sandwiched between two layers of α-helices. The secondary structural elements are related by a pseudo twofold axis suggesting that the protomer resulted from gene duplication. The proenzyme consists of 334 amino acid residues and the enzyme undergoes autoprocessing to give the α and the β subunits (*22*).

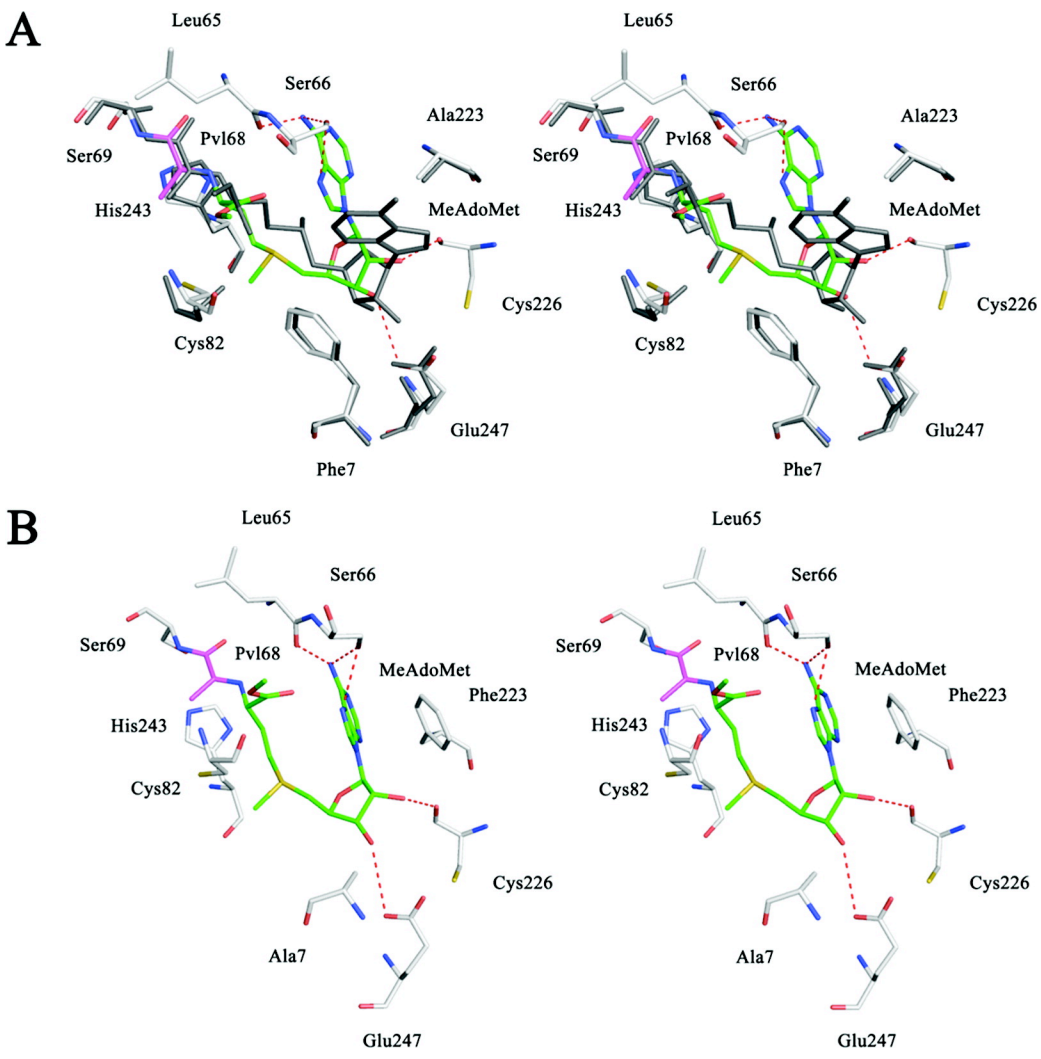

Figure 4.8 Comparison of modeling of hAdoMetDC F223A and hAdoMetDC F7A each complexed with MeAdoMet with the crystal structure of F223A mutant with MeAdoMet bound. Global minimum of modeling of MeAdoMet in the active site of the F223A mutant superposed with the crystal structure (A) and the F7A mutant (B) of hAdoMetDC (see Materials and Methods for details). The crystal structure has all atoms colored grey. The pyruvoyl group is shown in magenta and the ligand carbon atoms are shown in green for the models. Hydrogen bonds are shown as dashed lines. The adenine base attains an *anti* conformation in the models. The ribose makes one hydrogen bond to Glu247 and the other to the backbone carbonyl of Cys226. The adenine base makes three hydrogen bonds to Ser66. In the F7A model (B) the Phe223 residue changes its conformation to stack with the adenine base of MeAdoMet in the *anti* conformation.

The autoprocessing reaction yields the active enzyme with the pyruvoyl cofactor. The pyruvoyl group is located at the end of the N terminal β-sheet and the active site involves residues from both of the β-sheets. The binding site of putrescine, which activates both the autoprocessing and decarboxylation reactions of hAdoMetDC, is located well away from the ligand binding site within the wild-type enzyme. Experimental conditions for the purification of the enzyme included putrescine at sufficient concentration to ensure high occupancy of the putrescine binding site. The loops between the residues 1-4, 21-27, 165-173, 288-299, 329-334 are disordered in the crystal structures.

The crystal structure of hAdoMetDC F223A complexed with MeAdoMet was solved using molecular replacement. The difference F_o-F_c density shows that MeAdoMet is covalently bound to the enzyme and the nucleoside adopts a clear *syn* conformation (Figure 4.8 A). As expected, the composite omit map density shows no density for the Phe223 side chain. The ribose makes two hydrogen bonds to Glu247, which anchor the ligand, and the base is held in *syn* conformation by stacking interactions with Phe7 and hydrogen bonds between the adenine and Glu67. One molecule of putrescine per monomer is present in the expected putrescine binding site. A superposition of the F223A/MeAdoMet structure and the wild type structure with MeAdoMet shows that there is no appreciable change in the position or conformation of the ligand. The loops disordered in the mutant are also disordered in the wild type protein.

Biochemical Analysis of Potential Inhibitors of hAdoMetDC. The demonstrated importance of the *syn* conformation of the adenine base of the AdoMet substrate for binding in the active site of the enzyme led us to explore whether this could be exploited in designing better hAdoMetDC inhibitors. It is known that 8-substitution on adenine rings causes the nucleotide to favor a *syn* conformation in

solution (*26, 27, 46, 47*). It was thought that structural analogues of AdoMet that preferred the *syn* conformation in solution would lead to improved hAdoMetDC inhibition. Modeling of the active site had indicated that there was sufficient room to accommodate even rather large substituents at C^8 of adenine. Several series of AdoMet structural analogues were synthesized with substituents ranging from a methyl group to a phenyl group at the 8-position of adenine. Each of these compounds was then assayed for their ability to inhibit hAdoMetDC and IC_{50} values for the inhibition were determined (Table 4.3).

The inhibitors tested fall into four groups as described in the "Chemical Synthesis" sub section. One group (**12a-c**, **14a-f**, **5**) has an aminooxyalkyl side chain at C-5′, which can form a Schiff base with the pyruvate of AdoMetDC(*20, 48-50*) Compounds of this group were potent inhibitors with a 4-aminooxybutyl group being slightly superior to a 2-aminooxyethyl addition. A second group of compounds (**17d**,**e**,**f**,**j**,**k**,**l**,**m**) had an amide or a hydrazide side chain at C-5′ and a third group of inhibitors (**18a**,**b**,**d,e,f**; **19a,b,c,d; 21c**,**d**) had an aminoalkylamino side chain at C-5′. Also related to the third group by the synthetic method are **22a** and **22c**, which, respectively, have a guanidine and an amidoxime at the end of the C-5′ side chain. The compounds of groups 2 and 3 were less potent (particularly those with the aminoalkylamino, guanidine, or amidoxime side chain) but are more likely to be stable under *in vivo* conditions. The final group of compounds consisted of 5′-dimethylamino (**23a,b)** or 5′-dimethylsulfonio (**25b,d)** compounds. Compound **25d** has previously reported to be an AdoMetDC inhibitor with a K_i in the μM range (*32*). As shown in Table 4.3, the replacement of sulfur by nitrogen slightly improves the AdoMetDC inhibition.

Table 4.3. Inhibition of hAdoMetDC[a].

Compound	IC_{50}
12a	7 nM
12b	86 nM
12c	< 5% inhibition at 100 μM
14a	49 nM
14b	< 5% inhibition at 100 μM
14c	11 nM
14d	5 nM
14e	15 nM
14f	18 nM
5 (MAOEA)	55 nM
17d	400 nM
17e	4 μM
17f	< 5% inhibition at 100 μM
17j	7 μM
17k	170 nM
17l	1.5 μM
17m	31 μM
18a	440 μM
18b	< 5% inhibition at 100 μM
18d	500 μM
18e	< 5% inhibition at 100 μM
18f	88 μM
19a	< 5% inhibition at 100 μM
19b	< 5% inhibition at 100 μM
19c	< 5% inhibition at 100 μM
19d	< 5% inhibition at 100 μM
21c	70 μM
21d	420 μM
22a	< 5% inhibition at 100 μM
22c	157 μM
23a	600 nM

Table 4.3. (Continued)

23b	9 μM
25b	3 μM
25d	15 μM

[a] Each of the potential inhibitors was assayed for the ability to inhibit hAdoMetDC. At least five concentrations of each compound were used and IC_{50} values were calculated from curve fits to plots of inhibitor concentration versus % inhibition of hAdoMetDC.

Within each of these groups, there was a consistent improvement of inhibitory activity when an 8-methyl substituent was added to the adenine ring. The reduction in the IC_{50} value varied from 3.4-fold for compound **14d** to 15-17-fold for compounds **23a** and **17d**. There was an 8-fold increase in potency when an adenine 8-methyl substituent was added to compound **5** (MAOEA) forming compound **12a**. This is consistent with the concept that the 8-methyl substitution on adenine biases the corresponding nucleoside toward the *syn* conformation and that this is the form that is bound at the active site. An adenine 8-hydroxy substituent resulted in slightly increased potency compared to no substituent, but was not as effective as the 8-methyl substituent (compare **14c** to **14f** and **14d**). Larger 8-substitutions did not improve the effectiveness. An 8-phenyl addition to compounds **5**, **14f** and **18d** abolished the inhibitory activity. Smaller additions such as 8-ethyl (compare **14d** and **14e**, **17d** and **17e**, and **21c** and **21d**) or 8-methylamino (compare **12a** and **12b** and **21c** and **18a**) were tolerated but were not as potent as 8-methyl.

Crystal Structures of hAdoMetDC Complexes. The crystal structure of native hAdoMetDC with **12a** was solved using molecular replacement (Figure 4.9 A). As noted above, **12a** is structurally similar to the previously studied inhibitor MAOEA **5** except that it has a methyl substitution at the 8-position on the adenine base. The electron density indicates that the amino terminus of **12a** forms a Schiff base with the pyruvoyl group of the enzyme. The adenine base of **12a** adopts a *syn* conformation in

the crystal structure as expected. There is one molecule of putrescine bound in the putrescine binding site.

The crystal structure of native hAdoMetDC with **14e** was solved using molecular replacement (Figure 4.9 B). Compound **14e** is similar to MAOEA **5** except for an ethyl substituent on the 8-position of the adenine base and two extra carbon atoms between the tertiary nitrogen (near ribose) and the terminal nitrogen. The presence of a three-carbon linker between the ribose and the amino terminus makes this ligand interesting to study. The electron density maps show no density for Schiff base formation between the pyruvoyl group and the amino terminus of the ligand. There is no density for the terminal three atoms of the ligand but there is good density for the rest of the ligand. The position of the last three atoms was obtained by modeling them to an energetically favorable conformation using molecular modeling. The density around the pyruvoyl group fits it well and does not show any evidence of formation of a Schiff base. The ribose makes the critical hydrogen bonds to Glu247 and anchors the ligand. The nucleoside is held in the *syn* conformation and is stabilized by π-π stacking. The density of the ethyl substituent on the base is well defined indicating that the substituent is not disordered.

The crystal structures of hAdoMetDC with **17d** (Figure 4.9 C), **17f** (Figure 4.9 D) and **21c** (Figure 4.9 E) were also determined by molecular replacement. The three ligands have 8-methyl substituents; the first two have carboxamide end groups at the 5′-tail, while the third ligand has an amino group in this position. All three ligands showed clear electron density and all three ligands bound in the *syn* conformation.

Section 4.3. Discussion

The active site of AdoMetDC contains a bound pyruvoyl cofactor. The interactions of various ligands at the active site were previously elucidated from the

Figure 4.9 Complexes of hAdoMetDC with inhibitors having 8-substitutions. The carbon atoms of the inhibitor are shown in green and the pyruvoyl group is shown in magenta. Water molecules are shown as red spheres and hydrogen bonds are shown as dashed lines. (A) Complex with **12a**. The ligand makes a Schiff base linkage to the active site pyruvoyl group. (B) Complex with **14e**. There is no evidence from the electron density for the formation of a Schiff base and there is no density for the terminal three atoms of the ligand. The position of the terminal three atoms is determined by modeling. (C) Complex with **17d**. The carboxy terminus of the ligand makes hydrogen bonds to Leu65 and Ser229. (D) Complex with **17f**. The carboxy terminus of the ligand makes water mediated hydrogen bonds to Glu11 and Gly9. (E) Complex with **21c**. The amino terminus of the ligand makes water mediated hydrogen bonds to Glu11 and Gly9. The inhibitors **17d**, **17f** and **21c** do not make a Schiff base to the enzyme and are hence competitive inhibitors. The adenine base of all the inhibitors attains a *syn* conformation.

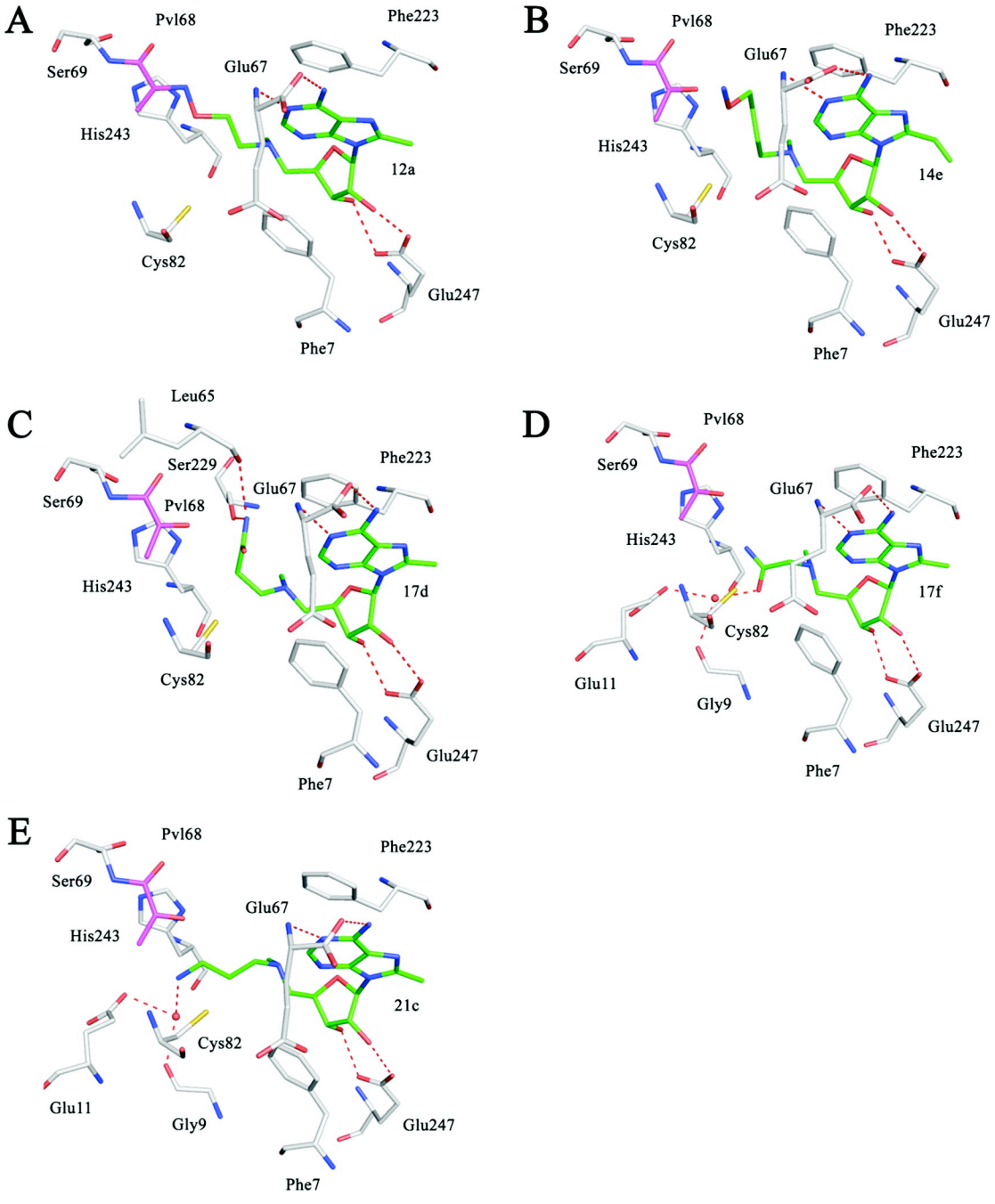
A
Pvl68
Phe223
Ser69
Glu67
His243
12a
Cys82
Glu247
Phe7
B
Pvl68
Phe223
Ser69
Glu67
His243
14e
Cys82
Glu247
Phe7
C
Leu65
Ser229
Phe223
Glu67
Ser69
Pvl68
His243
17d
Cys82
Glu247
Phe7
D
Pvl68
Ser69
Phe223
Glu67
His243
17f
Cys82
Glu11
Gly9
Glu247
Phe7
E
Pvl68
Phe223
Ser69
Glu67
His243
21c
Cys82
Glu11
Gly9
Glu247
Phe7

crystal structures obtained from complexes of the enzyme with the inhibitors MHZPA **3** (PDB 1I79), MAOEA **5** (PDB 1I72), MeAdoMet (PDB 1I7B), MGBG **1** (PDB 1I7C), and CGP48664A **2** (PDB 1I7M) (*25*). The crystal structure of MeAdoMet covalently bound to the enzyme most closely approximates the substrate AdoMet in the active site. The crystal structure shows key interactions of MeAdoMet with the enzyme including: (1) hydrogen bonding of the ribose oxygens with Glu247, (2) π-π stacking interactions of the adenine ring with Phe223 and Phe7, (3) hydrogen bonding of the 6-amino substituent of the adenine ring with the Glu67, the C-terminal residue of the β-chain and (4) hydrogen bonding of N-1 of the adenine ring with the backbone amide group of Glu67 (Figure 4.7). Similar interactions are also present in the structures of MHZPA **3** and MAOEA **5** complexed with hAdoMetDC. The glycosidic angle for the adenine base in the structures ranges from 128° to 139°, which demonstrates a preference for the *syn* conformation of the nucleoside when bound to the active site. Crystal structures of MGBG **1** and CGP48664A **2** with the enzyme show that they stack between the two phenyl rings and make hydrogen bonds to Glu247.

The molecular modeling of MeAdoMet in the active site of hAdoMetDC was performed by using mixed Monte Carlo/Low Mode conformational searching as described above. The glycosidic torsional angle was free to rotate during the conformational search, which would allow a wide range of rotomers that are compatible with the steric constraints of the active site before energy minimization. The low energy structures show that the adenine-derived nucleosides prefer the *syn* conformation in the active site of hAdoMetDC. Markham *et al.* have studied the conformational preferences of AdoMet in solution and *in vacuo* (*44*). These studies based on ^{1}H NMR and calculations based on NMR constraints have showed that AdoMet prefers an *anti* conformation in solution and a *syn* conformation *in vacuo*. In

solution, the energy difference between the *anti* and the corresponding *syn* conformation, which includes steric, electrostatic and the solvation contributions, is around -34 kJ/mol. However, these calculations were based on molecular mechanics without polarization effects and it is likely that the energy difference is much less negative. Our crystal structures and modeling results show that hAdoMetDC binds ligands in the *syn* conformation and that the energy difference is overcome by hydrogen bonding and π-π interactions Phe7 and Phe233. Typical π-π interactions of parallel geometry account for a stabilization of 8-12 kJ/mol (*51*), suggesting that other factors may be involved.

The roles of Phe223 and Phe7 in AdoMetDC were previously studied through crystal structures and kinetic experiments (*25*). Kinetic data from reaction of hAdoMetDC F223A and Phe7A mutants with the substrate AdoMet have shown that there is a 45-fold reduction of efficiency (k_{cat}/k_m) for the F7A mutant and a 1400-fold decrease with the F223A mutant. In addition, MGBG **1** and CGP48664A **2** show a significant increase in the IC_{50} values for both the F7A and F233A mutants when compared to the wild-type enzyme, with decrease in binding greater for the F223A than for F7A. Therefore, we chose to investigate the structural and conformational properties of MeAdoMet in the active site of the F223A mutant.

Our conformational searches with virtual mutations were done to understand the roles of Phe223 and Phe7 in stabilizing the *syn* conformation. In contrast to calculations done with the wild type enzyme structure, in which only the *syn* conformation was observed for the ensemble of lowest energy structures, the global minimum from both the mutations has the base in an *anti* conformation and the next higher energy structure has the base in a *syn* conformation. The difference in the energy between these conformations is about 2 kJ/mol, which we estimate to be within the error limit of our molecular mechanics based calculations. The energy difference

between the *syn* and *anti* conformation of both structures is low, and based on the X-ray structure of hAdoMetDC F223A with bound MeAdoMet, the enzyme binds the ligands in the *syn* conformation, suggesting that π-π interactions with Phe7 are sufficient to maintain the *syn* conformation. Thus, although the modeling studies were incapable of accurately predicting that the *syn* conformation of the nucleoside would be maintained in the F223A mutant, it was possible to infer from these studies that the binding affinity of the nucleoside for the enzyme would be diminished.

Our attempts to exploit the requirement by AdoMetDC for a ligand with a *syn* conformation were successful as demonstrated by the 8 to 18-fold improvement in inhibition when a methyl group is attached to C-8. However, the larger substituents that we tested provided no benefit over the unsubstituted parent compounds. In fact, the 8-phenyl substituent rendered the compounds much less potent than the unsubstituted analogue. Modeling studies of the active site had indicated that there should be sufficient space to accommodate the larger groups with the adenine in the *syn* conformation. A more detailed look at the area occupied by adenine C-8 substituents has indicated that this area is near the solvent interface. Based on our biochemical results, although large 8-substituents were structurally compatible with the active site, the penalty of incompletely burying a large hydrophobic group within a hydrophobic cavity is apparently greater than the gain from favoring the *syn* conformation. We are now exploring the effect of more hydrophilic C-8 adenine substituents that should be more compatible with proximity to the solvent. Such substituents may be useful in maintaining the inhibitory potency associated with the *syn* structure while still allowing species specific binding.

Structures of many of the AdoMet analogues bound to AdoMetDC have shown that they inhibit the enzyme through Schiff base formation with the pyruvoyl group of the enzyme. The linker length between the tertiary ammonium/sulfur and the terminal

nitrogen of those inhibitors is typically 3-4 atoms, which makes the formation of a Schiff base geometrically and sterically feasible. Compound **14e** has a linker length of five atoms. The electron density map for the complex of **14e** shows a break in the density after the pyruvoyl group, suggesting that there is no Schiff base formation. There is good density for the ligand except at the three terminal atoms, which are disordered and have no density. The positions of the last three atoms were fixed in an energetically favorable conformation using computer modeling. The five atoms of the linker region appear to cause a sterically unfavorable orientation for formation of the Schiff base. The ligand is still held rigidly in the active site by hydrogen bonds to Glu247 and the π-π stacking interactions with Phe7 and Phe223 and thus little movement is allowed to accommodate Schiff base formation for the longer linker region. Even though compound **14e** is not covalently attached to the pyruvoyl group its potency is better than MAOEA **5** and nearly as good as compound **12a**.

Conclusion. Previous structural studies showed that AdoMet binds to the active site of hAdoMetDC in the *syn* conformation, suggesting that adenosine analogues favoring the *syn* conformation in solution might be more potent inhibitors than corresponding analogues favoring the lower energy *anti* conformation. 8-Substituted nucleoside analogues favor the *syn* conformation because of unfavorable interactions in the *anti* conformation between a bulky 8-substituent and ribose. We used computer simulations to predict 8-substituted compounds that might bind to hAdoMetDC, and synthesized and assayed the most promising candidates. We also determined crystal structures of several compounds bound to hAdoMetDC to validate the predictions; the structures confirmed that the 8-substituted analogues bound in the *syn* conformation and retained the previously identified features of AdoMet binding, namely, purine stacking between Phe7 and Phe223, and hydrogen bonding between the ribose hydroxyl groups and Glu247. A group of adenosine analogues was

generated by varying the size and nature of the both the 8-substitutent and the 5'-modification. In general, 8-substituted analogues bound with a potency of 8 to 18-fold higher compared to the corresponding compound with a hydrogen atom at the 8-position; however, 8-substituents larger then methyl often showed lower potency than the corresponding 8-H compound. The observation results from excessive solvent exposure for large 8-substituents. Computer modeling and X-ray crystallography were also used to understand the preference for the *syn* conformation. Modeling studies suggested an important role for the two active site phenylalanine residues in addition to Glu247; however, the crystal structure of the F223A mutant hAdoMetDC showed that AdoMet still binds in the *syn* conformation, suggesting that other factors that favor the *syn* conformation remain to be identified.

REFERENCES

1. Hackert, M. L., and Pegg, A. E. (1997) Pyruvoyl-dependent enzymes, in *Comprehensive Biological Catalysis* (Sinnott, M. L., Ed.), pp 201-216, Academic Press, London.
2. Pegg, A. E., Xiong, H., Feith, D., and Shantz, L. M. (1998) *S*-adenosylmethionine decarboxylase: structure, function and regulation by polyamines, *Biochem. Soc. Trans. 26*, 580-586 526.
3. Tabor, C. W., and Tabor, H. (1984) Polyamines, *Annu. Rev. Biochem. 53*, 749-790.
4. Tabor, C. W., and Tabor, H. (1984) Methionine adenosyltransferase (*S*-adenosylmethionine synthetase) and *S*-adenosylmethionine decarboxylase, *Advan. Enzymol. Related Areas Mol. Biol. 56*, 251-282.
5. Casero, R. A., Jr., Celano, P., Ervin, S. J., Applegren, N. B., Wiest, L., and Pegg, A. E. (1991) Isolation and characterization of a cDNA clone that codes for human spermidine/spermine N^1-acetyltransferase, *J. Biol. Chem. 266*, 810-814.
6. van Poelje, P. D., and Snell, E. E. (1990) Pyruvoyl-dependent enzymes., *Ann. Rev. Biochem. 59*, 29-59.
7. Wallace, H. M., Fraser, A. V., and Hughes, A. (2003) A perspective of polyamine metabolism, *Biochem. J. 376*, 1-14.
8. Gerner, E. W., and Meyskens, F. L., Jr. (2004) Polyamines and cancer: old molecules, new understanding, *Nat. Rev. Cancer 4*, 781-792.
9. Pegg, A. E. (1988) Polyamine metabolism and its importance in neoplastic growth and as a target for chemotherapy, *Cancer Res. 48*, 759-774.
10. Metcalf, B. W., Bey, P., Danzin, C., Jung, M. J., Casara, P., and Vevert, J. P. (1978) Catalytic irreversible inhibition of mammalian ornithine decarboxylase

(E. C. 4. 1. 1. 17) by substrate and product analogues, *J. Am. Chem. Soc. 100*, 2551-2553.

11. Bewley, M. C., Graziano, V., Jiang, J., Matz, E., Studier, F. W., Pegg, A. E., Coleman, C. S., and Flanagan, J. M. (2006) Structures of wild-type and mutant human spermidine/spermine N^1-acetyltransferase, a potential therapeutic drug target, *Proc. Natl. Acad. Sci. U. S. A. 103*, 2063-2068.
12. Alhonen-Hongisto, L., Seppanen, P., and Janne, J. (1980) Intracellular putrescine and spermidine deprivation induces increased uptake of the natural polyamines and methylglyoxal bis(guanylhydrazone), *Biochem. J. 192*, 941-945.
13. Basuroy, U. K., and Gerner, E. W. (2006) Emerging concepts in targeting the polyamine metabolic pathway in epithelial cancer chemoprevention and chemotherapy, *J. Biochem. 139*, 27-33.
14. Fabian, C. J., Kimler, B. F., Brady, D. A., Mayo, M. S., Chang, C. H., Ferraro, J. A., Zalles, C. M., Stanton, A. L., Masood, S., Grizzle, W. E., Boyd, N. F., Arneson, D. W., and Johnson, K. A. (2002) A phase II breast cancer chemoprevention trial of oral alpha-difluoromethylornithine: breast tissue, imaging, and serum and urine biomarkers, *Clin. Cancer Res. 8*, 3105-3117.
15. Meyskens, F. L., Jr., and Gerner, E. W. (1999) Development of difluoromethylornithine (DFMO) as a chemoprevention agent, *Clin. Cancer Res. 5*, 945-951.
16. Meyskens, F. L., McLaren, C. E., Pelot, D., Fujikawa-Brooks, S., Carpenter, P. M., Hawk, E., Kelloff, G., Lawson, M. J., Kidao, J., McCracken, J., Albers, C. G., Ahnen, D. J., Turgeon, D. K., Goldschmid, S., Lance, P., Hagedorn, C. H., Gillen, D. L., and Gerner, E. W. (2008) Difluoromethylornithine Plus Sulindac

for the Prevention of Sporadic Colorectal Adenomas: A Randomized Placebo-Controlled, Double-Blind Trial, *Cancer Prev. Res. Phila. Pa. 1*, 9-11.

17. Raul, F., Gosse, F., Osswald, A. B., Bouhadjar, M., Foltzer-Jourdainne, C., Marescaux, J., and Soler, L. (2007) Follow-up of tumor development in the colons of living rats and implications for chemoprevention trials: assessment of aspirin-difluoromethylornithine combination, *Int. J. Oncol. 31*, 89-95.
18. Williams-Ashman, H. G., and Schenone, A. (1972) Methylglyoxal bis(guanylhydrazone) as a potent inhibitor of mammalian and yeast *S*-adenosylmethionine decarboxylases, *Biochem. Biophys. Res. Commun. 46*, 288-295.
19. Millward, M. J., Joshua, A., Kefford, R., Aamdal, S., Thomson, D., Hersey, P., Toner, G., and Lynch, K. (2005) Multi-centre Phase II trial of the polyamine synthesis inhibitor SAM486A (CGP48664) in patients with metastatic melanoma, *Invest. New Drugs 23*, 253-256.
20. Shantz, L. M., Stanley, B. A., Secrist, J. A., and Pegg, A. E. (1992) Purification of human *S*-adenosylmethionine decarboxylase expressed in *Escherichia coli* and use of this protein to investigate the mechanism of inhibition by the irreversible inhibitors, 5'-deoxy-5'-[(3-hydrazinopropyl)methylamino]adenosine and 5'{[(Z)-4-amino-2-butenyl]methylamino-5'-deoxyadenosine, *Biochemistry 31*, 6848-6855.
21. Danzin, C., Marchal, P., and Casara, P. (1990) Irreversible inhibition of rat *S*-adenosylmethionine decarboxylase by 5'-{[(Z)-4amino-2-butenyl]methylamino}-5'-deoxyadenosine, *Biochem. Pharmacol. 40*, 1499-1503.

22. Ekstrom, J. E., Matthews, I. I., Stanley, B. A., Pegg, A. E., and Ealick, S. E. (1999) The crystal structure of human *S*-adenosylmethionine decarboxylase at 2.25 Å resolution reveals a novel fold, *Structure 7*, 583-595.

23. Ekstrom, J. L., Tolbert, W. D., Xiong, H., Pegg, A. E., and Ealick, S. E. (2001) Structure of a human *S*-adenosylmethionine decarboxylase self-processing ester intermediate and mechanism of putrescine stimulation of processing as revealed by the H243A mutant, *Biochemistry 40*, 9495-9504.

24. Tolbert, W. D., Zhang, Y., Cottet, S. E., Bennett, E. M., Ekstrom, J. L., Pegg, A. E., and Ealick, S. E. (2003) Mechanism of human *S*-adenosylmethionine decarboxylase proenzyme processing as revealed by the structure of the S68A mutant, *Biochemistry 42*, 2386-2395.

25. Tolbert, D. W., Ekstrom, J. L., Mathews, I. I., Secrist, J. A. I., Kapoor, P., Pegg, A. E., and Ealick, S. E. (2001) The structural basis for substrate specificity and inhibition of human *S*-adenosylmethionine decarboxylase, *Biochemistry 40*, 9484-9494.

26. Secrist III, J. A. (1987) New substrate analogues as inhibitors of *S*-adenosylmethionine decarboxylase, *Nucleosides Nucleotides 6*, 73-83.

27. Mitsunobu, O. (1981) The use of diethyl azodicarboxylate and triphenylphosphine in synthesis and transformation of natural products, *Synthesis*, 1-28.

28. Khomutov, A. R., Vepsalainen, J. J., Shvetsov, A. S., Hyvonen, T., Keinanen, T. A., Pustobaev, V. N., Eloranta, T. O., and Khomutov, R. M. (1996) Synthesis of hydroxylamine analogs of polyamines, *Tetrahedron 52*, 13751-13766.

29. Webb, R. R., II, and Kaneko, T. (1990) Synthesis of 1-(aminooxy)-4-[(3-nitro-2-pyridyl)dithio]butane and 1-(aminooxy)-4-[(3-nitro-2-pyridyl)dithio]-2-

butene, novel heterobifunctional crosslinking reagents, *Bioconjugate Chem. 1*, 96-99.

30. Kucznierz, R., Grams, F., Leinert, H., Marzenell, K., Engh, R. A., and von der Saal, W. (1998) Tetrahydro-isoquinoline-based factor Xa inhibitors, *J. Med. Chem. 41*, 4983-4994.
31. Pankaskie, M., and Abdel-Monem, M. M. (1980) Inhibitors of polyamine biosynthesis. 8. Irreversible inhibition of mammalian *S*-adenosyl-L-methionine decarboxylase by substrate analogues, *J. Med. Chem. 23*, 121-127.
32. Borchardt, R. T., Huber, J. A., and Wu, Y. S. (1976) Convenient preparation of *S*-adenosylhomocysteine and related compounds, *J. Org. Chem. 41*, 565-567.
33. Otwinowski, Z., and Minor, W. (1997) Processing of x-ray diffraction data collected in oscillation mode, *Methods Enzymol. 276*, 307-326.
34. Brünger, A. T., Adams, P. D., Clore, G. M., DeLano, W. L., Gros, P., Grosse-Kunstleve, R. W., Jiang, J. S., Kuszewski, J., Nilges, M., Pannu, N. S., Read, R. J., Rice, L. M., Simonson, T., and Warren, G. L. (1998) Crystallography & NMR system: A new software suite for macromolecular structure determination, *Acta Crystallogr. D 54*, 905-921.
35. Jones, T. A., Zou, J.-Y., Cowan, S. W., and Kjeldgaard, M. (1991) Improved methods for the building of protein models in electron density maps and the location of errors in these models, *Acta Crystallogr. A 47*, 110-119.
36. Emsley, P., and Cowtan, K. (2004) Coot: model-building tools for molecular graphics, *Acta Crystallogr. D 60*, 2126-2132.
37. Kleywegt, G. J., and Jones, T. A. (1998) Databases in protein crystallography, *Acta Crystallogr. D 54*, 1119-1131.
38. Mohamadi, F., Richards, N. G. J., Guida, W. C., Liskamp, R., Lipton, M., Caufield, C., Chang, G., Hendrickson, T., and Still, W. C. (1990) Macromodel

- an Integrated Software System for Modeling Organic and Bioorganic Molecules Using Molecular Mechanics, *J. Comput. Chem. 11*, 440-467.

39. Chang, G., Guida, W. C., and Still, W. C. (1989) An Internal Coordinate Monte Carlo Method for Searching Conformational Space, *J. Am. Chem. Soc. 111*, 4379-4386.

40. Kolossvary, I., and Guida, W. C. (1999) Low-mode conformational search elucidated: application to C39H80 and flexible docking of 9-deazaguanine inhibitors into PNP, *J. Comput. Chem. 20*, 1671-1684.

41. Weiner, S. J., Kollman, P. A., Case, D. A., Singh, U. C., Ghio, C., Alagona, G., Profeta, S., Jr., and Weiner, P. (1984) A new force field for molecular mechanical simulation of nucleic acids and proteins, *J. Am. Chem. Soc. 106*, 765-784.

42. Weiner, S. J., Kollman, P. A., Nguyen, D. T., and Case, D. A. (1986) An all atom force field for simulations of proteins and nucleic acids, *J. Comput. Chem. 7*, 230-252.

43. Ponder, J. W., and Richards, F. M. (1987) An efficient Newton-like method for molecular mechanics energy minimization of large molecules, *J. Comput. Chem. 8*, 1016-1024.

44. Markham, G. D., Norrby, P. O., and Bock, C. W. (2002) *S*-adenosylmethionine conformations in solution and in protein complexes: conformational influences of the sulfonium group, *Biochemistry 41*, 7636-7646.

45. Shantz, L. M., and Pegg, A. E. (1998) Assay of S-adenosylmethionine decarboxylase, in *Methods in Molecular Biology, Vol 79: Polyamine Protocols* (Morgan, D. M. L., Ed.), pp 45-50, Humana Press Inc., Totowa, NJ.

46. Ikehara, M., Uesugi, S., and Kaneko, M. (1967) Bromination of adenosine nucleosides and nucleotides, *Chem. Commun.*, 17-18.

47. Van Aerschot, A. A., Mamos, P., Weyns, N. J., Ikeda, S., De Clercq, E., and Herdewijn, P. A. (1993) Antiviral activity of C-alkylated purine nucleosides obtained by cross-coupling with tetraalkyltin reagents, *J. Med. Chem. 36*, 2938-2942.

48. Chattopadhyaya, J. B., and Reese, C. B. (1977) Reaction between 8-bromoadenosine and amines. Chemistry of 8-hydrazinoadenosine, *Synthesis*, 725-726.

49. Kohyama, N., Katashima, T., and Yamamoto, Y. (2004) Synthesis of novel 2-aryl AICAR derivatives, *Synthesis*, 2799-2804.

50. Long, R. A., Robins, R. K., and Townsend, L. B. (1967) Purine nucleosides. XV. Synthesis of 8-amino- and 8-substituted aminopurine nucleosides, *J. Org. Chem. 32*, 2751-2756.

51. Gani, D., and Johnson, A. W. (1982) The base-sugar conformation of certain derivatives of adenosine, *J. Chem. Soc., Perkin Trans. 1*, 1197-1204.

CHAPTER 5

COMPLEXES OF *THERMOTOGA MARITIMA S*-ADENOSYLMETHIONINE DECARBOXYLASE WITH SUBSTRATE ANALOGS PROVIDE INSIGHTS INTO SUBSTRATE SPECIFICTY AND INHIBITOR DESIGN

Section 5.1. Introduction

S-Adenosylmethionine decarboxylase (AdoMetDC) is a critical enzyme at a key branch point in the polyamine biosynthetic pathway (*1-4*). AdoMetDC catalyzes the decarboxylation of *S*-adenosylmethionine (AdoMet) to *S*-adenosyl-5′-(3-methylthiopropylamine) (dcAdoMet). The propylamine group from dcAdoMet is transferred to putrescine and spermidine to form spermidine and spermine respectively. The primary role of AdoMet in cells is as a methyl group donor to a variety of substrates. After the decarboxylation process, dcAdoMet is committed to polyamine biosynthesis. The polyamines putrescine, spermidine and spermine are ubiquitous across all forms of life and are implicated in cellular growth and differentiation. Elevated levels of polyamines are associated with various tumors and parasitic diseases (*5, 6*). AdoMetDC and other enzymes in the polyamine biosynthetic pathway are promising targets for anti-tumor and anti-proliferative diseases (*7, 8*).

AdoMetDC is expressed as a proenzyme and undergoes an internal serinolysis reaction as part of a post-translational modification to generate the active site pyruvoyl group. This process cleaves the peptide chain to α and β chains with the pyruvoyl group generated at the N-terminus of the α chain. The α chain is derived from the carboxy end of the proenzyme and the β chain is derived from the amino end of the proenzyme. The crystal structures of wild type human AdoMetDC (hAdoMetDC) and the H243A and S68A mutants provided insights into the mechanism of auto-processing of the enzyme (*9-11*). The crystal structures of AdoMetDC from plants

and *Thermotoga maritima* have also been determined (*12, 13*). The dimeric fold of *T. maritima* AdoMetDC (TmAdoMetDC) is similar to the monomeric protomer of human and plant AdoMetDC, suggesting evolutionary links of gene duplication and fusion.

The crystal structure of the human enzyme has been determined complexed to various ligands and substrate analogs (*14*). The complex of the human enzyme with *S*-adenosylmethionine methyl ester (MeAdoMet) reveals key interactions of the ligand with the active site residues and the binding conformation of the ligand. The ligand makes a Schiff base with the pyruvoyl group and the adenine base binds in an unusual *syn* conformation stabilized by stacking interactions with Phe223 and Phe7 and hydrogen bonds to Glu67. The hydroxyl groups of the ribose make two hydrogen bonds to Glu247. No information is available in terms of the substrate/ligand binding conformation for prokaryotic AdoMetDCs. The crystal structures of the proenzyme and the non-processible S63A mutant of TmAdoMetDC have been reported previously (*13*). In this paper, we report the crystal structure of processed TmAdoMetDC and the complexes with MeAdoMet and 5′-deoxy-5′-dimethyl thioadenosine (MMTA). We compare the complexes from *T. maritima* with the complexes from hAdoMetDC. The comparison and the conservation of the active site residues reveal recurring themes for substrate recognition and inhibitor design

Section 5.2. Materials and Methods

Protein expression, processing and purification. The expression and purification protocol of TmAdoMetDC is described in a previous paper(*13*). The pTmSpeD.28 plasmid encoding the enzyme was transformed into the B834(DE3) strain of *E. coli*. An overnight starter culture of 10 mL was grown in LB media supplemented with 35 μg/mL kanomycin. It was then introduced into a 1 L cell culture and grown until the $O.D_{600}$ reached 0.6 and subsequently induced with 1 mM

isopropyl β-D-thiogalactoside. The temperature was reduced to 15 °C and the protein expressed overnight. The cells were harvested by centrifugation and stored at –80 °C.

The cells were suspended in a wash buffer consisting of 50 mM Tris-HCl, pH 8.0, 10 mM imidazole, and 500 mM NaCl and lysed using a sonicator. Processing of the enzyme was induced by heating the lysate at 80 °C for 1 h. The heating process also served as a partial purification step. The lysate was centrifuged and the supernatant was passed through a Ni-NTA column equilibrated with the wash buffer. The column was washed with 100 mL wash buffer followed by 50 mL of buffer containing 50 mM Tris-HCl, pH 8.0, 35 mM imidazole, and 500 mM NaCl. The protein was eluted with elution buffer containing 50 mM Tris-HCl, pH 8.0, 150 mM imidazole, and 500 mM NaCl, and dialyzed into 20 mM Tris-HCl, pH 8.0, and 1 mM dithiothreitol. The protein was concentrated to 6 mg/mL and stored at –80 °C.

Crystallization conditions. The protein was crystallized using the hanging drop vapor diffusion method at room temperature. The crystallization conditions were 2.4 – 2.8 M ammonium formate, and 100 mM HEPES, pH 8.0. Crystals appeared in 2 weeks and grew to a maximum size of 0.2 × 0.15 × 0.1 mm in 3-4 weeks. For the crystals of the complexes, the crystals were transferred into a well solution containing 5 mM MeAdoMet or MMTA, respectively, for 4 h to allow the ligands to soak into the active site of the enzyme.

Data collection and processing. The data for the processed enzyme was collected at our home source on a Rigaku R-AXIS IV^{++} detector with Cu Kα radiation from a Rigaku RU-300 rotating anode generator. Data were collected over 100° with a 0.5° oscillation range and 15 min exposure per frame at a crystal to detector distance of 180 mm. Crystals of the complexes were sequentially transferred into well solution containing 5%, 10%, 15% and 20% glycerol and 200 mM concentrations of ammonium formate prior to freezing in liquid nitrogen. The data for the complexes

were collected at the 24-ID-E beamline at the NE-CAT sector of the Advanced Photon Source. Data were collected over 140° and 150° for the MeAdoMet and MMTA complexes, respectively, with a 1° oscillation range and 1 s exposure per frame at a crystal to detector distance of 260 mm. The data were indexed, integrated and scaled using the HKL2000 program suite (*15*). The data collection statistics are summarized in Table 5.1.

Structure determination and Refinement. The structures of the processed enzyme and the complexes were solved by molecular replacement using the CNS program suite (*16*). The structure of the wild type proenzyme (PDB code 1TLU) was used as the search model for molecular replacement. The model building for the protein was done by the program COOT (*17*). The refinement process included successive rounds of simulated annealing, B factor refinement, minimization and calculation of composite omit maps and difference Fourier maps. Model building was done against the composite omit maps. After several rounds of refinement and model building, the difference Fourier and composite omit maps were used to identify missing ligands and water molecules. The topology and parameter files for MeAdoMet and MMTA were obtained from the HIC-UP server (*18*). The ligand and water molecules were added to the structure followed by a few rounds of refinement as mentioned above. The final refinement statistics are shown in Table 5.2.

Figure preparation. Figures were prepared using PyMOL (*22*) and ChemDraw.

Table 5.1. Summary of Data Collection and Processing Statistics

	TmAdoMetDC Processed	TmAdoMetDC + MeAdoMet	TmAdoMetDC + MMTA
Wavelength (Å)	1.5418	0.9792	0.9792
Space group	R3	R3	R3
a = b (Å)	104.71	105.20	105.47
c (Å)	69.84	70.06	70.11
Resolution (Å)	2.06	1.90	1.90
Total reflections	49357	91891	101615
Unique reflections	16833	22459	22388
Redundancy[a]	2.9 (1.7)	4.1 (2.3)	4.5 (2.8)
Completeness (%)	95.4 (71.2)	98.9 (90.4)	97.6 (79.6)
I/σ	23.1 (4.1)	17.9 (3.1)	24.4 (2.9)
R_{sym}[b]	4.5 (21.0)	9.6 (21.6)	6.5 (23.6)
Matthews no.	2.49	2.52	2.54
Solvent content (%)	49.7	50.3	50.8

[a]Values for the highest resolution shell are given in parentheses.
[b]Rsym=ΣΣi $|$ Ii - <I> $|$ /Σ<I>, where <I> is the mean intensity of the N reflections with intensities Ii and common indices h,k,l.

Table 5.2. Refinement statistics for processed TmAdoMetDC and complexes

	TmAdoMetDC Processed	TmAdoMetDC + MeAdoMet	TmAdoMetDC + MMTA
Resolution (Å)	2.06	1.90	1.90
R factor[a](%)	0.233	0.212	24.9
R_{free}[b] (%)	0.262	0.238	28.0
No of non-H atoms			
Protein	1868	1917	1900
Ligand	-	56	42
Water	115	108	61
B factors ($Å^2$)			
Protein	28.3	33.5	31.0
Ligand ($Å^2$)	-	54.6/44.4	46.1/41.9
Rms deviations			
Bonds (Å)	0.011	0.031	0.006
Angles (º)	1.4	1.5	1.2
Dihedrals (º)	25.0	27.2	25.3
Ramachandran plot			
Most favored region (%)	94.5	95.6	95.6
Additional allowed region (%)	5.5	4.4	4.4
Disallowed region (%)	0.0	0.0	0.0

[a]R factor = $\Sigma_{hkl}||F_{obs}|-k|F_{cal}|/\Sigma_{hkl}|F_{obs}|$, where F_{obs} and F_{cal} are observed and calculated structure factors respectively.
[b]For R_{free}, the sum is extended over a subset of reflections (5% for processed; 10% for TmAdoMetDC/MeAdoMet and TmAdoMetDC/MMTA) excluded from all stages of refinement.

Section 5.3. Results

Overall structure of processed enzyme. Heating TmAdoMetDC in crude lysate of *E. coli* induces processing of the enzyme. The structure of the processed enzyme was solved by molecular replacement using the structure of the proenzyme as the search model. The overall structure of processed enzyme in the asymmetric unit is a dimer comprised of two 2-fold related protomers. The protomer is a two-layer αβ sandwich with an anti-parallel β-sheet flanked by two α-helices (similar to the monomer of the proenzyme). The dimer interface is formed by the interaction of the β-sheets of the protomers. The autoprocessing occurs between residues Glu62-Ser63 located in a β-turn between residues Val59-His64. The electron density maps show a break in the main chain density and the formation of a pyruvoyl group at Ser63. Residues Ser61 and Glu62 are disordered in the processed enzyme and become ordered upon ligand binding (see next section). The active site is at the dimeric interface and contains residues from both protomers. A comparison of the processed structure and the proenzyme shows no significant change in the overall secondary structure. The overall structure of the processed enzyme is shown in Fig. 5.1 (A). A stereoview of the comparison of the proenzyme and the processed enzyme at the processing site is shown in Fig. 5.1 (B).

Complex with MeAdoMet. The crystal structure of TmAdoMetDC complexed to MeAdoMet was solved by molecular replacement. The difference F_o- F_c density shows that MeAdoMet binds to the enzyme by making a Schiff base with the active site pyruvoyl group in both protomers. The 2′ and 3′ oxygen atoms of the ribose make hydrogen bonds to the carboxylate group of Glu72′ (′ marks residues from the two-fold related protomer). The adenine base of MeAdoMet binds in the unusual *syn* conformation stacking against Phe49′. Residue Phe49′ undergoes a torsional change in N-CA-CB-CG angle by 90° to stack against the adenine base. Residue His47′

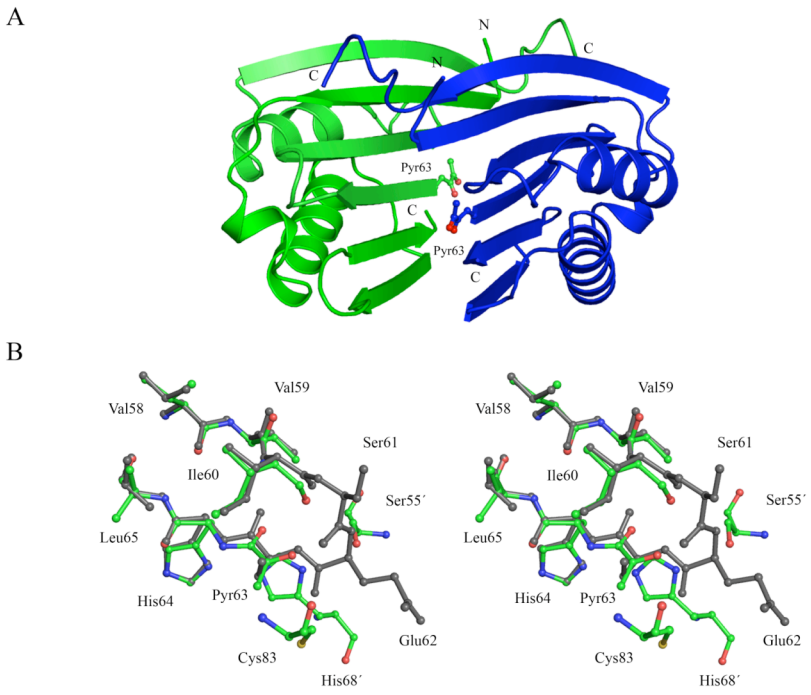

Figure 5.1. (A) Overall structure of processed TmAdoMetDC. The dimeric structure of the enzyme is shown with the monomers colored green and violet. The pryuvoyl group formed is shown in ball-and-stick and labeled. (B) Stereoview of the superposition of processed enzyme (carbon atoms colored green) and the proenzyme (shown in black). Residues Ser61 and Glu62 are disordered in the processed enzyme.

undergoes a torsional change in N-CA-CB-CG angle by 130° to stack edge-to-face against Phe49´. Residues Ser61 and Glu62 become ordered upon binding of MeAdoMet. The N6 and N1 atoms of the adenine base make two hydrogen bonds to the carboxylate and amide group of Glu62, respectively. The sulfonium ion of MeAdoMet is sandwiched between the aromatic rings of Phe49´ and Trp70´. The sulfonium atom is 4.4 Å from the CZ2 atom of the tryptophan ring, which is also the closest contact of the sulfonium with Trp70´. The sulfonium atom is 4.7 Å away from the center of the six membered ring of tryptophan. The sulfonium is 4.2 Å from the center of the Phe49´ ring and 3.8 Å from the CD2 and CE2 atoms of the ring, which is

also the closest contact of the sulfonium with Phe49′. Residue Tyr52′ undergoes a torsional change in the N-CA-CB-CG angle by 100°, moving closer into the active site upon ligand binding. Tyr52′ partially shields MeAdoMet from the external solvent. A stereoview of MeAdoMet bound to TmAdoMetDC is shown in Fig. 5.2 (A). A schematic view of the interactions of MeAdoMet with the active site residues is shown in Fig. 5.3.

Complex with MMTA. The crystal structure of TmAdoMetDC complexed to MMTA was solved by molecular replacement. MMTA lacks the terminal nitrogen group necessary to make a Schiff base to the enzyme and binds as a competitive inhibitor. The difference F_o- F_c maps show MMTA binding in the active site in both protomers. The enzyme undergoes conformational changes in residues Phe49′, His47′ and Tyr52′ (as explained in the previous section) upon MMTA binding. The adenine base of MMTA binds in the *syn* conformation stacking against Phe49′. The 2′ and 3′ oxygen atoms of the ribose make hydrogen bonds to the carboxylate group of Glu72′. The N1 atom of the adenine base makes a hydrogen bond to the amide group of Glu62. The carboxylate end of Glu62 is disordered in chain D and attains an alternate conformation in chain B. The density for the terminal end of Glu62 is too weak to assign a second hydrogen bond between the N6 atom of the adenine base and the carboxylate end of Glu62 as seen in the MeAdoMet complex. The sulfonium atom is 4.3 Å from the CZ2 atom of the tryptophan ring, which is also the closest contact of the sulfonium with Trp70′. The sulfonium atom is 4.5 Å away from the center of the six membered ring of tryptophan. The methyl group on the sulfonium is partially positive charged and is 4.1 Å from the center of the Trp70′ ring and 3.6 Å from the

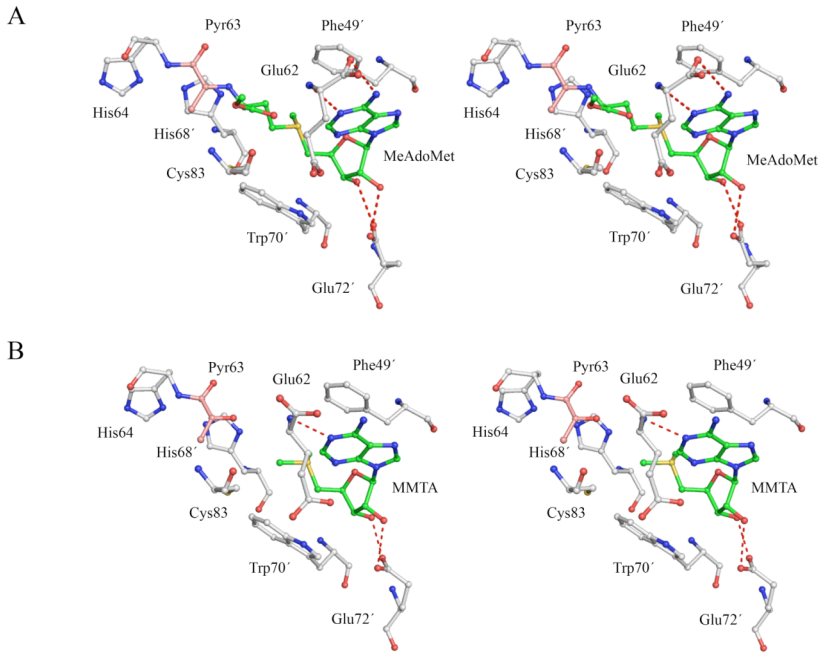

Figure 5.2. Complexes of TmAdoMetDC. (A) Stereoview of MeAdoMet covalently bound to the enzyme. The pyruvoyl group has carbon atoms colored pink and MeAdoMet has carbon atoms colored green. (B) Stereoview of MMTA bound to the enzyme. The pyruvoyl group has carbon atoms colored brown and MMTA has carbon atoms colored green. Hydrogen bonds are shown as dashed lines.

CZ2 atom of the ring, which is also the closest contact of the methyl group with Trp70´. The sulfonium is 4.5 Å from the center of the Phe49´ ring and 4.0 Å from the CD2 and CE2 atoms of the ring, which is also the closest contact of the sulfonium with Phe49´. A stereoview of MMTA bound to TmAdoMetDC is shown in Fig. 5.2 (B).

Section 5.4. Discussion

Processing of AdoMetDC. AdoMetDC is ubiquitously expressed as a proenzyme and undergoes internal serinolysis to mature to the active enzyme. The self-processing occurs between a glutamate and serine residue resulting in the formation of a pyruvoyl group from the serine residue. Processing occurs

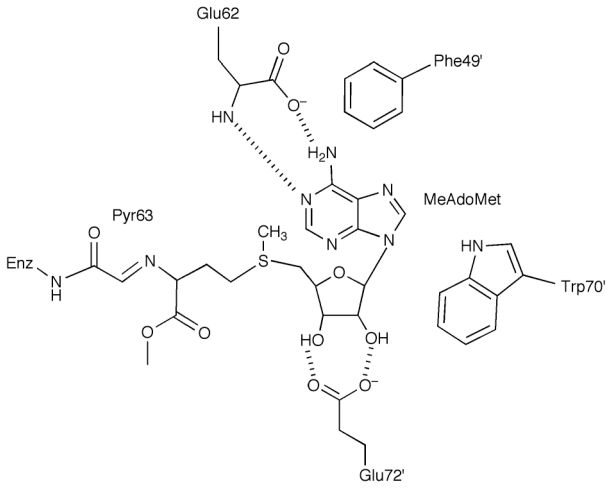

Figure 5.3. Schematic view of interactions of MeAdoMet in the active site of TmAdoMetDC.

spontaneously in the human and the potato enzyme as seen in the crystal structures and supported by the activity studies (*9, 10, 12*). Putrescine activates the processing and decarboxylation rates of hAdoMetDC (*10, 23*). Mechanical strain in the β-turn preceding the cleavage site has been implicated in autoprocessing in histidine decarboxylase and aspartate decarboxylase (*24, 25*). The processing site in TmAdoMetDC is in a β-turn and processing was induced by heating the enzyme for 1 h at 80 °C. The heat treatment for processing might be a physiologically relevant step as *T. maritima* is a thermophilic bacteria with an optimum growth at 80 °C. Comparison of the processed enzyme and the proenzyme reveals no significant changes in the secondary structure, suggesting that mechanical strain might not play a role in processing of the enzyme.

The mechanism of processing of hAdoMetDC has been extensively studied through site directed mutagenesis and crystal structures as reported previously (*10, 11, 13*). The conservation of active site residues in TmAdoMetDC suggests that the mechanism of processing is similar. The hydroxyl group of Ser63 attacks the carbonyl atom of the adjacent Glu62 resulting in the formation of an oxyoxazolidine

intermediate. The hydroxyl group needs to be activated for such an attack and there is no basic residue in the vicinity for such a role. The activation of Ser63 could occur by a water molecule, but there is no clear evidence for the activation process. The oxyoxazolidine intermediate collapses to generate the ester intermediate. The amide hydrogen of Ser63 is abstracted by His68′ resulting in the cleavage of the protein backbone to the α and β chains. The dehydroalanine residue at the N-terminus of the α chain undergoes tautomerization and subsequent hydrolysis to generate the pyruvoyl group.

Substrate specificity of AdoMetDC. Biochemical studies have shown that substrate analogs lacking a positive charge do not bind to hAdoMetDC (*26, 27*). The crystal structure of hAdoMetDC has been determined with various ligands that are substrate analogs (*14*). Substrate analogs lacking positive charge at the sulfonium position do not bind to the enzyme as analyzed from the crystal structures (data not shown). The crystal structures of the enzyme with various ligands reveal that the positive center stacks between Phe223 and Phe7 and the substrate specificity arises from the favorable cation-π interactions between the sulfonium and the aromatic rings.

The complexes of TmAdoMetDC with MeAdoMet and MMTA reveal similar interactions to those seen in the human enzyme. The sulfonium center of MeAdoMet and MMTA is sandwiched between Trp70′ and Phe49′. The geometry and distance of the sulfonium center from the aromatic rings are favorable for a cation-π interaction. Cation-π interactions in biology are implicated in protein stability, ligand recognition, catalysis and ion channels (*28, 29 , 30*). The strength of the interaction depends on the distance and geometry of the cation from the aromatic ring and also on the nature of the cation and the interacting aromatic group. There are no negative charged residues around the sulfonium center in either enzyme and the critical necessity of the positive

charge for binding suggests that the cation-π interaction plays a significant role in ligand recognition in AdoMetDC.

Ligands binding to AdoMetDC. The adenine base of the ligand binds in an unusual *syn* conformation in hAdoMetDC. The base is sandwiched between Phe223 and Phe7 for favorable π stacking interactions. The N6 and N1 atoms of the adenine base make two hydrogen bonds to the carboxylate and amide group of terminus of Glu67, respectively. The *syn* conformation is further stabilized by electrostatic interactions between the N3 atom of the base and the sulfonium center (unpublished data). The crystal structure of the F223A mutant with MeAdoMet shows that the adenine base still binds in the *syn* conformation, suggesting that π stacking to Phe7, hydrogen bonding to Glu67 and electrostatic effects are sufficient to stabilize the adenine base in the higher energy conformation (*31*).

Both of the ligands MeAdoMet and MMTA bind to TmAdoMetDC in the high energy *syn* conformation. The *syn* conformation is stabilized by π-π interactions with Phe49′. The adenine base is positioned edge-to-face 5.4 Å away from Trp70′ (residue identical to Phe7 in hAdoMetDC) and does not have a favorable geometry or distance for stabilization by the aromatic ring. In the *syn* conformation, the N3 atom of the adenine base is partially negatively charged and is present 3.7 Å away from the positive charge of the sulfonium center in the MeAdoMet complex. In the MMTA complex, the distance between the corresponding atoms is 3.4 Å. Electrostatic interactions and hydrogen bonding to Glu62 further stabilize the *syn* conformation of the adenine base.

Comparison of T.maritima and Human AdoMetDC. The crystal structure of the processed form of TmAdoMetDC provides the first insight into the active form of the enzyme from prokaryotes. The similarity in the overall structure of TmAdoMetDC and hAdoMetDC also presents a strong case of protein evolution as

discussed previously. TbAdoMetDC is a homodimer formed by two protomers related by 2-fold symmetry. Processing is observed in both the protomers are the active sites in the dimer are separated by ~26 Å. The human enzyme is a homodimer comprising of two ($\alpha\beta$) protomers. The N-terminal and C-terminal halves of hAdoMetDC are structurally homologous to each other and also to the protomer of TbAdoMetDC suggesting that the human enzyme evolved by gene duplication and subsequent fusing. The superposition of the processed from of TbAdometDC and hAdoMetDC is shown in Figure 5.4. The human enzyme has two extra β strands extending out the central β sheet in both the N-terminal and C-terminal half when compared to TbAdoMetDC.

The complexes of TmAdoMetDC with MeAdoMet and MMTA further elucidate the role of the active site residues in binding the substrate as well as the autoprocessing and decarboxylation reactions. The comparison of the active site reveals the absolute conservation of the residues involved in the autoprocessing and decarboxylation processes of both the enzymes (shown in Table 5.3). The only outlier of the absolute conservation is Trp70′ that is mutated to a phenylalanine in the human enzyme. The mutation from tryptophan to phenylalanine would conserve the role of the amino acid residue in stacking the adenine base of the substrate. The processing site in the C-terminal half of the enzyme is lost due to the mutation of Glu-Ser (essential motif for processing) to Gly-Thr, mutation of residues essential for substrate binding/decarboxylation and an insertion of an amino acid in the β turn Lys234-Thr238 (comparison of residues shown in Table 5.4).

As discussed in the previous sections, cation - π interactions determine the substrate specificity in both the AdoMetDCs and the enzymes would bind the substrate AdoMet in the *syn* conformation. The role of AdoMet in cells is predominantly a methyl group donor. The process would be facilitated if AdoMet is in the more open *anti* conformation. For the decarboxylation process, the substrate

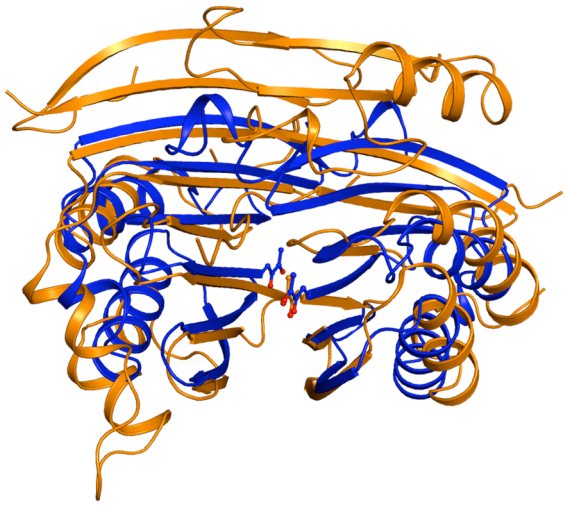

Figure 5.4. Superposition of processed form of TbAdoMetDC (blue) and hAdoMetDC (orange). The pyruvoyl cofactor is shown as sticks.

Table 5.3. Active site residues in TmAdoMetDC and hAdoMetDC

T. maritima[a]	Human	Role
Pyr63	Pyr68	Schiff base to the substrate
His68′	His243	Base for autoprocessing
Phe49′	Phe223	Stacking adenine base & sulphonium of substrate
Trp70′	Phe7	Stacking adenine base & sulphonium of substrate
Glu72′	Glu247	Hydrogen bonding to ribose moiety of substrate
Cys83	Cys82	Acid for decarboxylation
Glu62	Glu67	Hydrogen bonding to adenine base of substrate
Ser55′	Ser229	Positioning base for autoprocessing

[a] Residues labelled (′) come from the two-fold related protomer

assumes the unusual, closed *syn* conformation which is stabilized by residues conserved in prokaryotes and higher organisms.

Implications for drug design. Regulating the polyamine biosynthetic pathway and maintaining polyamine levels is a promising therapeutic strategy for cancer and parasitic diseases. Inhibitors of AdoMetDC have potential application as anti-cancer agents and have been a subject of clinical trials (*32, 33*). The development of substrate analogs such as MHZPA and MAOEA as inhibitors resulted in compounds that inhibit human AdoMetDC with IC_{50} values in the nM to pM range (unpublished data). The key interactions of the inhibitors with the active site of the enzyme include: (a) hydrogen bonding to Glu247 and Glu67, (b) stacking interactions with Phe7 and Phe223, (c) cation-π interactions to Phe223, and Phe7 (d) interactions with the pyruvoyl group. The complexes of TmAdoMetDC reveal the conservation of key interactions mentioned above in prokaryotes when compared to higher organisms (Figure 5.5).

The inhibitors of polyamine biosynthesis have potential applications in the treatment of African trypanosomiasis and other parasitic infections. The crystal structure of AdoMetDC from *T. brucei (*TbAdoMetDC) has not been determined. The structure of TbAdoMedDC would provide a template for structure-based drug design for AdoMetDCs relevant to parasitic infections. It has been recently discovered that TbAdoMetDC exists as a heterodimeric complex formed by the active enzyme and a catalytically inactive homolog termed the prozyme (*34*). The sequence alignment between human and TbAdoMetDC shows that residues Glu266, Tyr242, Phe28 and Glu85 in TbAdoMetDC are likely to be involved in substrate binding. Residues Glu266 and Glu85 are equivalent to Glu247 and Glu67, and residues Tyr242 and Phe28 are equivalent to Phe223 and Phe7 in the human enzyme, respectively. The conservation of the nature of the substrate binding residues suggests that the parasitic

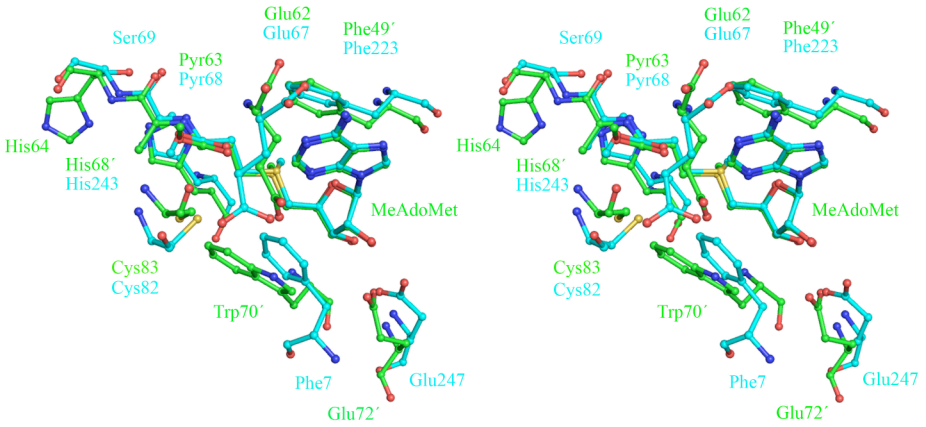

Figure 5.5. Stereoview of the comparison of active sites of TmAdoMetDC (carbon atoms colored green) and human AdoMetDC (carbon atoms colored cyan) with MeAdoMet bound. Hydrogen bonds are omitted for clarity.

Table 5.4. Comparison of residues in the second "active" site[a]

T. maritima	Human	Role
Ser63	Thr238	Pyruvoyl froming residue
Glu62	Gly237	Residue in the β turn
Ser61	Asp236	Residue in the β turn
-	Ser235	Residue in the β turn
Ile60	Lys234	Residue in the β turn
Val59	Met233	Residue in the β turn
His68	Ser73/Arg76	Base for processing
Ser55	Gln60	Base for processing
Cys83	-	Acid for decarboxylation

[a]Ser73 and Arg76 are positioned in a similar position to His68. Missing residues in equivalent positions in the human enzyme are indicated by a dash.

AdoMetDC binds ligands in a similar fashion to the human and the prokaryotic enzymes. The similarity also suggests that inhibitors designed for hAdoMetDC have a potential to block activity of AdoMetDCs in other species

REFERENCES

1. Hackert, M. L., and Pegg, A. E. (1997) Pyruvoyl-dependent enzymes, in *Comprehensive Biological Catalysis* (Sinnott, M. L., Ed.), pp 201-216, Academic Press, London.
2. Pegg, A. E., Xiong, H., Feith, D., and Shantz, L. M. (1998) *S*-adenosylmethionine decarboxylase: structure, function and regulation by polyamines, *Biochem. Soc. Trans. 26*, 580-586 526.
3. Tabor, C. W., and Tabor, H. (1984) Polyamines, *Annu. Rev. Biochem. 53*, 749-790.
4. Tabor, C. W., and Tabor, H. (1984) Methionine adenosyltransferase (*S*-adenosylmethionine synthetase) and *S*-adenosylmethionine decarboxylase, *Advan. Enzymol. Related Areas Mol. Biol. 56*, 251-282.
5. Gerner, E. W., and Meyskens, F. L., Jr. (2004) Polyamines and cancer: old molecules, new understanding, *Nat. Rev. Cancer 4*, 781-792.
6. Pegg, A. E. (1988) Polyamine metabolism and its importance in neoplastic growth and as a target for chemotherapy, *Cancer Res. 48*, 759-774.
7. Casero, R. A., Jr., Frydman, B., Stewart, T. M., and Woster, P. M. (2005) Significance of targeting polyamine metabolism as an antineoplastic strategy: unique targets for polyamine analogues, *Proc. West Pharmacol. Soc. 48*, 24-30.
8. Casero, R. A., Jr., and Marton, L. J. (2007) Targeting polyamine metabolism and function in cancer and other hyperproliferative diseases, *Nat. Rev. Drug Discov. 6*, 373-390.
9. Ekstrom, J. E., Matthews, I. I., Stanley, B. A., Pegg, A. E., and Ealick, S. E. (1999) The crystal structure of human *S*-adenosylmethionine decarboxylase at 2.25 Å resolution reveals a novel fold, *Structure 7*, 583-595.

10. Ekstrom, J. L., Tolbert, W. D., Xiong, H., Pegg, A. E., and Ealick, S. E. (2001) Structure of a human *S*-adenosylmethionine decarboxylase self-processing ester intermediate and mechanism of putrescine stimulation of processing as revealed by the H243A mutant., *Biochemistry 40*, 9495-9504.

11. Tolbert, W. D., Zhang, Y., Cottet, S. E., Bennett, E. M., Ekstrom, J. L., Pegg, A. E., and Ealick, S. E. (2003) Mechanism of human S-adenosylmethionine decarboxylase proenzyme processing as revealed by the structure of the S68A mutant, *Biochemistry 42*, 2386-2395.

12. Bennett, E. M., Ekstrom, J. E., Pegg, A. E., and Ealick, S. E. (2002) Monomeric *S*-Adenosylmethionine Decarboxylase from Plants Provides an Alternative to Putrescine Stimulation, *Biochemistry 41*, 14509-14517.

13. Toms, A. V., Kinsland, C., McCloskey, D. E., Pegg, A. E., and Ealick, S. E. (2004) Evolutionary links as revealed by the structure of *Thermotoga maritima* *S*-adenosylmethionine decarboxylase, *J Biol Chem 279*, 33837-33846.

14. Tolbert, D. W., Ekstrom, J. L., Mathews, I. I., Secrist, J. A. I., Kapoor, P., Pegg, A. E., and Ealick, S. E. (2001) The structural basis for substrate specificity and inhibition of human *S*-adenosylmethionine decarboxylase, *Biochemistry 40*, 9484-9494.

15. Otwinowski, Z., and Minor, W. (1997) Processing of x-ray diffraction data collected in oscillation mode, *Methods Enzymol. 276*, 307-326.

16. Brünger, A. T., Adams, P. D., Clore, G. M., DeLano, W. L., Gros, P., Grosse-Kunstleve, R. W., Jiang, J. S., Kuszewski, J., Nilges, M., Pannu, N. S., Read, R. J., Rice, L. M., Simonson, T., and Warren, G. L. (1998) Crystallography & NMR system: A new software suite for macromolecular structure determination, *Acta Cryst. D 54*, 905-921.

17. Emsley, P., and Cowtan, K. (2004) Coot: model-building tools for molecular graphics, *Acta Crystallogr. D 60*, 2126-2132.

18. Kleywegt, G. J., and Jones, T. A. (1998) Databases in protein crystallography, *Acta Cryst. D 54*, 1119-1131.

19. Eswar, N., Marti-Renom, M. A., Webb, B., Madhusudhan, M. S., Eramian, D., Shen, M., Pieper, U., and Sali, A. (2007) Comparative Protein StructureModeling with MODELLER, in *Current Protocols in Protein Science*, pp 2.9.1-2.9.31, Wiley, John & Sons, Inc.

20. Sali, A., and Blundell, T. L. (1993) Comparative protein modelling by satisfaction of spatial restraints, *J. Mol. Biol. 234*, 779-815.

21. Thompson, J. D., Higgins, D. G., and Gibson, T. J. (1994) CLUSTAL W: improving the sensitivity of progressive multiple sequence alignment through sequence weighting, position-specific gap penalties and weight matrix choice, *Nucleic Acids Res. 22*, 4673-4680.

22. DeLano, W. L. (2002) The PyMOL Molecular Graphics System, DeLano Scientific, San Carlos, CA.

23. Bale, S., Lopez, M. M., Makhatadze, G. I., Fang, Q., Pegg, A. E., and Ealick, S. E. (2008) Structural basis for putrescine activation of human *S*-adenosylmethionine decarboxylase, *Biochemistry 47*, 13404-13417.

24. Gallagher, T., Rozwarski, D. A., Ernst, S. R., and Hackert, M. L. (1993) Refined structure of the pyruvoyl-dependent histidine decarboxylase from *Lactobacillus* 30a, *J. Mol. Biol. 230*, 516-528.

25. Schmitzberger, F., Kilkenny, M. L., Lobley, C. M., Webb, M. E., Vinkovic, M., Matak-Vinkovic, D., Witty, M., Chirgadze, D. Y., Smith, A. G., Abell, C., and Blundell, T. L. (2003) Structural constraints on protein self-processing in L-aspartate-a-decarboxylase, *EMBO J. 22*, 6193-6204.

26. Pegg, A. E., and Jacobs, G. (1983) Comparison of inhibitors of *S*-adenosylmethionine decarboxylase from different species, *Biochem. J. 213*, 495-502.

27. Pankaskie, M., and Abdel-Monem, M. M. (1980) Inhibitors of polyamine biosynthesis 8: Irreversible inhibition of mammalian *S*-adenosyl-L-methionine decarboxylase by substrate analogs, *J. Med. Chem. 23*, 121-127.

28. Gallivan, J. P., and Dougherty, D. A. (1999) Cation-πinteractions in structural biology, *Proc. Natl. Acad. Sci. U. S. A. 96*, 9459-9464.

29. Ma, J. C., and Dougherty, D. A. (1997) The Cation-π Interaction, *Chem. Rev. 97*, 1303-1324.

30. Zacharias, N., and Dougherty, D. A. (2002) Cation-π interactions in ligand recognition and catalysis, *Trends Pharmacol. Sci. 23*, 281-287.

31. McCloskey, D. E., Bale, S., Secrist, J. A., Tiwari, A., Moss, T. H., Valiyaveettil, J., Brooks, W. H., Guida, W. C., Pegg, A. E., and Ealick, S. E. (2009) New Insights into the Design of Inhibitors of Human S-Adenosylmethionine Decarboxylase: Studies of Adenine C(8) Substitution in Structural Analogues of S-Adenosylmethionine, *J. Med. Chem. 52*, 1388-1407.

32. Millward, M. J., Joshua, A., Kefford, R., Aamdal, S., Thomson, D., Hersey, P., Toner, G., and Lynch, K. (2005) Multi-centre Phase II trial of the polyamine synthesis inhibitor SAM486A (CGP48664) in patients with metastatic melanoma, *Invest. New Drugs 23*, 253-256.

33. Williams-Ashman, H. G., and Schenone, A. (1972) Methylglyoxal bis(guanylhydrazone) as a potent inhibitor of mammalian and yeast *S*-adenosylmethionine decarboxylases, *Biochem. Biophys. Res. Commun. 46*, 288-295.

34. Willert, E. K., Fitzpatrick, R., and Phillips, M. A. (2007) Allosteric regulation of an essential trypanosome polyamine biosynthetic enzyme by a catalytically dead homolog, *Proc. Natl. Acad. Sci. U. S. A. 104*, 8275-8280.

CHAPTER 6

CONCLUSIONS

Structure based drug design employing X-ray crystallography as a tool is gaining wider acceptance by pharmaceutical companies and academia in reducing the costs associated with drug discovery and reduce the time frame involved for drug development. *S*-Adenosylmethionine decarboxylase (AdoMetDC) is an attractive target for inhibitor design in the polyamine biosynthetic pathway. The enzyme is expressed as an inactive proenzyme which undergoes internal serinolysis as a post-translational modification to mature into the active form. In humans, the rate of the autoprocessing and decarboxylation reactions are activated by putrescine which binds at the allosteric site in the enzyme. Biochemical assays indicate that a positive charge at the position of the sulphonium of the substrate is essential for substrate analogs to inhibit AdoMetDC. Previously obtained crystal structures showed that AdoMetDC binds substrate analogs in the unusual and higher energy *syn* conformation. The existence of a proenzyme, activation by putrescine, requirement of positive charge for inhibition and the binding of ligands in the *syn* conformation make AdoMetDC an interesting target to pursue for inhibitor design.

The tools of structure based drug discovery were used in understanding the molecular details of inhibition of human AdoMetDC at various sites and stages of the enzyme lifetime. The activity of AdoMetDC can be blocked by (1) Inhibiting the putrescine binding site (2) Inhibiting the active site (3) Inhibiting the autoprocessing reaction. The crystal structures of human AdoMetDC solved previously identified the putrescine binding site and the interactions putrescine would make with the enzyme. To investigate the structural basis of putrescine activation, the crystal structure of the wild type AdoMetDC, D174N, E178Q, and E256Q mutants in the putrescine free form were obtained. The comparison of the crystal structures revealed that putrescine

effects are primarily electrostatic that orient the catalytic residues through a hydrogen bonding network mediated by Lys80.

The crystal structure of AdoMetDC with substrate analogs 5′-deoxy-5′-[*N*-methyl-*N*-(3-hydrazinopropyl)amino]adenosine (MHZPA), 5′-deoxy-5′-[*N*-methyl-*N*-[(2-aminooxy)ethyl]amino]adenosine (MAOEA), and the methyl ester of *S*-adenosylmethionine (MeAdoMet) elucidated the interactions of potential inhibitors with the active site of the enzyme. The structural information obtained from these complexes was used to rationally design inhibitors to the active site of the enzyme. The inhibitors synthesized broadly fall into four categories based on the terminal group at the 5′ end of the ribose moiety. The crystal structure of human AdoMetDC was obtained cocrystallized with a representative ligand from each of the category of ligands synthesized.

The complexes of AdoMetDC with competitive inhibitors 5′-deoxy-5′-(dimethylsulfonio)adenosine (MMTA) and 5′-deoxy-5′-(*N*-dimethyl)amino-8-methyladenosine (DMAMA) were obtained. The structural information from the complexes combined with quantum chemical calculations and stopped flow experiments provided insights into ligand specificity of AdoMetDC. The positive charge on the central sulphur/nitrogen atom of the ligands stacks between Phe223 and Phe7 and is stabilized by favorable cation - π interactions to the aromatic rings. The stabilization obtained by cation - π interactions is ~ 4.5 kcal/mol as obtained from quantum chemical calculations. The stopped flow experiments demonstrate that the importance of residues in binding ligands follows the order Phe223 ~ Glu247 >> Phe7.

The crystal structure of the F223A mutant of AdoMetDC complexed to MeAdoMet revealed that the ligand binds to the enzyme in the *syn* conformation. The crystal structure of human AdoMetDC was obtained complexed with 5′-deoxy-5′-[(3-

aminopropyl)methylamino]-8-methyl-adenosine, 5′-deoxy-5′-[(2-carboxamidoethyl)methylamino]-8-methyl-adenosine, 5′-deoxy-5′-[(2-aminooxyethyl)methylamino]-8-methyl-adenosine, 5′-deoxy-5′-[(4-aminooxybutyl)methylamino]-8-ethyl-adenosine, and 5′-deoxy-5′-[(carboxamidomethyl)methylamino]-8-methyl-adenosine. All these ligands have a substituent at the C^8 position. The substituent would favor a *syn* conformation of the adenine base in solution. The inhibitors mentioned above also have a variety of terminal groups at the 5′ end to investigate the possibility of formation of a Schiff base to the active site pyruvoyl group. The crystal structures revealed that a linker length of two carbon atoms between the central sulphur/nitrogen and the terminal group is ideal for the formation of a Schiff base. The inhibition studies of these ligands suggest that the C^8 substituted ligands were 5-18 times more potent than the unsubstituted parent compounds.

In addition to the material discussed in chapters 2 - 5, complexes of AdoMetDC with 5′-deoxy-5′-[(2-aminooxyethyl)ethylamino]-adenosine, 5′-deoxy-5′-[(2-hydrazinocarbonylethyl)methylamino]-8-adenosine, 5′-deoxy-5′-[(2-carboxamidoethyl)amino]-adenosine, and 5′-deoxy-5′-[(2-hydrazinocarbonylethyl)amino]-adenosine were also obtained (data not shown). The latter two inhibitors do not have a third substituent on the central nitrogen atom but still maintain a positive charge at physiological pH for binding to AdoMetDC.

Human AdoMetDC undergoes processing between residues Glu67 and Ser68 to mature the active enzyme. The S68A mutant prevents processing and traps the enzyme in the form of the proenzyme. The crystal structure of the S68A mutant of AdoMetDC complexed to competitive inhibitors MMTA and DMAMA were obtained (data not shown). The binding of the inhibitors induced a conformational change in the β turn containing the processing site. The structural information could be used in

designing inhibitors to the proenzyme that block the autoprocessing reaction and hence block AdoMetDC activity.

In addition to the inhibitor design of human AdoMetDC, the crystal structure of *Thermotoga maritima* AdoMetDC (TmAdoMetDC) in the processed form and complexed to MeAdoMet and MMTA were obtained. The similarity between the prokaryotic and human enzyme suggests a case of evolution of the human enzyme by gene duplication and fusion. In addition to the overall structure, the active site residues involved in autoprocessing and decarboxylation reactions in human AdoMetDC are also conserved in TbAdoMetDC. The ligands MeAdoMet and MMTA bind to TbAdoMetDC in a similar pose as to the human enzyme and make similar interactions to the residues in the active site as in the human enzyme. The comparison of the crystal structures of TbAdoMetDC and human AdoMetDC reveal recurring themes for substrate recognition and inhibitor design.